Controls on Arsenic Mobility in Contaminated Wetland and Riverbed Sediments

by

Nicole E. Keon

B.S. Environmental Science
University of Rochester, 1996

B.A. Chemistry
University of Rochester, 1996

Submitted to the Department of Civil and Environmental Engineering
in Partial Fulfillment of the Requirements for the Degree of

Doctor of Philosophy in Environmental Engineering

at the

Massachusetts Institute of Technology

September 2002

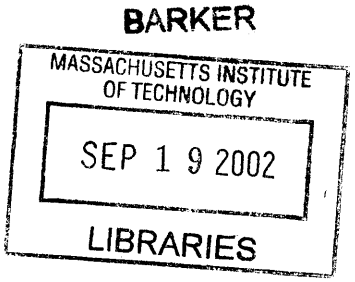

Signature of Author: _____
Department of Civil & Environmental Engineering
August 12, 2002

Certified by: _____
Harold F. Hemond
Professor of Civil and Environmental Engineering
Thesis Supervisor

Accepted by: _____
Oral Buyukozturk
Chairman, Committee on Graduate Students

Controls on Arsenic Mobility in Contaminated Wetland and Riverbed Sediments

by

Nicole E. Keon

Submitted to the Department of Civil and Environmental Engineering
on August 12, 2002 in Partial Fulfillment of the Requirements
for the Degree of Doctor of Philosophy in Environmental Engineering

ABSTRACT

Arsenic mobility and transport in the environment are strongly influenced by associations with solid phases. This dissertation investigates the mechanisms affecting arsenic retention in contaminated wetland and riverbed sediments.

A sequential extraction procedure was designed and tested to differentiate solid phase arsenic speciation, including adsorbed As and As coprecipitated with amorphous and crystalline oxides and sulfides. The sequential extraction was performed on Wells G & H wetland (Woburn, MA) sediments, and the inferred As associations were compared to XANES analyses. Geochemical modeling was used to predict redox conditions and As associations. We found that most As in the wetland was adsorbed onto amorphous Fe (hydr)oxide phases. Riverbed sediments differed from wetland sediments in that redox conditions were more reducing, and As was associated with more reducing and crystalline phases, including sulfides. As(III) and As(V) oxidation states coexist in the wetland and riverbed sediments, with more oxidized As in the wetland.

We tested the hypothesis that As associations with more oxidized phases in the wetland may result from wetland plant activities, including root oxygenation in anoxic sediments. We investigated the extent of Fe plaque formation on *Typha latifolia* roots (cattail), and the mechanism of As sequestration in plaques and (near-root) rhizosphere sediment. The plaque was approximately 30 μm thick, with a strong correlation between As and Fe, as determined by XRF microtomography. Most As was adsorbed, likely to Fe hydroxides in the plaque. Root plaque oxidation state maps showed that both As(III) and As(V) were retained in the plaque, suggesting that the plaque sequesters even the more mobile As(III) species. Mass balance analysis of As revealed that the plaque was a significant sink of aqueous As.

We concluded that the As retained in the Wells G & H wetland is susceptible to redox changes (particularly reduction of Fe hydroxides onto which most As is adsorbed) and displacement by competitive anions. Iron plaque formation on *T. latifolia* roots was shown to affect As cycling within root zone contaminated sediments by providing a substrate onto which aqueous As can adsorb.

Thesis Supervisor: Harold F. Hemond
Title: Professor of Civil and Environmental Engineering

ACKNOWLEDGMENTS

This work has been financially supported by the NIEHS Superfund Basic Research Program Grant #5P42ES04675-06 and the EPA NCERQA STAR Fellowship Program.

I owe special thanks to many people who have offered assistance and encouragement in the completion of this thesis, a few of whom I mention here.

Thank you to my advisor, Harry Hemond, for helping me to become a confident and competent scientist, undaunted in getting to the bottom of instrumental problems and contradictory literature. To other members of my thesis committee: Tina Voelker, for precision editing and many helpful aquatic chemistry discussions; Charlie Harvey, for making me part of the Bangladesh research team.

Thank you also to Dan Brabander (also a committee member) and Chris Swartz— both postdoctoral fellows while I was a graduate student. They have both been great hands-on advisors in the field and lab, as well good friends. We have traveled far and worked some very long days together, which has been enjoyable because of you.

Thank you to Jenny Jay, who welcomed me into the lab, then helped with endless extractions and lab equipment repairs in later years. You spark my interest in environment issues time and again, and have been a good friend and role model.

Thank you to my teachers in x-ray absorption spectroscopy – Satish Myneni, at Princeton and Berkeley Labs, who introduced me to the method; and Steve Sutton and Matt Newville, at Argonne National Lab, who have helped me with much of the root imaging.

Thank you to other Parsons Lab friends and Hemond group members, who understood the challenging grad school experience and helped to make it fun: Dave Senn; Megan Kogut; Kristen Jellison; Rachel Adams; Jim Gawel; Wendy Pabich; and Rich Camilli. Thank you also to UROPs who have worked on this project, especially Rachel Stanley and Yukie Tanino.

Thank you to those who keep everything running at Parsons and always lend an ear: Sheila Frankel, who is the heart of the Parsons Lab; John MacFarlane, who lent me many a piece of lab equipment, always with a smile; Vicki Murphy; Sheila Anderson; Cynthia Stewart; and Pat Dixon.

Thank you to my advisor at Woods Hole, Kathleen Ruttenberg, who taught me amazing organizational skills and how to keep perspective about things that matter most.

Thank you to my family (my mother Lee, my father John, my grandmother Leonora, and my sister Kristen), who have always stressed the value of education, hard work, and finding your passion. They always believed in me and told me so – it is truly a gift to have such a wonderful family. Thank you also to my "new" family (in-laws Sally, John, Meghan, and Sarah), for welcoming me into their home during my final thesis year of commuting between LA and MIT. They too have made it all possible in many ways.

Finally, thank you to my husband Matt, who has been there every step of the way— from my grad school interviews to my defense. I dedicate this thesis to you – it was your unwavering support that made this dream possible.

Table of Contents

Chapter 1. Introduction 8

Chapter 2. Validation of a Sequential Extraction Method for Evaluating Arsenic Mobility in Sediments

2.1 Abstract..... 16
2.2 Introduction..... 16
2.3 Experimental Section..... 18
2.4 Results & Discussion..... 24
2.5 References..... 28

Chapter 3. Geochemical Controls on Arsenic Speciation in Contaminated Wetland Peat and Riverbed Sediments

3.1 Abstract..... 37
3.2 Introduction..... 38
3.3 Site Description..... 40
3.4 Sample Collection..... 41
3.5 Analytical Techniques..... 43
3.6 Results..... 48
3.7 Discussion..... 55
3.8 Conclusions..... 65
3.9 References..... 67

Chapter 4. Arsenic Distribution and Speciation in Iron-Rich Root Plaques: The influence of *Typha latifolia* on arsenic cycling in the Wells G & H Wetland

4.1 Abstract..... 86
4.2 Introduction..... 86
4.3 Methods..... 90
4.4 Results & Discussion..... 95
4.5 Conclusions..... 104
4.6 References..... 106

Appendices

A. Sediment Cores 123
B. Construction of pH-pe Diagrams 126
C. Mineral Identification in Sediment Cores 133
D. X-Ray Absorption Spectroscopy Data Fitting 141
E. *T. latifolia* SEM Images & Elemental Maps 148

List of Figures & Tables

Chapter 2

Table 1.	Sequential extraction method	32
Table 2A.	Reproducibility of total As and As distribution in subsamples by extractions	33
Table 2B.	Reproducibility of total As by acid digestion	33
Table 3A.	Extractant distribution of As in sediment used for spike recovery experiments.	34
Table 3B.	Spike recovery of As-bearing solid phases in the sequential extraction	34
Figure 1.	Distribution of As extracted from spiked and unspiked sediment samples	35

Chapter 3

Table 1.	Sequential extraction procedure	72
Figure 1.	Map of Aberjona Watershed and Wells G & H Wetland	73
Figure 2.	Wetland & riverbed solid phase & aqueous profiles of arsenic	74
Figure 3.	Microelectrodes (pH, PEP), Fe (porewater & solid phase), and AVS wetland & riverbed measurements	75
Figure 4.	Wetland & riverbed pH-pe diagrams	76
Figure 5.	XRF elemental concentrations for one wetland core & one riverbed core	78
Figure 6.	Wetland extraction results: As	79
Figure 7.	Riverbed extraction results: As	80
Figure 8.	Wetland extraction results: Fe	81
Figure 9.	Riverbed extraction results: Fe	82
Figure 10.	Wetland and riverbed extraction results: Al	83
Figure 11.	XANES solid phase speciation of As	84

Chapter 4

Table 1.	Root separation methodology	110
Table 2.	Abbreviated sequential extraction used to extract root plaques	111
Table 3.	As and Fe distribution in root plaque, determined by extractions	112
Figure 1.	pH and PEP measurements of *T. latifolia* root zone	113
Figure 2.	SEM images of *T. latifolia* roots	114
Figure 3.	XRF microtomography elemental maps of a *T. latifolia* root	115
Figure 4.	Correlation plot of As and Fe in root plaque	116
Figure 5.	As XANES spectrum through a root with data fit	117
Figure 6.	Fe XANES spectrum through a root with model compound spectra	118
Figure 7.	Oxidation state maps of As in the root plaque	119
Figure 8.	Distribution of sediment and biomass in root cores	120
Figure 9.	As concentrations and proportion in each biomass & sediment pool	121

Appendices.

A.

Table I.	Sediment cores	123
Figure I.	Map of sediment coring	124
Figure II.	Corer design	125

B.

Table I.	Redox reactions used in model construction	126
Table II.	pH reactions	127
Table III.	Mineral formation reactions	128
Table IV.	pH-PEP measurements for wetland sediment depths	130
Table V.	pH-PEP measurements for riverbed sediment depths	131

C.

Figure I.	Optical microscope images of wetland dense minerals	137
Figure II.	Optical microscope images of magnetic, dense minerals	138
Figure III.	X-ray diffraction scans of unseparated sediment & dense minerals	139
Figure IV.	Electron microprobe images of unseparated sediment & Fe-rich regions	140

D.

Figure I.	Wetland sediment depth 30-35 cm: XANES spectra & curve fit	141
Figure II.	Wetland sediment depth 65-70 cm: XANES spectra & curve fit	142
Figure III.	Wetland sediment depth 90-95 cm: XANES spectra & curve fit	143
Figure IV.	Riverbed sediment depth 30-35 cm: XANES spectra & curve fit	144
Figure V.	Riverbed sediment depth 40-45 cm: XANES spectra & curve fit	145
Figure VI.	Riverbed sediment depth 95-100 cm: XANES spectra & curve fit	146
Figure VII.	Arsenic model compounds used for curve fits	147

E.

Figure I.	Map of wetland plant species in the Wells G & H wetland	148
Figure II.	BSE image of a root cross section showing plaque ring	149
Figure III.	BSE image of a root cross-section highlighting SEM method limitations	150
Figure IV.	BSE image of rhizome rhizosphere sediment and x-ray elemental maps	151
Figure V.	Higher magnification image of rhizosphere sediment	152
Figure VI.	SIMS step scan of As and Fe across a root fragment	153
Figure VII.	XRF microtomography of a smaller *T. latifolia* root	154
Figure VIII	Correlation of As & Fe in smaller root plaque	155
Figure IX.	XRF microtomograms of a rhizome section	156
Figure X.	As XANES spectra of apex region of a *T. latifolia* root	157

Chapter 1

Introduction

Introduction & Motivation for Research

The occurrence of toxic levels of arsenic (As) in drinking water around the world has focused much attention on the metalloid during the past decade. Increased awareness of the ubiquity of As and the effects of As on human health has promoted a flurry of research investigating ways to mitigate exposure. In 2002, the EPA mandated a revised arsenic standard for drinking water, five times lower than the current standard, after review of existing epidemiological data. The National Academy of Sciences report to the EPA underscored the potential cancer risk from low, chronic doses of arsenic in drinking water (*1*).

Arsenic exposure risk to humans is determined primarily by the mobility, fate and transport of the element. Arsenic contamination of drinking water sources may occur by natural release of arsenic from the solid phase or from industrial pollution. As the 20th most abundant element in the earth's crust, As is found at low concentrations in most soils and sediments (*2; 3*). In addition to originating from natural sources, arsenic has been introduced into many environments by anthropogenic industrial effluents, pesticides and herbicides, and mine drainage. Certain deposits, notably sulfide deposits, are commonly enriched in As (usually as arsenian pyrite). Mine drainage of As-enriched ores and the subsequent effluent from ore processing in the last two centuries have yielded a legacy of As contamination in many parts of the U.S., including Coeur d'Alene, Idaho (*4*) and Iron Mountain, California (*5*). In Woburn, Massachusetts, As-rich Iberian Pyrite ore was used in the manufacture of sulfuric acid, which yielded hundreds of tons of As-laden waste (*6*).

In the environment, As can cycle between the solid and aqueous phase depending on various conditions. The mobility of aqueous phase As can be reduced by sequestration in the solid phase via mechanisms of adsorption, coprecipitation, and precipitation of As minerals. Redox conditions and pH are the principal determinants of As retention in the solid phase, as the availability of substrates onto which As sorb and aqueous elements with which As can

precipitate are controlled by these two key parameters. The chemical speciation of inorganic As also depends on redox and pH, which in turn affects mobility due to oxidation state and charge. In addition, the speciation of As can be important from a toxicological and exposure standpoint, as reduced As is thought to be more toxic than oxidized As and more difficult to remove from drinking water.

The primary purpose of this research was to identify and closely examine the relative importance of mechanisms that limit As mobility in a contaminated wetland. From the outset, we identified the lack of sufficiently tested methods for assessing solid phase As associations. Chapter 2 builds on existing sequential extraction procedures by specifically testing common As phases in sediments and establishing constraints on reproducibility and applicability. The validated method was then applied in each of the following chapters to assess As solid phase associations and mobility. Speciation of solid phase As in an As-contaminated wetland was investigated in Chapter 3. Results obtained in Chapter 3 led to the exploration of the role of *Typha latifolia* (cattail plants) in reducing As mobility in the contaminated root zone, which was the subject of Chapter 4. In Chapter 4, mechanisms and distribution of As sequestration by *T. latifolia* roots were determined. Subsequently, the impact of *T. latifolia* in reducing aqueous concentrations of As was examined by quantifying the fraction of solid phase As directly associated with the roots. The appendices include supporting data and calculations that expand upon the information included in the chapters.

To assess solid phase As mobility, the integration of numerous analytical techniques is necessary, particularly in contaminated environmental sediments with a complex mixture of phases. Chapter 2, published under the title "Validation of an Arsenic Sequential Extraction Method for Evaluating Mobility in Sediments" in *Environmental Science & Technology* (v. 35, p.2778-2784, July 2001), focuses on the most widely available technique to researchers: sequential chemical extractions. Extractions take advantage of differential dissolution of As phases and the substrates that may retain As. The usefulness of extractions is directly

dependent on appropriate standard-testing in conjunction with other methods to predict expected redox-sensitive solid phases.

In Chapter 3, the speciation of aqueous and solid phase As was investigated to determine the retention mechanisms of As in the Wells G & H Wetland Superfund Site in Woburn, Massachusetts. The wetland contains approximately 10 tons of arsenic, primarily contained within the upper 50 cm of sediment. Although aqueous concentrations of As in this zone exceed the EPA maximum contaminant level for drinking water, the aqueous phase has relatively little compared to the amount of As in the solid phase. The Aberjona River runs from the upstream Industri-Plex site, the likely source of the As contamination, through the towns of Woburn and Winchester. Arsenic exposure risk from the wetland contamination to residents along the downstream flood plain of the Aberjona is dependent on the mobility of As and changes in geochemistry that could release stored solid phase As. This chapter investigates the processes controlling As retention in the solid phase, using the standard-tested sequential extraction method (Ch. 2), x-ray absorption near-edge spectroscopy (XANES) to directly probe solid phase As speciation, and various other measurements to detemine the redox conditions of the sediments as a function of depth. Predictions of solid phase As speciation, based on *in-situ* pH and platinum electrode potential porewater measurements, were developed using pH-pe diagrams and compared to the conclusions from solid phase analyses. In Chapter 3, a comparison of vegetated wetland sediments and nearby unvegetated riverbed sediments showed that the upper contaminant zone of the wetland was more oxidizing and As was mostly adsorbed, most likely to Fe oxyhydroxides.

In Chapter 4, we tested the hypothesis that wetland As sequestration may be partly explained by the metabolic activity of the wetland plants (i.e. the near-root (rhizosphere) oxygenation and exudation of organic complexes). The role of cattail roots in rhizofiltration of aqueous As at the root surface was explored, and potential mobilization mechanisms of plant-associated As were considered. *T. latifolia* was selected for the investigation, as this invasive

wetland plant species is dominant in the Wells G & H wetland and in wetlands throughout the United States and Europe. The presence of an iron (Fe) plaque on wetland plant root surfaces has been previously documented (*7*), and the likelihood of a strong As affinity for the plaque suggested (*8; 9*). However, until recently the experimental capability did not exist to probe trace contaminants at the micron-scale. Chapter 4 aims to use the new x-ray fluorescence (XRF) microtomography technique to develop a better understanding of root plaques in *T. latifolia*, including Fe plaque thickness and composition, spatial distribution of As in the plaque and in the interior of roots, and the mechanism of As retention in the plaque. XRF microtomography enabled us to produce cross-sectional elemental maps (Fe, As, As(III) vs. As(V)) of roots on a micron scale to determine how wetland plants in As-rich sediments affect the cycling of the As.

Findings of root plaque geochemistry from XRF microtomographic analysis were then coupled to root quantification methods to evaluate the relative importance of root-associated As compared to the aqueous and total solid phase As concentrations. To accomplish this, live and dead roots were separated by hand from several plant cores and adhering rhizosphere (near-root) sediment was removed by washing. This is the first study in which deoxygenated water washes were used to separate the rhizosphere soil from the plaque, which is critical to avoid oxidation of As(III) or Fe(II) induced by the experimental procedure. Arsenic associated with separated live roots, dead roots, and rhizosphere soil from all roots was quantified to determine the proportion of root-associated As compared to other mineralogical and organic soil components. Live roots were also measured for diameter and length. Root surface area was calculated and the volume of plaque was estimated from the thickness determined by XRF microtomography. Arsenic content in the plaque and rhizosphere soil were compared to total solid phase As and aqueous As, to determine if *T. latifolia* roots are important in immobilizing wetland As.

In all, Chapters 2 through 4 comprise a research project that was dynamic in its progression. Each layer of understanding that was revealed along the way led us to refine our hypotheses, conclusions, and course of research. Due to the complexity in data interpretation at an impacted and reworked environmental field site, we integrated a wide range of experimental methods to investigate As immobilization mechanisms, from the very small scale (XRF microtomography) to bulk measurements of As speciation (chemical extractions). While the findings are accompanied by unanswered questions and apparent puzzles, we have gained an increased understanding of real-world As immobilization, notably in system that poses an exposure health risk to nearby residents. I hope that this research will provide a foundation for studies of arsenic that follow at this particular field site and around the world.

References

(1) (2001) Arsenic in Drinking Water: 2001 Update. National Research Council.

(2) Cullen W. R.; Reimer K. J. (1989) Arsenic speciation in the environment. *Chem. Rev.* 89, 713-764.

(3) (1977) Arsenic. National Research Council.

(4) Mok W.; Wai C. (1990) Distribution and mobilization of arsenic and antimony species in the Coeur D'Alene River, Idaho. *Environ. Sci. Technol.* 24, 102-108.

(5) Nordstrom D. K.; Alpers C. (1999) Negative pH, efflorescent mineralogy, and consequences for environmental restoration at the Iron Mountain Superfund Site, California. *PNAS* 96, 3455-3462.

(6) Aurilio A.; Durant J. L.; Hemond H. F.; Knox M. L. (1995) Sources and distribution of arsenic in the Aberjona watershed, Eastern Massachusetts. *Water, Air, Soil Poll.* 81, 265-282.

(7) Armstrong W. (1979) Aeration in higher plants. *Adv. Botanical Res.* 7, 226-332.

(8) Doyle M. O.; Otte M. L. (1997) Organism-induced accumulation of iron, zinc, and arsenic in wetland soils. *Environ. Poll.* 96, 1-11.

(9) Otte M. L.; Kearns C. C.; Doyle M. O. (1995) Accumulation of arsenic and zinc in the rhizosphere of wetland plants. *Bull. Environ. Contamin. Toxicol.* 55, 154-161.

Chapter 2

Validation of an Arsenic Sequential Extraction Method For Evaluating Mobility in Sediments

This paper is reproduced with permission from N. E. Keon, C. H. Swartz, D. J. Brabander, C. **Harvey, and** H. F. Hemond (2001) Validation of an arsenic sequential extraction method for **evaluating** mobility in sediments. *Environmental Science and Technology* **35**, p. 2778-2784.

1. Abstract

Arsenic (As) mobility and transport in the environment are strongly influenced by arsenic's associations with solid phases in soil and sediment. We have tested a sequential extraction procedure intended to differentiate the following pools of solid phase arsenic: loosely- and strongly- adsorbed As; As co-precipitated with metal oxides or amorphous monosulfides; As co-precipitated with crystalline iron (oxyhydr)oxides; As oxides; As co-precipitated with pyrite; and As sulfides. Additions of As-bearing phases to wetland and riverbed sediment subsamples were quantitatively recovered by the following extractants of the sequential extraction procedure: As adsorbed on goethite, 1M NaH_2PO_4; arsenic trioxide (As_2O_3), 10M HF; arsenopyrite (FeAsS), 16N HNO_3; amorphous As sulfide, 1N HCl, 50mM Ti-citrate-EDTA and 16N HNO_3; and orpiment (As_2S_3), hot concentrated HNO_3/H_2O_2. Wet sediment subsamples from both highly contaminated wetland peat and less As-rich sandy riverbed sediment were used to test the extraction procedure for intra-method reproducibility. The proportional distribution of As among extractant pools was consistent for subsamples of the wetland and for subsamples of the riverbed sediments. In addition, inter-method variability between the sequential extraction procedure and a single-step hot concentrated HNO_3 / H_2O_2 acid digestion was investigated. The sum of the As recovered in the different extractant pools was not significantly different than results for the acid digestion.

2. Introduction

High concentrations of As in sediments and soils (relative to a crustal average of 1-10 mg As kg^{-1} soil) occur in many areas due to industrial contamination and pesticide or herbicide applications, as well as natural processes (*1*). In order to accurately predict As mobility, it is necessary to both quantify the As bound to sediments and evaluate its dominant associations with the several likely solid phases. Adsorption and mineral precipitation of As depend strongly on oxidation state and, where present as an oxyanion, its aqueous acidity constants. In aqueous solutions of neutral pH, arsenate, As(V), is present predominantly as $H_2AsO_4^-$, while

arsenite, As(III), is uncharged as H_3AsO_3 (*2*). The distribution of As between these species is important due to the higher toxicity and enhanced mobility of As(III) (*3*). In oxic sediments, As(V) forms strong inner-sphere complexes with iron hydroxides (*4*) or may be present in oxide minerals. Iron-reducing conditions often coincide with the reduction of As(V) to As(III) and studies suggest that As(III) can adsorb onto remaining Fe oxides (*5; 6*). In sulfidic environments, As may adsorb onto pyrite, co-precipitate with authigenic pyrite, or form As(III) sulfide minerals (*7-9*). In organic-rich sediments and porewater, humic acid amine groups may also complex As(V) and As(III) (*10*).

The solid phases of As in sediments may be investigated by a range of methods, including x-ray absorption spectroscopy (XAS), x-ray diffraction (XRD), and chemical extractions. XAS can provide detailed information on the speciation and coordination environment of As in the solid phase (*11; 12*), but this technique is not practical in many cases due to limited access to instrumentation and difficulty of data analysis for heterogeneous, natural samples (*13*). XRD analysis enables identification of As-bearing solid phases and is more widely accessible than XAS, but the As minerals must have a high degree of crystallinity and comprise at least a few weight percent of the sediment. Dense minerals (e.g. many minerals associated with As) may be separated from sediment matrices to facilitate XRD analysis, although there are difficulties with density separations in wetland and other organic-rich sediments (*14*).

Sequential chemical extractions have the advantage of sufficient sensitivity to quantify mg kg^{-1} concentrations of As and apportion the As into pools based on chemical properties of the target binding phases. Extractions also require little specialized instrumentation compared to other methods. Weaknesses include their operationally-defined nature, the potential for alteration of the sediment during extraction, and the lack of well-tested extractions for specific elements. Standard-testing of extraction methods can improve upon the interpretation of the sequential extraction results (*15; 16*). Although extraction techniques are widely used to characterize sediments, we found that information on the extraction of known As-bearing phases was insufficient to interpret extraction data from natural samples. Thus, we proposed a sequence of

extraction steps specifically designed to apportion As based on the nature of its associations with solid phase components of sediments and tested the method with known As phases.

The method of Tessier (*17*) provides a foundation for many extraction procedures, including ours. However, it was designed for the extraction of cationic metals, which may be associated with a different suite of solid phases than As. Our method is closely based on procedures developed to extract As, especially that of Huerta-Diaz and Morse (*14*), which splits As into a 1N HCl-extractable fraction (targeting acid volatile sulfides and amorphous metal oxides), a 10M HF-extractable fraction (silicates), and a 14N HNO_3 fraction (pyrite). We have included additional steps to further partition As, with the final extraction protocol as follows: 1M $MgCl_2$ (loosely-adsorbed As), 1M NaH_2PO_4 (strongly-adsorbed As) (*18*), 1N HCl (see above), 0.2M oxalic acid (As incorporated in amorphous iron and aluminum oxides), 0.05M Ti-citrate-EDTA (As incorporated in crystalline iron oxides) (*19-21*), 10M HF (As oxides and As in silicate minerals), 16N HNO_3 (As in pyrite), and hot concentrated HNO_3 & H_2O_2 (crystalline As sulfides).

We standard-tested the sequential extraction method by submitting As-contaminated wetland and riverbed sediments both with and without spikes of well-characterized, common As phases to the extraction procedure. We also investigated the reproducibility of the method for wet As-rich wetland sediments and riverbed sediments containing lesser amounts of As. Our findings suggest that this method will be useful for quantifying As associations with solid phases under different environmental redox conditions and levels of As concentration.

3. Experimental Section

Site Description. The sediments used in the sequential extraction procedure were obtained from Woburn, MA, at the Wells G & H Superfund site. This 16-hectare wetland consists of deposits of peat 2 to 8 meters thick, underlain by 50 meters of sand and gravel glacial deposits in the Aberjona River Valley (*22*). The Wells G & H wetland contains approximately 10 metric tons of arsenic within the top meter of peat. Arsenic contamination of the wetland resulted from riverine transport and deposition of waste As, much evidently originating from pyrite roasting for

sulfuric acid manufacturing (with likely waste products of As_2O_3 or pyrite cinders) and lead arsenate pesticide manufacturing at the upstream IndustriPlex Superfund site in the early 1900s (*23*). Industrial- (including mining) and pesticide- derived As contamination has been observed in wetlands and riverbed sediments around the world (*9; 24-26*), which highlights the need for method development for predicting the stability of As in sediments.

We applied the sequential extraction method to (a) sulfidic riverbed sediments composed of silty-sand and (b) iron-reducing wetland peat. The upper meter of riverbed and wetland sediments are characterized by solid phase As concentrations in the range of 100-10,000 mg kg^{-1}, with porewater concentrations in the range of 5 to 600 $\mu g\ L^{-1}$. Solid-phase iron concentrations range from 1 to 25 % by weight, and dissolved iron (<30 nm filtered) porewater concentrations of 5 to 1500 mg L^{-1} have been measured. Porewater pH ranges from 5.0 to circumneutral in the riverbed sediments and peat.

Sample Collection and Handling. To test our extraction procedure, we retrieved sediment cores in thick-walled (0.25"), 3" ID tubes (Lexan™) using a vacuum-action piston corer (*22; 27*). Sample contact with oxygen was avoided to obtain meaningful extraction results from redox-sensitive solid phases. These sediment cores were immediately placed in N_2-purged field-portable glove bags for transport back to the laboratory. All subsequent sediment preparation and extraction steps in the lab were performed in an acrylic glove box or polyethylene glove bag (Cole-Parmer™) purged with high-purity N_2 gas (from liquid N_2). The core was subsectioned into 5 cm increments using a hacksaw, and sediment that came in contact with the hacksaw was removed with a Teflon spatula and discarded. Each increment was then placed into 250 mL polycarbonate Sep-Cor™ centrifuge bottles, and the porewater was removed by centrifugation at 11,000 × *g* for 25 minutes. Samples for inter- and intra-method reproducibility experiments were frozen until needed, then thawed. These samples came from a wetland core (depth 35-40 cm) and river core (depth 30-35 cm) collected in May 2000. Another wetland core collected

in December 1998 (depth increments 25-30 and 30-35 cm) was used as the matrix to which As-bearing spike phases were added.

Fresh or frozen samples should be subjected to the extraction procedure, as it has been observed that freeze-drying may alter speciation in anoxic sediments (*28*). Ideally, the sediment should be homogenized with mortar and pestle until near uniform consistency, preferably to pass through a <125 μm sieve (*15*). However, we found that the ability to effectively grind and homogenize these samples (which contain significant root mass) when wet was greatly diminished. In spite of insufficient homogenization, we determined that As distribution among the various extracted pools from fresh peat was relatively uniform (see Results).

However, a higher degree of variability was found for total As recovery in wet sediments compared to freeze-dried counterparts. Since a necessary validation step for the extraction procedure was quantifying recovery of As-bearing spikes added to sediment matrices, we chose to use homogenized freeze-dried sediment as the matrix for spike recovery assessment. To minimize potential redox alterations in the freeze-dried sediment, we prepared the sediments in a N_2 atmosphere and loaded the samples into a nitrogen-purged dessicator for freeze-drying (Corning™ dessicator attached to a -50°C cold trap coil and vacuum pump at 0.02 mm Hg pressure). As shown in Results, the freeze-dried matrix sediment used for the standardization did not appear to affect the recovery of spikes, and we were able to quantitatively determine spike recoveries.

Reagents. All extractant solutions were prepared from Milli-Q (18.2 megaohm-cm resistivity) water deoxygenated by sparging with N_2 gas for 2 hours. The deoxygenated water contained less than 0.03 mg O_2 L^{-1} as measured by Vacu-Vials™ (Chemetrics) using the Rhodazine D™ method. Ultra-pure HCl, HF, and HNO_3 acids (Ultrex™) and reagent grade $MgCl_2$, NaH_2PO_4, ammonium oxalate, oxalic acid, $TiCl_3$, citrate, bicarbonate, and tetrasodium EDTA were used to prepare the extractants. Extractant pH was adjusted with HCl or NaOH to the desired value

listed in Table 1. Reagent blanks for all extractants were analyzed in parallel with the samples and found to have negligible levels of As in all cases.

Safety. Special caution must be exercised in the use of concentrated acids, particularly hydrofluoric acid, and titanium (III) chloride. HF attacks bone by complexing calcium, a process that can be fatal if HF is spilled onto one's skin even in small amounts (*29-31*). Preparation of the Ti extractant must be conducted in an inert atmosphere because Ti (III) chloride is spontaneously combustible in contact with air.

Analysis techniques. Aqueous As concentrations were measured using graphite furnace atomic absorption spectroscopy (GFAAS, Perkin Elmer 4100ZL), or hydride generation atomic fluorescence spectroscopy (HG) for more dilute (< 5 $\mu g\ L^{-1}$) or high PO_4 and Mg (>10 mM) samples. Calibration curves were determined using standards prepared in matrices that mirrored extractant solutions, and palladium and magnesium nitrate matrix modifiers were used to help minimize interferences in GFAAS (*32*). High concentrations of phosphate (in the PO_4 extraction step) interfered greatly in the GFAAS analysis (*33*) but did not affect HG-fluorescence analysis. The use of HG also allows speciation of As liberated by the Mg and PO_4 steps.

Sequential extraction procedure. Table 1 summarizes the sequential extraction procedure, the solid phases targeted by each extractant, and references to the application of similar extractants elsewhere. In a glove box, a 0.4 g subsample of sediment was added to a 50 mL polypropylene centrifuge tube (Sep-Cor™) along with a 40 mL volume of the first extractant (1M $MgCl_2$). Reagent concentrations and sediment-to-extractant ratios of 1:100 (0.4 g to 40 mL) for each step were selected to assure that each extractant did not become exhausted (e.g. oxalate fully complexed by iron, leading to iron oxide dissolution being limited by oxalate concentration).

These suspensions were tumble-shaken (outside the glove box) in the sealed Sep-Cor™ tubes for the specified duration, then centrifuged for 25 minutes at 11,000 × *g*. The tubes were

transferred to the glove box, where the supernatant was decanted using a teflon-tip syringe (with care taken not to remove sediment) and filtered through 200 nm polycarbonate filters. The next extractant was added to the remaining residue and the procedure repeated. Decanted extractants were removed from the glove box and acidified to 1% with concentrated HNO_3 for GFAAS analysis or concentrated HCl for HG analysis. The detection limit for extractable As in each of the fractions is less than 1 mg As kg^{-1} sediment, given an analytical detection limit of 5 μg L^{-1} for GFAAS and 0.15 μg L^{-1} for HG, for a sediment-to-extractant ratio of 0.4 g to 40 mL.

In parallel to each multi-step sequential extraction, we carried out a separate acid volatile sulfide (AVS) extraction (which also uses a 1N HCl solution) on wet sediment to obtain a more complete geochemical characterization of the sediments (*34*). A 1 hour 1N HCl extraction will dissolve many amorphous sulfides but does not attack crystalline sulfides such as pyrite (*14; 21; 35-37*). To quantify AVS in our sediments, we preserved a 2.0 g wet sediment sample for AVS extraction by storage at -30°C until ready for extraction. After thawing, 40 mL of 1N HCl was added to the sediment in a 50 mL centrifuge tube tightly capped with a two-holed stopper. The mixture was bubbled with N_2 gas (flow rate approximately 40 mL min^{-1}) for one hour. During bubbling, liberated hydrogen sulfide (H_2S) gas was carried, via rigid PFA Teflon tubing, to the bottom of two serially connected 250 mL bottles containing 0.3M Zn acetate and 0.12M Na acetate. Sulfide was precipitated as ZnS in the solutions as the bubbles traveled up the bottle, and was measured by the methylene blue method to calculate the amount of AVS initially present in the sediment (*38*).

Method verification with spiked minerals. We standardized our extraction procedure by adding known amounts of five common As-bearing minerals and phases (each done in duplicate) separately to subsamples of freeze-dried, homogenized wetland sediment (as noted above). The As phases we tested included: orpiment (As_2S_3), amorphous As sulfide, arsenopyrite (FeAsS), arsenic trioxide (As_2O_3), and adsorbed As (V) on goethite. The additions of As spikes to the unspiked sediment constituted approximately 25-40% of the original unspiked sediment As

load. Sequential extractions were carried out as described in Table 1, and recoveries of the spiked minerals were compared to the As added.

Orpiment and arsenopyrite originating from Niñas de Panasqueira, Peru and Quiruvilco, Portugal, respectively, were purchased from Ward's Scientific. High-purity arsenic trioxide was obtained from Spex Certiprep, Inc. The stoichiometries of the FeAsS and As_2S_3 were verified using wavelength-dispersive electron microprobe analyses (JEOL 733) after mineral grains were mounted in Buehler™ epoxy and polished with diamond paste. The possibility of elemental impurities in the minerals in excess of a few weight percent was ruled out by an initial energy-dispersive spectroscopy scan. The molar percentage composition (average of ten locations on the mineral) was determined to be (mean ± 1 σ): FeAsS (Fe: 33.82 ± 0.13, As: 34.60 ± 0.25, S: 31.58 ± 0.22) and crystalline As_2S_3 (As: 39.27 ± 0.16, S: 60.73 ± 0.16). The mass of As in the mineral spikes was calculated by converting the molar percentages to elemental weight percentages, from which the amount of As was obtained.

Amorphous arsenic sulfide was synthesized according to the experimental procedure detailed by Eary (*39*), with the modification of adding three times as much potassium hydrogen phthalate as recommended to lower the pH to 4. The amorphous As sulfide was aged for 3 days, centrifuged and decanted, rinsed with deoxygenated Milli-Q water three times, and freeze-dried. We used freeze-dried amorphous As sulfide in the spiking experiments because moist amorphous As sulfide appeared to age over the time required to complete the extraction tests, losing a more labile fraction and becoming more recalcitrant compared to the freeze-dried amorphous As sulfide (see Results). This aging prevented the determination of reproducibility for the moist amorphous As sulfide spiking tests, necessitating the use of the more stable freeze-dried amorphous As sulfide. The As content of this freeze-dried amorphous As sulfide was found to be 49 ± 2% (by weight) by hot digestion in aqua regia. X-ray diffraction (Rigaku RU 300) confirmed the amorphous nature of the synthesized As sulfide.

Crystalline goethite was synthesized by the method of Atkinson (*40*). We added 10.1 grams of $Fe(NO_3)_3 \cdot 9H_2O$ to 50 mL Milli-Q water at 45°C, then increased the pH to 9.0 with 2.5N

NaOH. The suspension was heated for 4 days at 62°C, washed with Milli-Q water until the conductivity of the suspension was comparable to that of Milli-Q water, and vacuum-filtered on a Büchner funnel. 98 mL of 1 mM Na_2HASO_4 was added to the goethite, the pH was adjusted to 6.6 to mimic our wetland conditions, and the mixture was shaken for 48 hours. The product was washed three times with Milli-Q water to leave only strongly adsorbed As, and again vacuum-filtered to remove excess water. The As-spiked goethite contained 0.132 ± 0.005 % As by weight, as determined by hot 12N HCl digestion of three subsamples of the goethite.

4. Results & Discussion

Method Reproducibility. We investigated the relative importance of sediment subsample heterogeneity in evaluating inter-method (extraction vs. digestion) reproducibility for quantifying total As. Six wet 0.4 g subsamples of both the high-As wetland and lower-As riverbed samples were sequentially extracted (SE) (Table 2A), and another six 0.4 g subsamples of each were digested by the EPA acid digestion method 3050B (hot HNO_3 and H_2O_2 digestion) (AD) (Table 2B). The wetland sediment was found to contain 1939 ± 175 mg As kg^{-1} by SE and 2161 ± 324 mg As kg^{-1} by AD, where the error is 1σ for n=6. River sediments contained 40 ± 3 mg As kg^{-1} by SE and 36 ± 4 mg As kg^{-1} by AD. Relative standard deviations (RSD) of the SE and AD replicate totals were similar for both wetland (9% SE, 15% AD) and riverbed (7% SE, 11% AD) sediments, suggesting similar extraction precision for these two sample sets despite the factor of fifty difference in concentration. T-testing at 95% confidence intervals showed that the means for AD versus SE (total As extracted) are not significantly different for both the wetland and riverbed sediments. The RSD and t-test findings suggest that, in our sediments, subsample heterogeneity is more responsible for variability in total As recoveries than the method used.

Intra-method reproducibility for the sequential extraction procedure was also found to be good, as the percentage distribution of As (Table 2A, in italics) among the extracted pools was very similar among replicates for both the wetland and riverbed sediments. Most of the extractant pools (except for Ox and hot HNO_3/ H_2O_2) are represented by at least 5% of total

extractable As for either the wetland or riverbed sediments, with approximately 50% of total As extracted by PO_4 (strongly-adsorbed As) in both sediments. Notable differences between the two sediments include a greater percentage of Mg-extractable, HF-extractable As, and HNO_3-extractable As in the riverbed sediments, and a higher percentage of HCl- and Ox- extractable As in the wetland sediment.

Method Standardization. Two general observations can be drawn from the results of the spiked phase tests. First, the recoveries of As from the spiked phases in natural sediment were very good, in the range of 92-127% (Table 3). Second, the added As phases were mainly extracted by the chemical extractants that were intended to target those phases (Figure 1). Arsenic adsorbed on goethite was liberated by competitive desorption with orthophosphate (PO_4). Arsenic trioxide was dissolved predominantly by 10M HF, arsenopyrite was extracted by 16N HNO_3, and orpiment was dissolved by hot concentrated HNO_3 / H_2O_2.

The freeze-dried amorphous As sulfide was extracted in different pools than we initially expected. We hypothesized that amorphous As sulfide would be targeted by either HCl (as an acid volatile sulfide) or HNO_3 (as a more crystalline sulfide). Nine percent of the amorphous As sulfide was extracted in the HCl step, 43% was recovered in the Ti step, and 40% was extracted by HNO_3. The observed apportionment of As from the amorphous As sulfide may be due to the acid dissolution of an AVS component (extracted in HCl), ligand-promoted dissolution by citrate and EDTA (in the Ti reagent), and oxidation of more recalcitrant components (by HNO_3). To examine these hypotheses, we subjected subsamples of the amorphous As sulfide in the absence of the sediment matrix individually to 1N HCl and 50 mM citrate-EDTA extractions. The HCl step was found to extract 7% of the As from As sulfide, and the citrate-EDTA solution extracted 33±3% compared to recovery of 3% of As in Q-water. These results from the individual extractions are similar to the spiked-sediment sequential extraction results. The observed range of extractability in a freshly-precipitated, amorphous sulfide As may be due to a greater recalcitrance of the interior of nucleated particles to extractants.

As noted in the Methods section, moist amorphous As sulfide appeared to age during the course of the extraction experiments. Initially (one day following vacuum-filtration), the moist amorphous As sulfide showed an extractability in 50 mM citrate-EDTA of 53% of the total As extracted in solution (compared to 33% for the freeze-dried sample). No HCl-extractable As was found in the moist amorphous As sulfide, in contrast to the samples immediately freeze-dried. After two weeks, only 25% of the As in the moist As sulfide was extracted by citrate-EDTA (compared to 53% initially), the rest having become more recalcitrant and extractable only by HNO_3.

As our extraction results suggest, the nature of authigenic, amorphous As sulfides in the environmental samples may be variable in extractability. While the presence of As phases containing components that may be progressively leached by several extraction solutions can be problematic in interpreting extraction results for some sediments, the magnitude of the problem depends on the nature of the dominant phases. Arsenic in sediments mainly extracted by PO_4, HF, or HNO_3 may be easier to ascribe to certain As-bearing phases, whereas Ti-extractable As may be either due to reduction of crystalline oxide phases or ligand-promoted dissolution of amorphous As sulfide by citrate-EDTA. By their nature, extraction procedures are operationally-defined and may be incomplete in some cases; however, their utility lies in being able to narrow the list of possible phase associations and hypothesize an element's mobility under different conditions (e.g. redox). Supplementary geochemical data (such as AVS analysis, platinum electrode potential, porewater characterization, and microprobe analyses) are of assistance in the interpretation of extraction data.

Extraction Redistribution of Arsenic. Several researchers (*15; 41; 42*) have suggested that trace elements may readsorb onto surfaces of remaining phases after the targeted phase of a sequential extraction step has been eliminated. For phosphorus extraction from sediments, Ruttenberg (*15*) recommended that a $MgCl_2$ wash be administered between extraction steps to counter this effect. To test the redistribution effects for our sediments, we applied a PO_4 wash

between the extraction steps in one replicate of the wetland sediment sample extraction sequence to remove any readsorbed As. We used PO_4 because our data showed that arsenate strongly adsorbed on goethite was removed by PO_4 but not $MgCl_2$. Our analyses of the PO_4 washes found that less than 5% of the As liberated in the previous step was released by a PO_4 wash following the HCl and Ox extractions, the steps after which iron oxide surfaces may still be present in the sample for adsorption. We thus considered a water wash between each step to be sufficient for all subsequent experiments, thereby minimizing matrix effects in the measurement of washes. We caution that necessity of inter-step washes and the washing agent used should be verified, however, for different types of sediments.

Interpretation of Arsenic Mobility from Extraction Results. The sequential extraction procedure reported in this paper is an improvement over currently used methods because it allows the quantification of easily mobilized, adsorbed As and gives information about As associations with redox-dependent solid phases, including oxides and sulfides, as tested by spiking experiments. We believe that the application of this extraction procedure will yield practical information in assessing the potential mobility of As in sediments.

For example, several different geochemical processes might liberate the differently bound fractions of As in sediments. Ionically-exchangeable As, removed by the $MgCl_2$ extractant, could be mobilized by an increase in the ionic strength of the aqueous phase, such as might occur by road salting or seawater intrusion. Arsenic liberated by the PO_4 extractant is most likely that which is strongly complexed by either iron oxides or humic acids, and might for example be liberated by agricultural drainage (*10*). The introduction of groundwater containing species that can outcompete As(V) and As(III) for such adsorption sites, including $H_2PO_4^-$, might mobilize As by competitive displacement (*43*). Ligand-promoted dissolution (Ox step) of Fe and Al oxides and the reductive dissolution (Ti step) of Fe oxides liberates As co-precipitated with these phases. The Ox and Ti steps, although somewhat overlapping in target phases, provide important distinctions in evaluating the potential for As mobilization by geochemically reducing

conditions, as the more crystalline Fe oxides are generally more recalcitrant to reductive dissolution than amorphous iron oxides. Oxidation of sediments, such as by infiltration of oxygenated water or water containing high levels of nitrate, may also release As from sulfides (which may be quantified by the HCl, Ti, and HNO_3 steps).

Potential Method Modifications. Our sequential extraction procedure can be easily modified to suit the sediment characteristics to which the method is applied. For sediments containing low amounts of As (e.g. 100 mg As kg^{-1} or less), more dilute orthophosphate concentrations (e.g. 0.1M) may be used in the PO_4 step. If measuring As by GFAAS, dilution of the PO_4 extractant may be necessary to reduce matrix effects caused by high orthophosphate concentrations. If As oxides or As incorporated in silicates are not a likely sink (or source) for As in a certain environment, the hazardous HF step could be omitted. The applicability and utility of this method can be augmented by further testing in new environments and with additional As phases.

Acknowledgments. The first two authors equally contributed to the laboratory component of this paper. We gratefully acknowledge the assistance of Rachel Stanley and Yukie Tanino, and the support of the MIT UROP Program. We thank the three anonymous reviewers for their thorough reviews and insightful comments. This study was financially supported by the NIEHS Superfund Basic Research Program Grant #5P42ES04675-06, the EPA NCERQA STAR Fellowship Program, and the MIT/ETH/UT Alliance for Global Sustainability.

5. References

(1) Yan-Chu H. (1994) Arsenic Distribution in Soils. In *Arsenic in the Environment, Part I: Cycling and Characterization*, Vol. 26 (ed. Nriagu, J.), pp. 17-49. John Wiley & Sons, Inc.

(2) Cullen W. R.; Reimer K. J. (1989) Arsenic speciation in the environment. *Chem. Rev.* **89**, 713-764.

(3) Bhumbla D. K.; Keefer R. F. (1994) Arsenic mobilization and bioavailability in soils. In *Arsenic in the Environment. Part I: Cycling and Characterization*, Vol. 26 (ed. Nriagu, J. O.), pp. 51-82. John Wiley & Sons, Inc.

(4) Stumm W.; Morgan J. J. (1996) *Aquatic Chemistry*. John Wiley & Sons, Inc.

(5) Ahmann D.; Krumholz L. R.; Hemond H. F.; Lovley D. R.; Morel F. M. M. (1997) Microbial mobilization of arsenic from sediments of the Aberjona Watershed. *Environ. Sci. Technol.* **31**, 2923-2930.

(6) Pierce M. L.; Moore C. B. (1982) Adsorption of arsenite and arsenate on amorphous iron hydroxide. *Water Res.* **16**, 1247-1253.

(7) Newman D. K.; Beveridge T. J.; Morel F. M. M. (1997) Precipitation of arsenic trisulfide by *Desulfotomaculum auripigmentum*. *Appl. Environ. Microbiol.* **63**, 2022-2028.

(8) Mok W. M.; Wai C. M. (1994) Mobilization of arsenic in contaminated river waters. In *Arsenic in the Environment. Part I: Cycling and Characterization*, Vol. 26 (ed. Nriagu, J. O.), pp. 99-117. John Wiley & Sons, Inc.

(9) Moore J. N.; Ficklin W. H.; Johns C. (1988) Partitioning of arsenic and metals in reducing sulfidic sediments. *Environ. Sci. Technol.* **22**, 432-437.

(10) Thanabalasingam P.; Pickering W. F. (1986) Arsenic sorption by humic acids. *Environ. Poll. (Ser. B)* **12**, 233-246.

(11) Myneni S. C. B.; Traina S. J.; Waychunas G. A.; Logan T. J. (1998) Experimental and theoretical vibrational spectroscopic evaluation of arsenate coordination in aqueous solutions, solids, and at mineral-water interfaces. *Geochim. Cosmochim. Acta* **62**(19/20), 3285-3300.

(12) Waychunas G. A.; Rea B. A.; Fuller C. C.; Davis J. A. (1993) Surface chemistry of ferrihydrite: Part 1. EXAFS studies of the geometry of coprecipitated and adsorbed arsenate. *Geochim. Cosmochim. Acta* **57**, 2251-2269.

(13) Foster A. L.; Brown Jr. G. E.; Parks G. A.; Tingle T. N.; Voigt D. E.; Brantley S. L. (1997) XAFS determination of As(V) associated with Fe(III) oxyhydroxides in weathered mine tailings and contaminated soil from California, U.S.A. *J. Phys. IV France* **7**, C2-815-816.

(14) Huerta-Diaz M. A.; Morse J. W. (1990) A quantitative method for determination of trace metal concentration in sedimentary pyrite. *Mar. Chem.* **29**, 119-144.

(15) Ruttenberg K. C. (1992) Development of a sequential extraction method for different forms of phosphorus in marine sediments. *Limnol. Oceanogr.* **37**(7), 1460-1482.

(16) Nirel P.; Morel F. (1990) Pitfalls of sequential extractions. *Water Res.* **24**(8), 1055-1056.

(17) Tessier A.; Campbell P. G. C.; Bisson M. (1979) Sequential extraction procedure for the speciation of particulate trace metals. *Anal. Chem.* **51**, 844-851.

(18) Welch A. H.; Lico M. S. (1998) Factors controlling As and U in shallow ground water, southern Carson Desert, Nevada. *Appl. Geochem.* **13**(4), 521-539.

(19) Wallmann K.; Hennies K.; Konig I.; Petersen W.; Knauth H.-D. (1993) New procedure for determining reactive Fe(III) and Fe(II) minerals in sediments. *Limnol. Oceanogr.* **38**(8), 1803-1812.

(20) Ryan J. N.; Gschwend P. M. (1991) Extraction of iron oxides from sediments using reductive dissolution by titanium (III). *Clays Clay Miner.* **39**(5), 509-518.

(21) Canfield D. E. (1988) Sulfate reduction and the diagenesis of iron in anoxic marine sediments. Ph.D. Dissertation, Yale University.

(22) Zeeb P. (1996) Piezocone Mapping, Groundwater Monitoring, and Flow Modeling in a Riverine Peatland: Implications for the transport of arsenic. Ph.D. Dissertation, Massachusetts Institute of Technology.

(23) Aurilio A.; Durant J. L.; Hemond H. F.; Knox M. L. (1995) Sources and distribution of arsenic in the Aberjona watershed, Eastern Massachusetts. *Water, Air, Soil Poll.* **81**, 265-282.

(24) La Force M.; Hansel C.; Fendorf S. (2000) Arsenic speciation, seasonal transformations, and co-distribution with iron in a mine waste-influenced palustrine emergent wetland. *Environ. Sci. Technol.* **34**, 3937-3943.

(25) Kalbitz K.; Wennrich R. (1998) Mobilization of heavy metals and arsenic in polluted wetland soils and its dependence on dissolved organic matter. *Sci. Tot. Environ.* **209**, 27-39.

(26) Peryea F. J. (1991) Phosphate-induced release of arsenic from soils contaminated with lead arsenate. *Soil Sci. Soc. Am. J.* **55**, 1301-1306.

(27) Fifield J. (1981) Peat Hydrology in Two New England Salt Marshes. M.S. Thesis, Massachusetts Institute of Technology.

(28) Rapin F.; Tessier A.; Campbell P.; Carignan R. (1986) Potential artifacts in the determination of metal partitioning in sediments by a sequential extraction procedure. *Environ. Sci. Technol.* **20**(8), 836-840.

(29) Peters D.; Miethchen R. (1996) Symptoms and treatment of hydrogen fluoride injuries. *J. Fluor. Chem.* **79**, 161-165.

(30) Matsuno K. (1996) The treatment of hydrofluoric acid burns. *Occup. Med.* **46**, 313-317.

(31) Edinburg M.; Swift R. (1989) Hydrofluoric acid burns of the hands: A case report and suggested management. *Aust. N. Z. J. Surg.* **59**, 88-91.

(32) Schlemmer G.; Welz B. (1986) Palladium and magnesium nitrates, a more universal modifier for graphite furnace atomic absorption spectrometry. *Spectrochim. Acta* **41B**(11), 1157-1165.

(33) Chakraborti D.; Irgolic K. J.; Adams F. (1984) Matrix interferences in arsenic determinations by graphite- furnace atomic-absorption spectrometry - Recommendations for the determination of arsenic in water samples. *Intl. J. Environ. Anal. Chem.* **17**(3-4), 241-256.

(34) Huerta-Diaz M. A.; Morse J. W. (1992) Pyritization of trace metals in anoxic marine sediments. *Geochim. Cosmochim. Acta* **56**, 2681-2702.

(35) Morse J. (1999) Sulfides in sandy sediments: New insights on the reactions responsible for sedimentary pyrite formation. *Aquatic Geochem.* **5**, 75-85.

(36) Cooper D.; Morse J. (1999) Selective extraction chemistry of toxic metal sulfides from sediments. *Aquatic Geochem.* **5**, 87-97.

(37) Cornwell J. C.; Morse J. W. (1987) The characterization of iron sulfide minerals in marine sediments. *Mar. Chem.* **22**, 193-206.

(38) Cline J. D. (1969) Spectrophotometric determination of hydrogen sulfide in natural waters. *Limnol. Oceanogr.* **14**, 454-458.

(39) Eary L. E. (1992) The solubility of amorphous As_2S_3 from 25 to 90 C. *Geochim. Cosmochim. Acta* **56**, 2267-2280.

(40) Atkinson R. J.; Posner A. M.; Quirk J. P. (1968) *J. Inorg. Nucl. Chem.* **30**, 2371-2381.

(41) Ostergren J.; Brown Jr. G.; Parks G.; Tingle T. (1999) Quantitative speciation of lead in selected mine tailings from Leadville, CO. *Environ. Sci. Technol.* **33**, 1627-1636.

(42) Kheboian C.; Bauer C. (1987) Accuracy of selective extraction procedures for metal speciation in model aquatic sediments. *Anal. Chem.* **59**(10), 1417-1423.

(43) Manning B.; Goldberg S. (1996) Modeling competitive adsorption of arsenate with phosphate and molybdate on oxide minerals. *Soil Sci. Soc. Am. J.* **60**, 121-131.

Table 1. Extractants were added to a sediment subsample in sequential order (top to bottom), with removal of the supernatant after each step's time duration. Sediment was extracted with fresh solution for the number of consecutive times listed for each step (e.g. 2 repetitions for Mg). Samples were washed with Milli-Q water between each different extractant for 30 minutes. Each "pool" as designated in the text includes the two or three steps under each extractant heading (e.g. As content in Mg repetition 1, Mg repetition 2, and water wash were summed into one "pool" – loosely adsorbed As). Extractant solutions included in the method were chosen from literature-reported extractions (references in the right column are footnoted, as *p*: pH, *d*: time duration, *t*: temperature, *c*: concentration, to explain the selected conditions).

Sequential extraction procedure for As-bearing solid phases.

Step	Extractant	Target phase	Possible Mechanism	Ref.
Mg	**1M $MgCl_2$**, pH 8, 2hrs, 25°C • 2 repetitions + 1 water wash	Ionically bound As	Anion exchange of Cl for As; possible Mg-As complex formed	(*15pdct, 17c*)
PO_4	**1M NaH_2PO_4**, pH 5, 16 & 24hrs, 25°C • 1 repetition of each time duration + 1 water wash	Strongly adsorbed As	Anion exchange of PO_4 for AsO_4 & AsO_3	(*18*) (modified)
HCl	**1N HCl**, 1hr, 25°C • 1 repetition +1 water wash	As co-precipitated with acid volatile sulfides, carbonates, Mn oxides, and very amorphous Fe oxyhydroxides, amorphous Al hydroxides	Proton dissolution; Fe-Cl complexation	(*34c, 37ct, 19dct, 21dc)*
Ox	**0.2M Oxalate/ Oxalic Acid**, pH 3, 2hrs, 25°C, in dark (Al foil) • 1 repetition + 1 water wash	As co-precipitated with amorphous Fe oxyhydroxides, crystalline Al oxides	Ligand-promoted dissolution	(*47pdct, 45pdct*)
Ti	**0.05M Ti(III)-citrate-EDTA-bicarbonate**, pH 7, 2 hrs, 25°C • 2 repetitions + 1 water wash	As co-precipitated with crystalline Fe oxyhydroxides	Reduction of Fe(III) to Fe(II)	(*44pdc, 46, 20pdct*)
HF	**10M HF**, 1hr & 24 hrs, 25°C • Added 5g boric acid at 16hrs • 1 repetition of each time duration + 1 boiling water wash	Arsenic trioxide & As co-precipitated with silicates	Si-F tetrahedral coordination; dissolution of oxides	(*34dc*)
HNO_3	**16N HNO_3**, 2 hrs, 25°C • 2 repetitions + 1 water wash	As co-precipitated with pyrite & amorphous As_2S_3	Oxidation of crystalline sulfides	(*34dc, 37c*)

Table 2. A. Sequential extraction results for six fresh subsamples of a highly-contaminated wetland peat and a less-contaminated riverbed sediment collected in May 2000. Each extractant pool entry (e.g. 79 ppm for the Mg pool of subsample Wetland #1) gives the As extracted per 0.4 g wet sediment (in mg kg^{-1}). The percentage that each pool contributes to the total As extracted (e.g. 4 % for Mg Wetland #1) is listed to the right of each entry in italics. **B.** Hot concentrated nitric acid and peroxide digestion (acid digestion, AD) results for six additional subsamples of the wetland and riverbed sediments. Concentrations are in mg As kg^{-1} sediment for 0.4 g of sediment.

A. Sequential Extraction Method Reproducibility for Wet Sediment (concentrations in mg As/kg sediment)

Sample & Replicate #	Mg	(%)	PO4	(%)	HCl	(%)	Ox	(%)	Ti	(%)	HF	(%)	HNO_3	(%)	Hot HNO_3	(%)	Totals
Wetland #1	79	*4*	1105	*56*	356	*18*	56	*3*	181	*9*	13	*1*	155	*8*	33	*2*	1978
Wetland #2	79	*4*	1028	*56*	335	*18*	44	*2*	188	*10*	10	*1*	137	*7*	23	*1*	1843
Wetland #3	74	*4*	975	*55*	321	*18*	36	*2*	207	*12*	18	*1*	139	*8*	11	*1*	1781
Wetland #4	83	*4*	1205	*57*	378	*18*	54	*3*	233	*11*	10	*0*	147	*7*	15	*1*	2125
Wetland #5	78	*4*	1249	*58*	375	*17*	57	*3*	253	*12*	14	*1*	110	*5*	19	*1*	2155
Wetland #6	59	*3*	918	*52*	250	*14*	40	*2*	187	*11*	15	*1*	221	*13*	61	*3*	1749
AVERAGE	**75**	*4*	**1080**	*56*	**336**	*17*	**48**	*2*	**208**	*11*	**13**	*1*	**152**	*8*	**27**	*1*	**1939**
STD. DEV.	9	*0*	130	*2*	48	*1*	9	*0*	29	*1*	3	*0*	37	*2*	18	*1*	**175**
																RSD:	9%
River #1	5	*12*	20	*45*	0	*1*	1	*1*	8	*18*	4	*10*	6	*13*	0	*0*	45
River #2	5	*13*	16	*42*	1	*1*	1	*2*	8	*21*	4	*11*	4	*9*	0	*0*	39
River #3	5	*13*	18	*47*	1	*2*	0	*1*	9	*23*	3	*7*	3	*7*	0	*0*	38
River #4	5	*13*	16	*45*	1	*2*	0	*0*	6	*17*	4	*10*	5	*15*	0	*0*	36
River #5	5	*11*	17	*40*	0	*1*	0	*0*	10	*23*	4	*11*	6	*14*	0	*0*	42
River #6	5	*13*	19	*48*	0	*1*	0	*1*	7	*18*	3	*7*	4	*11*	0	*0*	39
AVERAGE	**5**	*13*	**18**	*44*	**0**	*1*	**0**	*1*	**8**	*20*	**4**	**9**	**5**	*12*	**0**	*0*	**40**
STD. DEV.	0	*1*	2	*3*	0	*0*	0	*1*	1	*3*	1	*2*	1	*3*	0	*0*	**3**
																RSD:	7%

B. Total As by Acid Digestion

Sample & Replicate #	Total As	Sample & Replicate #	Total As
Wetland #7	2546	River #7	35
Wetland #8	2282	River #8	35
Wetland #9	2297	River #9	36
Wetland #10	1852	River #10	30
Wetland #11	1684	River #11	37
Wetland #12	2305	River #12	42
AVERAGE	**2161**	**AVERAGE**	**36**
STD. DEV.	324	STD. DEV.	4
RSD	15%	RSD	11%

Table 3. A. Samples from a single wetland core collected in December 1998. Each sample (I, II, or III) was subsampled for replicate sequential extractions, and the average of the replicates was used in Table 3B for spike recovery calculations. **B.** Arsenic-containing phases were added as spikes either to the freeze-dried Unspiked Sediment I, II, or III, as listed in parentheses following the As spike. Bold entries for the spiked sediments denote the chemical pool that extracted the largest fractions of the spike. As spike added ± error (concentrations in mg As kg^{-1} dry sediment) are the mean and standard deviation (1σ) calculated for five mass measurements of each spike. Total minus unspiked is the difference between total As recovered and the average unspiked total As concentration for I, II, or III. The % spike recovered is calculated as total minus unspiked, divided by the As spike added.

A. Sequential extraction data for unspiked wetland sediment (in mg As/kg dry sediment)

	Sequential Extraction Results								
Sample & Replicate #	Mg	PO_4	HCl	Ox	Ti	HF	HNO_3	Hot HNO_3	TOTALS
Unspiked Sediment I-#1	221	3008	2302	1060	244	74	63	0	6972
Unspiked Sediment I-#2	196	4010	1310	786	583	29	0	0	6914
Unspiked Sediment I-#3	234	3757	1453	969	360	26	61	0	6860
Unspiked Sediment I-#4	214	3153	1125	1668	409	30	32	5	6637
Unspiked Sediment I-#5	207	3153	1129	1727	476	37	35	2	6767
Unspiked Sediment I Ave.	**214**	**3416**	**1464**	**1242**	**415**	**40**	**38**	**2**	**6831**
Unspiked Sediment I Std.Dev.	14	440	488	428	127	20	26	2	132
Unspiked Sediment II-#1	55	2369	329	720	282	18	29	0	3802
Unspiked Sediment II-#2	52	2268	270	718	178	15	20	0	3520
Unspiked Sediment II-#3	54	2397	306	692	196	12	17	0	3673
Unspiked Sediment II-#4	58	2379	278	733	310	7	14	0	3778
Unspiked Sediment II-#5	51	2357	273	680	272	6	19	0	3657
Unspiked Sediment II Ave.	**54**	**2368**	**276**	**707**	**291**	**6**	**17**	**0**	**3719**
Unspiked Sediment II Std.Dev.	3	50	25	22	57	5	6	0	112
Unspiked Sediment III-#1	162	3523	1202	607	273	28	62	2	5859
Unspiked Sediment III-#2	138	3734	1357	555	211	28	0	0	6023
Unspiked Sediment III Ave.	**150**	**3629**	**1280**	**581**	**242**	**28**	**31**	**1**	**5941**
Unspiked Sediment III Std.Dev.	17	149	110	37	44	0	44	1	116

B. Sequential extraction data for spiked wetland sediment (in mg As/kg dry sediment)

										Added As Spike & Percent Recovery		
As Spike										As Spike Added ± Error	Total - Unspiked ± Error	% Spike Recovered ± Error
As adsorbed on goethite (II)	73	**3737**	347	840	252	4	12	0	**5264**	1324 ± 46	1546 ± 95	**117** ± 8%
As adsorbed on goethite (II)	73	**3400**	365	698	396	2	12	0	**4944**	1225 ± 47	1225 ± 93	**100** ± 8%
As trioxide (III)	115	3043	2076	331	500	**2803**	314	366	**9547**	3593 ± 75	3448 ± 124	**96** ± 4%
As trioxide (III)	110	3191	2030	445	535	**2630**	233	309	**9483**	3424 ± 88	3384 ± 124	**99** ± 4%
Arsenopyrite (I)	321	3176	1416	1821	176	4	**2231**	17	**9162**	2479 ± 78	2331 ± 126	**94** ± 6%
Arsenopyrite (I)	216	3448	1271	1793	461	39	**2043**	101	**9371**	2444 ± 106	2540 ± 127	**104** ± 7%
Orpiment (I)	228	3115	1179	1764	458	47	249	**2089**	**9129**	2488 ± 134	2298 ± 126	**92** ± 7%
Orpiment (I)	318	3189	1504	1732	226	24	390	**2528**	**9912**	2434 ± 98	3081 ± 129	**127** ± 7%
Amorphous As sulfide (I)	279	3554	2421	560	**1743**	95	**1091**	21	**9764**	3063 ± 400	2933 ± 129	**96** ± 13%
Amorphous As sulfide (I)	193	3529	2315	620	**1518**	86	**1064**	13	**9340**	2581 ± 337	2509 ± 127	**97** ± 14%

Figure 1. Recoveries of As in a given extraction step from As-containing phases added to sediment matrices. The bars in the six panels show the As distribution in unspiked and spiked sediment samples among the following pools: Mg, PO_4, HCl + Ox + Ti, HF, HNO_3, and Hot HNO_3/H_2O_2. The key identifies the patterns representing each spike and the amount of As added to the matrix by the spike addition. The concentration of As present in each of the unspiked sediment matrices is shown in each panel as the solid bars. Dashed lines separate experimental groups that used different sediment matrices for spike additions. Due to the overlap in the phases targeted by the HCl, Ox, and Ti steps for our sediments (noted in Table 1), these steps were summed here. The data for the spiked samples shown represent the first of the two replicates for each spike listed in Table 3. Labeled arrows identify the spiked phase responsible for the increased As concentration (augmenting the unspiked As concentration) in each extractant pool. Percentages shown are the proportion of As recovered for a spiked phase in a particular step. Error bars represent 1σ error for unspiked replicates.

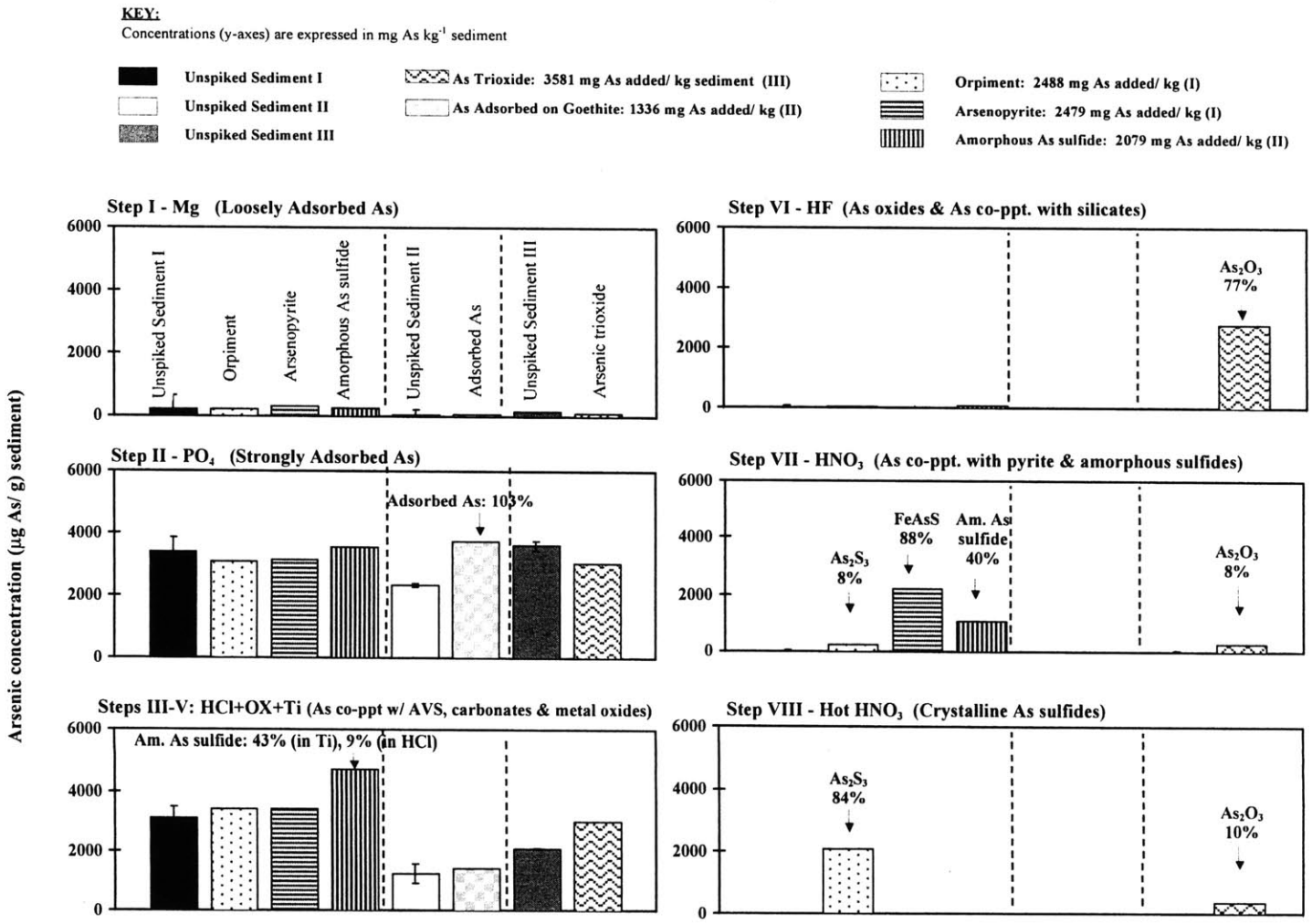

Chapter 3

Geochemical Controls on Arsenic Speciation in Contaminated Wetland Peat and Riverbed Sediments

This chapter is prepared for submission to *Geochimica et Cosmochimica Acta*. Co-authors on the manuscript include: C.H. Swartz, D.J. Brabander, S.C.B. Myneni, and H.F. Hemond.

1. Abstract

Mobility of arsenic (As) in the environment is controlled by binding mechanisms with solid phases and precipitation in minerals and amorphous solids. In this study, we probed the speciation of solid phase As and determined the sediment phases that sequester As in the Wells G & H wetland in Woburn, MA. The uppermost sediments in the wetland contain high concentrations of both dissolved and solid phase As (up to 2,000 μg/L and 15,000 μg/g, respectively) and a consistent depth maximum between 30-40 cm depth. Mechanisms of As retention in the solid phase were investigated using a sequential extraction method standard-tested with As phases, XANES analysis to directly probe solid phase As speciation, and geochemical equilibrium modeling (pH-pe diagrams, constructed using porewater measurements of various species) to predict the expected As solid phase associations.

We found that As in the upper 40 cm of the wetland was predominantly adsorbed onto amorphous Fe (hydr)oxide phases. Riverbed sediments differed from wetland sediments in that a greater proportion of As was associated with more reduced and crystalline phases, and adsorbed As was more likely associated with Al oxide phases. The presence of As sulfides in the riverbed sediments was indicated by extractions and confirmed by XANES. The coexistence of As(III) and As(V) oxidation states was consistently observed in upper depths in the porewater and in all depths of the solid phase, even under sulfidic conditions in which pH-pe modeling predicted the predominance of As(III). The association of As with more oxidized phases in the wetland compared to the riverbed sediments may result from a combination of plant activities, including evapotranspiration-driven water table depression and/or root oxygenation.

2. Introduction

Arsenic (As) contamination of water, soils, and sediments is found throughout the world, due to both natural sources and anthropogenic pollution (*1*). The occurrence of As in drinking water has fostered political debate regarding appropriate limits, given the public health implications of consumption of arsenic-contaminated waters (*2-4*). Underlying this debate is the need for a more thorough understanding of As sources to surface and ground waters, and the factors that affect mobilization of As from contaminated sediments into the aqueous phase.

The oxidation state of dissolved As affects its association with solid phases and therefore its mobility. Inorganic forms of As, including arsenate ($H_2As^{(V)}O_4^-$) and arsenite ($H_3As^{(III)}O_3$), differ in toxicity and are typically more prevalent than organic As species in groundwater systems (*5*). The primary mechanisms of inorganic As immobilization are adsorption onto surfaces and co-precipitation with minerals and amorphous solids. The adsorption binding mechanism affects As retention and mobilization behavior from the solid phase. Arsenate adsorbs by inner sphere surface complexation mechanisms onto both ferric and aluminum hydroxides; arsenite can also adsorb onto ferric hydroxides, both as inner and outer sphere complexes (*6; 7*), and onto aluminum hydroxides as outer sphere complexes (*8*). Arsenic can also be coprecipitated, for example when solids such as ferrihydrite are formed; this process may yield a higher As content compared to adsorbed As phases (*9*). Dissolution of the solid phase is required for coprecipitated As to be mobilized, whereas adsorbed As may be released by competitive adsorption with other anions.

Whether As is predominantly present in the aqueous or solid phase is largely determined by redox conditions. As(III) is thermodynamically stable and may be more mobile than arsenate under Fe-reducing conditions, due to the dissolution of iron oxyhydroxide sorbents and coprecipitates. In organic-rich and low-oxygen sediments, such as those in wetlands, reducing conditions characterized by Fe(II) predominance typically exist below a few centimeters depth (*10*). Following Fe reduction, sulfate reduction may become prominent in S-rich sediments (*11*),

such as at our study site. In reducing, sulfidic environments, As(III) may form aqueous sulfide complexes (*12*), precipitate as As_2S_3 (crystalline orpiment or the amorphous phase), and/or be incorporated in arsenopyrite or arsenian pyrite (*11*). The fate of As in reducing but non-sulfidic environments remains uncertain. It may be more mobile, although As(III) oxides may precipitate or As(III) may be sorbed onto Al oxides or clays (*8; 13*).

The thermodynamic redox sequence predicts that arsenate will be reduced prior to sulfate due to a higher energy yield from the reduction (*14*). Paradoxically, As(III) and As(V) have been shown to coexist under reducing conditions in which only As(III) is expected (*15; 16*). The presence of As(V) in sediments with a low platinum-electrode redox potential has been suggested to be due to slow reduction kinetics (*17*). In a study of As(V) reduction kinetics, Jones et al. (*18*) concluded that the reduction of adsorbed As(V) was highly dependent on the solid phase dissolution rate; aqueous As(V) was reduced more rapidly than solid phase-bound As(V). Similarly, another study found that the longer half life of As(V) in one reducing soil compared to a second was due to a higher sorptive capacity of the first, which limited availability of the As(V) for reduction (*19*). Contrary studies exist, however, which show that As(V) may be microbially reduced without dissolution of the sorbent (*15; 20*).

While studies of As speciation and mobility in lakes and oceans are numerous, few investigations of As cycling in wetland sediments have been reported. Wetlands have high capacities in retaining metals and nutrients, which has fostered interest in the use of natural and constructed wetlands in contaminant attentuation (*21-25*). To our knowledge, one of the only studies of solid phase As speciation in wetland sediments is that of La Force et al. (*26*). Their study explored As sequestration in mine-waste-contaminated wetland sediments and concluded that As solid phase associations in the upper 2 cm of sediment varied seasonally, including between As(III)-sulfides, As(III) and As(V) with Fe (hydr)oxides, carbonates, silicates, and As(III)-sulfides. However, the conclusions drawn by La Force et al. (*26*) were not corroborated with measured redox parameters (e.g. amorphous sulfides) and equilibrium modeling, which

could have better established their conclusions. In our study of contaminated wetland sediments, we adopted a more comprehensive approach, using equilibrium modeling to predict redox conditions and supplementary geochemical analyses to support extraction and x-ray absorption data.

The purpose of our study was to determine solid and aqueous phase As speciation in the sediments of the Wells G & H wetland, in order to predict the conditions that might mobilize solid phase As into the porewater. We expected that As species in the waterlogged, sulfur-rich wetland sediments would be dominated by sulfides if the sediments are at geochemical equilibrium (*11*). We also anticipated the coexistence of different As solid phase associations, which has been consistently observed (*11; 16; 26*). As part of this study, we explored whether a small subset of geochemical measurements could predict the redox-dependent speciation of As, Fe, and S. Finally, we expanded upon our understanding of the impact of wetland conditions (e.g. fluctuating water table, dense plant root zone) on As speciation by comparing the results with As speciation in riverbed sediments (e.g. consistently waterlogged, unvegetated sediments).

3. Site Description

The Wells G & H field site is a 16 hectare wetland located in Woburn, Massachusetts, approximately 15 kilometers north of Boston. The 65 km^2 Aberjona watershed contains two Superfund sites, including the Wells G & H wetland and Industri-Plex, which resulted from significant industrial pollution in the late 1800s and early 1900s (*27-29*) (Fig. 1). The Wells G & H wetland is approximately 2.5 kilometers south of Industri-Plex and 5 km north of the Mystic Lakes, connected by the Aberjona River. The Aberjona River has received waste streams from chemical manufacturers (*27*) and tanneries (*30*), which have contributed to a range of metal and organic contamination throughout the river and its floodplain.

High sediment and aqueous As concentrations at the Industri-Plex site, Wells G & H wetland, Mystic Lakes, and Aberjona River are likely resulting from two main industrial processes at Industri-Plex: sulfuric acid manufacturing involving the roasting of arsenian Iberian pyrite, and the production of lead arsenate pesticides (*27*). Extrapolation of As concentrations from the numerous sediment cores measured in this study to the wetland scale yields an estimate that 10 metric tons of As may be contained in the wetland, largely in the upper 40 cm of peat.

Using pollen profiles and other deposition rate estimation methods, Zeeb (*31*) found that the peak of As concentration at 40 cm depth corresponded to approximately 1890-1920, or the height of the sulfuric acid manufacturing industry at Industri-Plex. Iberian pyrite was imported during this time period and oxidized at high temperatures in lead-lined chambers at the Industri-Plex site to yield sulfuric acid (*27*). The waste products expected from this process include Fe_2O_3 (hematite), As_2O_3, and SO_4.

4. Sample Collection

4.1. Sediment Corer Design

Sediment cores 1 m in length were retrieved from the Wells G & H wetland using a modified piston corer (*32*) (App. A, Fig. II). The corer was designed with the following features: (i) a sharp cutting edge to penetrate through dense root systems, (ii) thick-walled (0.25 inch) Lexan™ to minimize core contact with the atmosphere, and (iii) steel foot pedals for advancing the core to one meter depth without the need for heavy machinery. After retrieval, sediment cores were capped with plastic caps, sealed with parafilm and duct tape, placed into nitrogen-purged glove bags in the field, and transported back to the laboratory. Predrilled holes in the Lexan at 5 cm increments were used as ports for microelectrodes. The sampling ports were sealed during core retrieval, then uncovered either in the field glove bag or in the laboratory glove box. No differences were found between field and laboratory microelectrode

measurements in the initial cores, allowing subsequent cores to be measured in the laboratory, which limited microelectrode destabilization due to temperature fluctuations in the field.

The sediment in the cores was subsampled in 5 cm increments by manually slicing through the Lexan and sediment using a hacksaw in the nitrogen glove box. Sediment that contacted the hacksaw was removed with a Teflon spatula to prevent contamination from the blade. The remaining sediment in each section was spooned into preweighed 250 mL polycarbonate SepCor™ bottles with rubber o-ring seals. The bottles were centrifuged at 11,000 g for 25 minutes and returned to the glove box, where the porewater was decanted by syringe. Sediment was mixed with a Teflon spatula for homogenization, and aliquots for solid phase analyses were removed (see Section 4.2). The remaining sediment in each Sep-Cor bottle was purged with N_2 gas, sealed with parafilm and electrical tape, and stored at -30°C until additional aliquots were needed.

Multiple cores were taken from the Wells G & H wetland to periodically provide fresh sediment for analysis. Six sediment cores were retrieved from a 120 m^2 area of the wetland between Well G, Well H, and the Aberjona river (Appendix A). Three additional cores were removed from the center of the adjacent Aberjona riverbed, which was approximately 3 m wide. Each core was assigned an identification code, by which they are referred throughout the paper.

4.2 Porewater Sampling

Porewater CO_2 was measured in the small amounts of porewater (typically < 2 mL) that could be removed with a Teflon-tipped syringe via the sampling ports. Removal of remaining porewater required centrifugation of the sediment (see Section 3.1). In the glove box, porewater removed from the sediment subsections by centrifugation was filtered through 200 nm and 50 nm acid-cleaned polycarbonate membranes. Approximately 1-2 mL of porewater could be passed through the 50 nm membranes (Nucleopore) in the time span of an hour, necessitating the use of the 50 nm filtrate solely for measurement of dissolved Fe(II) and As. Other

constituents including dissolved sulfide were measured in the 200 nm filtrate. Immediately following filtration, the filtrates were analyzed for Fe(II) and dissolved sulfide. Subsamples of the 50 nm filtrate were frozen in liquid nitrogen until As speciation could be measured (usually within a few weeks) by hydride generation (*33*). Metals (Fe, Al, Mn) and anions (PO_4, SO_4, SiO_4) were measured in 200 nm filtered porewater that had been acidified with 1% HCl and frozen at -30°C until analysis.

5. Analytical Techniques

5.1. Porewater Measurements

Geochemical parameters of pH and oxidation-reduction potential (pe) strongly affect the speciation of many elements (e.g. As, Fe, S). These parameters were used to predict aqueous and solid phases, using platinum electrode potential (PEP) as a measure of pe. Prior to sediment core sectioning, pH and PEP were measured in triplicate for each 5 cm depth increment by inserting microelectrode probes (Microelectrodes, Inc.) into the core through the predrilled holes. The pH microelectrode was an exposed-tip MI-4144 (1.7 mm needle diameter) glass combination probe calibrated with pH buffers before each analysis. PEP was measured with an exposed-tip MI-800 (1.7 mm diameter) Pt/ KCl Ag/AgCl combination microelectrode calibrated with ZoBell's solution before analysis. PEP measurements were converted to the standard hydrogen potential scale by adding +209 mV to the measured value (*34*). PEP measurements are traditionally used as an indicator of oxidizing or reducing conditions (approximate pe, related by the Nerst equation pe = 16.9 Eh, where Eh is in millivolts) (*35*). However, PEP should be considered no more than an analytical tool for predicting redox changes in systems. The limitations of PEP measurements, including the high electroactivity and rapid kinetics of the Fe couple compared to other redox couples, are discussed further by Chapelle et al. (*36*) and Christensen et al. (*37*).

To determine porewater concentrations, metals (total Fe, Al, Mn, Cr) and total As were measured by graphite furnace atomic absorption spectroscopy (Perkin Elmer 4100Z GFAAS). The ferrozine method (*38*) was used to analyze Fe(II) shortly after filtration using a Beckman DU640 spectrophotometer. Sulfide and molybdate-reactive silicate were also determined colorimetrically according to *Standard Methods* (*38*). Phosphate and sulfate were measured by ion chromatography using a Dionex model 16 with an anion self-regenerating suppressor column. Dissolved CO_2 (preserved in airtight syringes stored underwater) was detected by gas chromatography of the nitrogen-purged headspace (Hewlett Packard GC fitted with a CarboSieve column).

Low concentrations of As, below the GFAAS detection limits (< 5 μg/L), were measured by hydride generation atomic fluorescence spectrometry (HGAF, PSA Excalibur), which has a detection limit of 0.1 μg/L. Porewater As from cores was speciated by selectively reducing As species using a modified procedure based on Andreae (*39*) and Aurilio (*40*). Briefly, As(III) was selectively reduced to arsine gas (by maintaining a pH of 8 with Tris buffer) using a 9.6 g/L $NaBH_4$/ 48 mM NaOH reductant, and the arsine was measured by atomic fluorescence. To determine total As in the samples, additional subsamples were pre-reduced for at least 12 hours using 13.9 g KI/L sample and 2.8 g/mL ascorbic acid in 1N HCl, then reduced to arsine with 15 g/L $NaBH_4$ and 100 mM NaOH, immediately before measurement by HGAF. As(V) was then determined by difference and the total compared to GFAAS results.

5.2. Solid Phase Analyses

5.2.1 Acid Volatile Sulfides. To quantify the presence of solid phase amorphous sulfides in the sediments, 2.00 g wet aliquots of sediment were tested for acid volatile sulfides (AVS) as described in Keon et al. (*41*). Briefly, amorphous sulfides liberated by the 1 N HCl extraction were trapped in a 0.2 M zinc acetate/ 0.12 M sodium acetate solution as ZnS.

Trapped sulfide from the AVS extraction was quantified using the methylene blue method (*38*), with a detection limit of 1 μg sulfide/g sediment.

5.2.2 Elemental concentrations. Total solid phase element concentrations of sediment depth increments were determined by x-ray fluorescence. Sediment aliquots (approximately 25 g wet weight) were oven dried at 60°C for several days. 4.00 g of dried sediment was homogenized and ground to a fine powder in a tungsten carbide mixer mill, then pressed into a 32 mm diameter pellet under 20 tons of pressure using a Spectro™ stainless steel die set. The sediment pellets were analyzed using a Spectro Analytical™ energy-dispersive x-ray fluorescence X-Lab 2000 spectrometer (ED-XRF, TurboQuant software) for approximately thirty elemental concentrations. Accuracy and precision of XRF results for this instrument are described in more detail by Rogers et al. (*42*).

5.2.3 As speciation by sequential extraction. A sequential chemical extraction described in detail and tested previously in Keon et al. (*41*) was applied to wet 0.4 g sediment subsamples to determine how As is bound in the sediments. Table 1 provides an overview of the extraction steps and the As-associated phases targeted by each extractant. In addition to those discussed in the published method, we have included additional expected target phases from other literature-based extractions (e.g. Al phases (*35; 43*)). Care was taken to exclude oxygen from each stage of sampling, storage, and extraction. All solutions were deoxygenated to < 0.3 mg/L O_2 and all sediment transfers were conducted in a N_2 glove box. Reproducibility of the extraction method was investigated in Keon et al. (*41*) using 6 aliquots each of Wells G & H wetland and Aberjona river core depths, and the relative standard deviation was found to be less than 9%. Sediment extractants were filtered through 200 nm polycarbonate filters unless otherwise noted, and acidified to 1% HCl unless the medium was already acidic.

For the sequential extractions, fresh wetland sediment was used. We intended to use fresh riverbed core sediment also, but analysis circumstances prevented this. Sediment cores

on which both extraction and x-ray absorption analysis were to be conducted were collected four days prior to scheduled beamtime to provide the freshest samples possible for the XAS analysis. However, As concentrations found in the riverbed core collected on this date were too low to enable XANES analysis. Thus, for the XANES analysis, we had to use riverbed sediment samples collected and archived by freezing at –30°C ten months earlier. The remainder of the core sediment had been freeze-dried for other experiments. The frozen aliquots were not large enough to also complete the extraction analysis, but the freeze-dried subsamples from this core were available and hence used. To most closely match XANES and extraction data, freeze-dried sediment was used for extractions and frozen aliquots of the sediment were used for XANES. Freeze-drying as a method of sediment preservation has alternately been recommended (*44*) and criticized for possibly causing phase changes (i.e. oxidation of sulfides or crystallization of amorphous Fe oxides) (*45; 46*). As discussed in more detail in sections 5.4 and 5.5, our findings of As sulfide phases in freeze dried sediments indicate that the As sulfide phases may not be oxidized by our freeze drying process.

The wetland core analyzed by sequential extractions and XANES (#4W) differs from the core for which porewater measurements were made (#3W). We chose to obtain Core #4W the day before our XANES beamtime to minimize potential alterations in fresh sediment, which did not allow adequate time for microelectrode measurements, porewater separation and filtration. However, we found similar pH, PEP, aqueous As and Fe profiles for several different wetland cores taken at various times during the year (data not shown). Due to low As content in the fresh riverbed sediments (discussed above), the riverbed porewater data corresponds to the same core as the solid phase (#2R).

Extractant solutions were measured for As by GFAAS, except when high concentrations of $MgCl_2$ and NaH_2PO_4 required measurement by hydride generation due to matrix interferences on the GFAAS or when lower detection limits were needed. Iron and aluminum were also measured in the extractants by GFAAS, using matched matrices for standards. To check that

Fe in the Mg and PO_4 pools did not result from colloid mobilization, we filtered the extracts through 30 nm filters in addition to the usual 200 nm filtration. No difference in Fe content was observed between the two filtrates. Since filtration was slow, subsequent samples were filtered through 200 nm filters and acidified to prevent precipitation of solids before analysis.

5.2.4 As speciation by XANES. As stated above, fresh wetland sediment and frozen (10 month) archived riverbed sediment were analyzed at the Stanford Synchrotron Research Laboratory (SSRL) to obtain XANES spectra. Previous studies of As at the SSRL have demonstrated the feasibility of XANES analysis in investigating a range of As concentrations in contaminated sediments (*6; 26; 47; 48*). Sediment was kept anoxic from the time of collection until analysis at SSRL. In a N_2-purged glove bag, wet sediment was thinly smeared between a folded piece of Kapton polymide film attached to a slide holder. The sample holder was then transferred to a N_2-purged sample chamber placed between the ionizing chambers (which were flushed with air). SSRL was operated at 3 GeV, with beam current varying between 100 and 50 mA. Wiggler beamline 4-1 was run under dedicated conditions, using Si (2,2,0) monochromator crystals. The beamline was detuned by 50% at the end of the scan. Slits of 1 mm height by 18 mm width were used for maximum peak resolution. An argon-purged Lytle detector was used to collect fluorescence data. Each XANES spectrum was calibrated using an As reference foil (edge position of 11,867 eV) or As(V) in solution (11,873.2 eV), then the scans were averaged. Using the computer code WinXAS 2.1 (*49*), the average XANES spectra were background corrected, normalized above the edge, and fit with a linear combination of standard As phase spectra collected under the same experimental conditions.

5.2.5 Mineralogy. In order to characterize mineral assemblages in the wetland sediment, we performed density separations on wet sediment subsamples. However, the high organic content caused excessive floating of the wet sediment, prohibiting effective density separations. Huerta-Diaz (*50*) also noted that density separations in sediments with high

organic content are likely to be ineffective due to the association of heavy minerals with lower density organic matter. To circumvent this problem, we performed density separations on freeze-dried sediment that was thoroughly crushed with a Teflon spatula. A 10 g homogenized sample, obtained by combining 5 g samples from each of the 30-35 cm and 35-40 cm depths that had passed through a 250 μm sieve, was separated gravimetrically using acetylene tetrabromide (TBE, Geoliquids Inc., IL, density of 2.96 g cm^3). The separation yielded 0.1% by mass of the sediment used. Despite the low percent mass recovered, the identity of the minerals was investigated by splitting the sample and probing half of the minerals with XRD and half with electron microprobe.

X-ray diffraction (XRD) was applied to half of the dense minerals from the separated sample to determine whether a dominant crystalline phase could be identified. A Rigaku 300 diffractometer with a rotating copper anode was used, with the analysis software Jade™. Minerals were sprinkled onto a no-background silica wafer with collodium, dried for 5 minutes, and mounted on an Al holder well with a ball of clay to hold the silica wafer flush with the Al holder window.

6. RESULTS

6.1 Aqueous constituents & redox components

6.1.1 Comparison of solid phase and porewater As. Several sediment cores were obtained from the wetland to determine the depth-dependent distribution of As and to provide fresh material for various analyses of the solid phases. All of the wetland cores collected, ranging in distance between 1 m and 11 m from the river, show a relatively similar solid phase As profile (Fig. 2A). The peak in As concentration for all cores appeared between 20 and 40 cm, usually centered at 35 cm. Concentration maxima range from 5,000 μg/g for the core 11 m from the riverbed to 16,000 μg/g for the core closest to the riverbed.

Porewater As in wetland core #3W ranged from 55 μg/L near the surface to 1,800 μg/L at the peak (30 cm), decreasing to less than 50 μg/L at 100 cm depth (Fig. 2A). Oxidation state of As in the porewater was highly variable, with evidence of As(V) and As(III) to 40 cm depth. Note that the total solid phase As profile for this core corresponds well to the aqueous profile. The maximum arsenic concentration of 1.2% by weight (12,000 μg/g) was identified between 30-35 cm depth.

The riverbed cores (Fig. 2B) show more variability in solid phase As profiles, with concentration maxima differing by an order-of-magnitude within a stretch of 6 m in the river. In general, As concentrations in the riverbed are lower than in the wetland. Solid phase As in the core showed a distinct concentration peak between 15 and 20 cm. A smaller solid phase As peak is apparent below the sandy layer, and the depth corresponds to the highest As porewater concentrations of the meter-long riverbed core. Riverbed sediments from core #2R contained porewater As concentrations up to 750 μg/L, with mostly As(III). No porewater was recovered from the sandy, highly porous depths of 45-85 cm, due to losses during core retrieval. In general, solid and aqueous phase As in the riverbed core #2R show similar distribution patterns.

6.1.2 pH and platinum electrode potential. Depth profiles of microelectrode measurements of pH and PEP are shown in Fig. 3. In the wetland core (Fig. 3A), pH ranges from 5.5 to 6.5, with the highest variability in the upper 20 cm. The PEP profile shows that the wetland sediments transition from oxic to reducing throughout the contaminant horizon.

The riverbed core (Fig. 3B) has a slightly higher pH range of 6.4 to 7.0. PEP was lower in the upper sediments compared to the wetland core surface sediments, with reducing conditions reached by a depth of 10 cm.

6.1.3 Fe(II) and sulfide. Ferrous iron concentrations in wetland porewater ranged from 5 to 520 μM, with a depth profile maximum similar to the solid phase Fe profile (Fig. 3A). Fe-reducing conditions were observed at the depth of maximum aqueous As (35-40 cm). For most

depths, Fe(II) and total Fe were indistinguishable, as expected given the low solubility of Fe(III) solid phases. In the riverbed sediments, porewater Fe(II) ranged between 50 uM to 180 uM (Fig. 3B).

Although low solubility of amorphous sulfide phases in the presence of excess metal cations leads to non-detect levels of aqueous sulfide, measurement of AVS allowed us to quantify amorphous sulfidic phases in the sediments. In wetland sediments, amorphous sulfides were observed between 60-100 cm (Fig. 3A). Riverbed sediments, in contrast, exhibit amorphous sulfides from 0-40 cm, with little present at depth likely due to diagenesis of amorphous sulfides into crystalline sulfides (Fig. 3B). The occurrence of AVS reflects redox conditions rather than the distribution of total sulfur in the sediments, as the S profile is fairly constant with depth (Fig. 5).

6.1.4 Other porewater anions: PO_4, SiO_4, SO_4, and Cl. The extent of As adsorption to Fe phases is affected by the presence of other anions in the porewater, including $H_2PO_4^-$ & HPO_4^{2-}, H_4SiO_4 which compete strongly with As, and less competitive anions SO_4^{2-} and Cl^-. In the wetland porewater, inorganic PO_4 was below the ion chromatograph detection limit of 10 μM. Molybdate-reactive silicic acid (H_4SiO_4) ranged from 14 to 400 μM in the porewater, with the peak between 55-60 cm. Sulfate concentrations in surface sediment porewater (0-10 cm) were 200-600 μM, with the concentration decreasing to 20 μM at the peak depth of 30-40 cm. Chloride concentrations were constant at approximately 3 mM as a function of depth.

The concentrations of competitive anions in the riverbed were similar to those in the wetland. Phosphate was below the detection limit. H_4SiO_4 concentrations ranged from 40 to 450 μM. Sulfate measurements were between 90 and 150 μM, with river water concentrations of 270 μM. The concentration of Cl^- was 3 to 7 mM in the porewater and 2 mM in the river water. Taken collectively, this data suggests that competitive anion aqueous chemistry is not

playing a dominant role in controlling the partitioning of As between the solid and aqueous phases in the contaminated wetland and riverbed sediments.

6.2 Chemical equilibrium modeling from porewater measurements

6.2.1. Wetland modeling. A pH-pe diagram was prepared using oxidation-reduction and acid-base equations, together with average porewater values of pCO_2 (0.001 atm) and Fe(II) (200 μM) (*35; 51; 52*) (App. B). To calculate pe-dependent lines, species were set equal; vertical pH lines are pKa values. In the wetland core, pH-pe equilibrium modeling of the upper 100 cm of the wetland predicts that As(III) is stable only in the upper 10 cm (Fig. 4A). Fe oxyhydroxides are predicted in the upper 10 cm, with an Fe-reducing zone between 15-70 cm, below which sulfate reduction is expected.

6.2.2. Riverbed modeling. pH-pe equilibrium modeling of the riverbed core predicts that As(III) is stable throughout the profile, in contrast to the porewater mixed oxidation state observed in Fig. 2. Fe oxyhydroxides may only be stable in the uppermost 3 cm, with the sediments become sulfate-reducing rapidly, by 13 cm depth. Predictions of Fe-reducing versus sulfate-reducing conditions were compared with actual observations of porewater Fe(II) and solid phase AVS (see Discussion).

6.3 Solid phase elemental profiles

Total solid phase concentrations for a range of elements were determined by XRF, including elements that are possible sorbents or co-precipitated elements with As in various phases. Fe concentrations exceed those of Al in the upper sediment of both cores, but Al becomes more dominant in the lower depths. In the lower Fe-reducing depths, Al or aluminosilicate phases (note Si increases with depth and comprises a significant fraction of the solid phase) may provide sorbent sites for As (see Discussion). Sulfur concentrations are relatively high in the wetland core (ranging between 0.4 and 1.5%) and the riverbed core (>1%

except in the sandy layer between 45-80 cm). Manganese, which as MnO_2 can strongly bind and oxidize As(III), exhibits low concentrations below the uppermost sediment presumably due to reductive dissolution, indicating that Mn cannot account for the binding of As in the solid phase.

6.4. Solid phase As associations: sequential extractions

6.4.1. Depth-dependent As distribution.

6.4.1.1. Wetland. Solid phase As speciation was determined from extractions of wetland core #4W, for which XANES analysis was also done. Figure 6 shows that As at all depths is predominantly PO_4-extractable (strongly adsorbed). For the depths in which As concentrations are greatest (15-20 and 30-35 cm), approximately 20% of the As is co-precipitated with amorphous phases (HCl- and Ox-extractable). Little As (<3%) in these depths is co-precipitated in crystalline Fe phases (Ti-extractable). Up to 18% of the As at the peak is HNO_3 and hot HNO_3/H_2O_2-extractable, which suggests that a crystalline As sulfide component may be present. Lower depths (65-70 and 90-95 cm) contain As concentrations only a few times higher than background levels. Sediments at 65-70 cm depth showed a similar As distribution as the 30-35 cm depth, with the exceptions of less HCl-extractable As and more Ti- and HF-extractable As. At 90-95 cm depth, the HCl-extractable As was also low and 15% of As was likely associated with crystalline sulfidic phases (HNO_3-extractable).

6.4.1.2. Riverbed. In riverbed sediments from core #2R, between 7-21% of the As was loosely adsorbed (Mg-extractable), and 18-56% strongly adsorbed (PO_4-extractable) (Fig. 6). Riverbed sediments exhibit several differences in As distribution as a function of depth. The upper sediment (20-25 and 30-35 cm) contained approximately 20% Ti-extractable As, along with 8-18% HNO_3-extractable As. In contrast, 5% and 17% of the As in the lower two depths (40-45 and 95-100 cm, respectively) was HNO_3-extractable, but less than 1% was extracted by Ti. Only the 20-25 and 95-100 cm depths contained HCl-extractable As. Riverbed sediments

contained between 14-23% HF-extractable As, which is likely co-precipitated with silicates or As trioxide.

6.4.2. Fe distribution in extractants.

6.4.2.1. Wetland. Iron in the wetland As contaminant horizon (< 40 cm depth) was mainly HCl- and Ox-extractable (Fig. 8). The deeper two core depths (65-70 and 90-95 cm) contained much less HCl- and Ox-extractable Fe, with up to half extracted in HF (silicates) and HNO_3 (crystalline sulfidic phases) extractants. More Fe that can be desorbed is also evidenced in the deeper depths from the higher percentage of PO_4-extractable Fe.

6.4.2.2. Riverbed. The extractants from four riverbed core depths were similarly analyzed for Fe (Fig. 9). Fe in the As-rich sediments (< 40 cm depth) was mainly HCl-extractable (amorphous Fe phases). Exchangeable Fe was detected in all depths, with more than a third of the Fe as Mg-extractable in the lower depths. Like the deeper wetland sediments, riverbed sediments contained a greater fraction (up to 40%) of HF-extractable (silicates) and HNO_3-extractable (crystalline sulfidic) Fe in the lower sediments.

6.4.3. Al distribution in extractants.

6.4.3.1. Wetland. Figure 10A displays the Al concentrations in the sequential extraction steps for wetland depth 35-40 cm, which was measured for Al distribution to examine whether Al phases might be a main sorbent for As. Aluminum in the wetland core depth was mainly HCl-extractable (likely amorphous Al oxides, released by proton-dissolution (*35*)), followed by Ti-extractable (crystalline Al phases) and HF-extractable Al (aluminosilicates).

6.4.3.2. Riverbed. The riverbed sediment depth of 40-45 cm contains Al that is mostly Ox-extractable (Fig. 10B), which more likely includes crystalline Al oxides like gibbsite rather than amorphous phases dissolvable by HCl (*35; 43*). Other main extractants of Al in the riverbed include HCl (amorphous Al hydroxides), HF (aluminosilicates), and PO_4 (sorbed Al).

6.4.4. Mineralogy. Wetland sediment at the depth of maximum As concentration (30-40 cm) contained a vast range of minerals. Most of the minerals reported here were identified optically following density separation. Orange and red Fe (hydr)oxides phases were dominant, reflecting the high Fe content but perhaps resulting from exposure of the freeze-dried sediment to air during the density separation (App. C, Fig. 1). Orange-red Fe-filled plant cells were also observed. Some crystalline phases identified by optical microscopy, such as magnetite, are almost surely present in the undisturbed core, being unlikely to be formed after the sediment was separated from porewater (App. C, Fig. 2). Goethite was present in sufficient quantity in bulk sediment for detection by XRD (i.e. a few weight percent; App. C, Fig. 3A). In the dense mineral fraction, hematite was identified by XRD along with Zn or Fe sulfides (App. C, Fig. 3B). Optical microscopy revealed that, at the 30-40 cm depth in the wetland, amorphous ferric hydroxides, crystalline Fe oxides, and crystalline mixed valence Fe oxide phases may all be present in the wetland sediments.

6.4.5. XANES analysis.

6.4.5.1. Wetland sediment. Fresh aliquots of wetland core #4R, for which extractions were performed (Fig. 6), were also analyzed using XANES. The oxidation states of As for each depth were determined, along with the nearest neighbor atom if a discernable energy shift existed between different types of atoms (e.g S, O). Figure 11 shows the results of XANES analyses of sediment subsamples. Between 50-72% of the As was present as As(III) (bound to oxygen or sulfide). However, even the sediment that contained As sulfides had at least 28% As(V). The depth at which the maximum As occurs (30-35 cm) was characterized by 28% As(V), whereas the 65-70 and 90-95 cm depths contained 40-50% As(V). Seventeen percent of As was associated with sulfide at 30-35 and 65-70 cm depths, with 10% at 90-95 cm depth.

6.4.5.2. Riverbed sediment. Frozen aliquots of the riverbed core, for which extractions were performed and reported in Fig. 7 were analyzed using XANES (Fig. 11). As(III) comprised 78-85% of the total As. The riverbed core had between 15-22% As(V) in the three tested depths. The As-sulfide percentage increases as a function of depth, from 8% at 20-25 cm to 38% at 95-100 cm.

7. DISCUSSION

7.1 Deposition of As contamination in the wetland

Solid phase As profiles determined for numerous cores support the hypothesis that transport of As from the Aberjona River into the wetland is the source of As to the upper wetland sediments. The As maxima positions shown in Fig. 2 are similar and confined to the upper 50 cm for six wetland cores. Arsenic concentrations decrease with increasing distance from the river, which also suggests that the As came from the river.

Total concentrations and variability of As in the wetland and riverbed most likely differ due to variable physical deposition and resuspension of sediment. Wetland sediment accumulates during overbank flow, which is comprised of suspended particles likely with a high As content. The riverbed sediment experiences periodic resuspension and possibly scouring, notably during flood conditions.

7.2. Modeling predictions & measurements of redox conditions

Wetland sediment pH-pe equilibrium modeling suggested that depths between 20-70 cm are Fe-reducing (Fig. 4A). Measured porewater profiles of Fe(II) (Fig. 3) supported this prediction. Below 70 cm depth, sulfate reducing conditions were predicted by the pH-pe diagram. In agreement, AVS (Fig. 3) was detected below 60 cm. Assuming that FeS is present as AVS, we calculated that the aqueous sulfide concentration in equilibrium with the FeS would range from 0.03-0.3 nM for the 5.5-6.0 pH range corresponding to the 60-100 cm depths. Using

this aqueous sulfide concentration and aqueous As concentrations, we determined that amorphous As_2S_3 is undersaturated in the wetland sediments and crystalline As_2S_3 is only oversaturated between 90-100 cm depth (refer to Appendix B for solubility product and ion activity product calculations).

For the riverbed core, pH-pe modeling suggested that the riverbed sediments were Fe-reducing below 8 cm depth, and sulfate-reducing below 43 cm. Fe(II) was measured at all depths in the core, in agreement with predicted Fe-reducing conditions. In contrast to the modeling predictions of sulfate-reduction, AVS was detected even in the uppermost 5 cm increment. The lack of AVS at reducing at lower depths in the riverbed, despite high relative concentrations of total S (Fig. 5), may indicate the presence of crystalline sulfidic phases. However, riverbed sediments, due to their higher pH, are undersaturated with respect to both amorphous and crystalline As_2S_3 (App. B).

Contrary to the pH-pe modeling predictions of As(III) stability below 5 cm depth in both environments, measured As porewater speciation includes a mixture of As(III) and As(V) in the uppermost 50 cm of both cores (Fig. 2B). Similarly, a co-occurrence of these two oxidation states was found for sediments at all depths by XANES analysis (Fig. 11). The presence of As(V) in the solid phase at lower, sulfidic riverbed sediment depths may reflect the incorporation or adsorption of As in phases resistant to reduction, such as silicates. Consistent with this possibility, riverbed sediment contain between 10-20% HF-extractable As (Fig. 7), compared to XANES data which reports approximately 20% As(V)-O associations (Fig. 11).

In the wetland sediments, nearly half of the As at maximum depth is As(V) (Fig. 11); however, less than a few percent is HF-extractable (Fig. 6). Instead, most of the As in the wetland was either adsorbed or incorporated in sulfidic phases, the latter of which would not include As(V). Therefore, the As(V) in the wetland might be adsorbed and resistant to reduction. In fact, recent studies have shown that As(V) reduction kinetics may be restrained by sorption processes, essentially preventing As(V) reduction until the dissolution of the sorbent

(*18; 19*). This may explain how adsorbed As(V), when bound to non-redox-active Al oxides or silicates, can persist in sulfidic sediments.

7.3. Wetland sediment As speciation

7.3.1 Potential sorbents of As. Most solid phase As in the Wells G & H wetland sediment is adsorbed onto amorphous Fe. Extraction with $H_2PO_4^-$ removed 47-63% of As in the wetland core (Fig. 6), confirming that most As is strongly sorbed. By considering potential sorbents of As (discussed in the following paragraphs), we determined that amorphous Fe hydroxides appear to be the substrate adsorbing most of the As rather than crystalline Fe, other metal oxide phases, or sulfides.

First, we evaluated whether Fe hydroxides might be expected in the upper 40 cm of sediment, where As concentrations are greatest. Measurements of pH and PEP (Fig. 4A) suggest that Fe hydroxide phases may be present in the upper 25 cm but some Fe reduction is predicted. At the 30-35 cm depth of maximum As concentration where Fe reduction is expected, Fe is mostly HCl-extractable (Fig. 8), which includes FeS, amorphous Fe oxyhydroxides, and $FeCO_3$. AVS measurements (Fig. 3) showed no measurable amorphous Fe sulfides at this depth. pH-pe modeling (Fig. 4A) indicated that the pH was likely too low for $FeCO_3$ stability. Consequently, the most likely HCl-extractable Fe phase is amorphous Fe oxyhydroxides.

Next, we confirmed that the capacity of solid phase amorphous Fe oxyhydroxides to adsorb the observed As. At the 30-35 cm depth, the concentration of adsorbed As was 1,700 μg/g (Fig. 6). Assuming that the HCl- and Ox-extractable Fe is amorphous Fe hydroxides, the concentration of Fe available for sorption was 30,000 μg/g. If the Fe is hydrous ferric oxide (HFO), reported values of sorption site densities for HFO (200 mmoles/mole Fe) ((*53*) could account for five times the extracted adsorbed As.

We considered other potential sorbents of As to determine if they could be ruled out, supporting the conclusion that amorphous Fe oxyhydroxides are the most likely sorbent. First, we considered crystalline Fe oxide phases. Sorption site density generally varies by degree of crystallinity for different Fe phases, decreasing with increasing crystallinity. Sequential extractions of Fe phases in the upper 40 cm showed that 10% of the Fe was Ti-extractable (e.g. crystalline phases, including goethite). XRD confirmed the presence of goethite at the As peak depth (App. C). Using the average site density of goethite, reported as 16 mmoles/mole Fe (*9; 54; 55*), if we assumed that all of the Ti-extractable Fe is goethite (maximum concentration is 0.11 mmoles Fe/g sediment, or 5,900 μg/g), then a maximum of 13 μg As/g sediment (< 1%) could be sorbed to goethite in the sediments. Goethite therefore does not control As retention at the depth of maximum As content.

The role of mixed valence Fe phases, such as green rust ($Fe_4^{(II)}Fe_2^{(III)}(OH)_{12}SO_4 \cdot 3H_2O$) and magnetite ($Fe^{(III)}{}_2Fe^{(II)}O_4$), might be important in sediments that experience redox fluctuations, such as wetlands. Green rust is a potential reduction product of hydrous ferric oxides, which can be oxidized to either magnetite or lepidocrocite (γ-FeOOH). Recent research by Randall et al. (*56*) has demonstrated that As(V) can sorb onto green rust. The presence of magnetite in the wetland sediments was suggested by magnetic separation of dense minerals, although the concentration was not high enough to appear in XRD analysis (App. C). Despite indications that mixed valence Fe oxides may affect As mobility in sediments, the importance and stability of As sorption on these phases in nature are unclear due to a lack of studies.

The other potentially significant sorbent besides Fe in the wetland, in concentration and affinity for As, is Al oxide. About half of the Al in the 30-35 cm depth was HCl-extractable, likely amorphous $Al(OH)_3$. The concentration of this Al in the sediment was 5,000 μg/g, which is only 1/6 of the amorphous Fe hydroxide concentration. In addition, the sorption site density of $Al(OH)_3$ for As is less than that of ferrihydrite, reportedly around 2 mmoles/ mole Al ((*53*), which

would at a maximum provide sites to adsorb 28 μg As/g sediment (less than 2% of the measured adsorbed As). We conclude that, for the upper 40 cm of contaminated wetland sediments, hydrous Fe oxides are a more important sorbent for As than amorphous Al hydroxides.

Due to their prevalence in natural sediments, phyllosilicate clay minerals may also provide an important sorbent for As(V) (via $AlOH_2^+$ functional groups). Manning and Goldberg (*57*) reported surface site densities between 0.11 and 0.21 mmoles As(V)/kg for clays including kaolinite, montmorillonite, and illite. The Wells G & H Wetland lies in a valley formed by glacial geology, contributing potassium feldspar and other granitic erosional materials to the wetland (*58*), most likely including phyllosilicate clays. From sequential extractions, we determined that 20% of the Al was HF-extractable (i.e. likely clays). Since we observed similar total molar proportions of Al and Si phases, despite about only 20% of the Al associated with silicates, the remaining 80% of the Si must be present in a low-Al phase such as SiO_2. Of the 20% of Al that may be in clays, the sorption site density of 0.04 mmoles As/mole kaolinite (for example) would yield a maximum of 60 μg/g of adsorbed As, or less than 3%. Arsenic coprecipitated with silicates (HF-extractable, <1%) was also not a major phase, suggesting that silicates do not control As speciation in the contaminant zone.

7.3.2 Occurrence of As sulfides. Arsenic sulfide associations were found in all samples by XANES analyses, which is supported by extraction findings. Approximately 17% of the As at the 30-35 cm depth was As(III)-sulfide. Similarly, about 18% of the As in the extractions was found to be HNO_3- or hot HNO_3/ H_2O_2-extractable, the step intended to target As-sulfides. In the 30-35 cm depth increment, amorphous sulfides (as AVS) were not detected. The combination of XANES (Fig. 11), AVS extraction data (Fig. 3), and calculations of As_2S_3 undersaturation (App. B.2) suggests that As present in the sediments at 30-35 cm is associated with crystalline sulfides that might be detrital. Another possibility is that As might be precipitated

in reducing, acidic microzones or under periodic reducing conditions, which could allow the formation of As_2S_3 in sediments that appear to hinder precipitation.

7.3.3 Oxidation state of solid phase As. Throughout the wetland core, XANES analyses on sediment subsamples indicated that As in all depths was a mixture of oxidation states. Arsenate was more prevalent at depths below the depth of maximum As concentration. Efforts were made to minimize oxidation during sample collection, transport, and analysis; further, energy scans as a function of time do not show evidence of oxidation in the beam. A possible explanation of higher concentrations of As(V) at depth (nearly 50%, Fig. 11) may be that half of the As mobilized downward by well pumping or recharge is kinetically resistant to reduction. The 95-100 cm depth corresponds to approximately 2,000 years ago (from ^{14}C age dating in a nearby sediment core by Zeeb (*31*)), and the background concentrations are lower, which argues that the As was transported to this depth. Further, Wells G and H bordering the wetland were used as a municipal water source, pulling water in the wetland and riverbed downward through the sediment (*59*).

7.4 Speciation of As in the riverbed

7.4.1 Coprecipitation with more reducing and crystalline phases. Compared to the wetland, the riverbed sediments contained a larger proportion of As that was incorporated in crystalline phases such as HF-extractable phases and sulfides (Fig. 7). HF-extractable As may result from the dissolution of (i) As coprecipitated in Al- and/or Fe-containing silicates or (ii) As_2O_3, a waste product of lead chamber sulfuric acid manufacturing (*60*).

Arsenic sulfide phases in the riverbed sediments were confirmed by various methods. Arsenic coprecipitated in sulfidic phases (HNO_3-extractable) comprised between 5-18% of the total As. Consistently, the riverbed exhibited sulfate-reducing conditions with the precipitation of amorphous sulfides in the upper sediments (Fig. 3B). XANES spectra revealed that between 8-39% of the As was As(III)-sulfide (Fig. 11). No As incorporated in FeAsS was detected (the

slightly lower As oxidation state in FeAsS compared to As(III)-S is clearly distinguishable). Thus, HNO_3-extractable As is most likely crystalline As sulfides rather than As incorporated in pyrite.

The presence of As sulfide species in other steps of the sequential extraction (i.e. HCl and Ti steps, in addition to the HNO_3 step) was supported by the comparison of XANES with extraction data. For example, the presence of Ti-extractable As in sediments with significant quantities of HNO_3-extractable As, measurable AVS, and little Ti-extractable Fe suggest that Ti-extractable As may be co-precipitated in amorphous sulfides. In tests of the extraction method (*41*), dissolution of amorphous As sulfides was found to occur partially in several steps, with 9% in the HCl step (acid dissolution), 43% in the Ti step (complexation by citrate and EDTA), and 40% extracted in the HNO_3 step (oxidation).

To investigate whether HCl- and Ti-extractable (in addition to HNO_3-extractable) As was coprecipitated with sulfides, we compared the proportion of As-S determined by XANES with the As distribution determined by extractions. For example, in the 20-25 cm riverbed depth XANES analysis showed that 8% of As was associated with sulfides (Fig. 11), in agreement with 8% As extracted by HNO_3. However, 21% of the As was extracted by Ti, which in sulfidic sediments implies that the As is coprecipitated with sulfides. The precipitation of HCl-extracted As and later extraction in the Ti extractant step as an As sulfide might explain the discrepancy between extraction and XANES results.

The dissolution of HCl-extractable As concurrently with AVS phases in sulfidic sediments might lead to extraction-induced precipitation of As_2S_3 if concentrations of As and sulfide in the acidic solution are sufficiently high (*52*). In the multi-step sequential extraction procedure we used, adsorbed As is removed by the Mg and PO_4 extractants, thus leaving only coprecipitated As as HCl-extractable and minimizing any As sulfide precipitation that may occur during extraction. To calculate whether As_2S_3 precipitation might occur in the HCl step, we assumed that the Ti-extractable As (i.e. the portion of As-S not accounted for by XANES) is due to As_2S_3 precipitation from the HCl extraction. We determined that, for the 20-25 cm depth, Ti-

extractable As and HCl-extractable amorphous sulfide yields an oversaturated ion activity product (IAP) for amorphous As_2S_3 (log IAP of -20.8 compared to the log K for As_2S_3 of -23.8). The artifact of amorphous As_2S_3 precipitation in AVS- and As-rich sediments may therefore explain the additional As sulfides observed by extractions compared to XANES, which emphasizes the need for complementary methods in determining As speciation in sediments.

Where there was no AVS, such as in the lower 95-100 cm riverbed sediments, As sulfide precipitation in the HCl step would not occur and the XANES As-S associations should agree with extractions. XANES analysis showed 38% As(III)-S (Fig. 11), which is similar to the As coprecipitated in the sum of the HCl, Ti, HNO_3, and Hot HNO_3 phases (45%). Interestingly, the 95-100 cm depth contained 25% HCl-extractable As. While previous extraction method testing found that synthetic amorphous As_2S_3 could be only partially dissolved by the 1N HCl extraction (*41*), authigenic As_2S_3 may be extracted in different proportions than the synthetic phase (e.g., due to degree of order and particle size).

7.4.2 Adsorbed As. Despite the greater abundance of As in crystalline silicate and sulfide species in the riverbed compared to the wetland, nearly 40% of the solid phase As at 20-25 cm was adsorbed. As in the wetland sediments, we considered the possible adsorptive phases that might control adsorbed As in the riverbed. In the 20-25 cm depth, the presence of amorphous Fe sulfides was indicated by AVS analysis, which makes the presence of hydrous ferric oxides unlikely. To obtain an estimate of the As to Fe ratio in the riverbed sediments, we calculated the ratio of adsorbed As to Fe in the HCl, Ox, and Ti steps (which would include FeS, $FeCO_3$, and Fe(II) oxides) to be 9 mmoles As/ mole Fe. The sorption capacities of FeS and other reduced Fe oxide species for As are not well-known, although this should be somewhat lower than around the estimate for goethite of 16 mmoles As/mole Fe.

To evaluate other potential sorbents, we determined the distribution of Al in one riverbed sediment depth was most likely crystalline Al oxide (Fig. 10B). Higher Al concentrations in the riverbed, compared to Fe, increase the potential relative importance of Al surfaces in

immobilizing As. Riverbed sediments contained between 2-8 times higher Al concentrations than the wetland. If we assumed that the Ox-extractable Al phase provides the sorption sites for adsorbed As in this depth, we found a ratio of 0.5 mmoles As/ mole Al. This ratio is within the reported values for Al oxides to support measured values of adsorbed As onto gibbsite ((*53*), which suggests that crystalline Al oxides could adequately sorb the As in the riverbed depth. Further, the non-redox-active chemical nature of Al oxides could provide As sorption sites under reducing conditions.

7.4.3 Oxidation state of solid phase As. Like in the wetland sediments, XANES analysis showed that most of the As in riverbed sediments was As(III), with a persistent As(V) component. As(V) ranged between 15-22% with depth (Fig. 11), despite sulfidic conditions and predominantly aqueous As(III) at depth. The solid phase associations of the As(V) phase in the riverbed must be either adsorbed or incorporated in silicates (that is, as long as the HF-extractable As is not As_2O_3, which would mean that all of the As(V) was adsorbed).

7.5. Potential causes of wetland and riverbed differences in As distribution

The main differences between As associations in wetland and riverbed sediments are due to differences in redox conditions. The upper 40 cm of wetland sediments is predominantly Fe-reducing, with evidence of amorphous Fe oxyhydroxide phases onto which most of the As is adsorbed. In contrast, the upper 40 cm of riverbed sediments is more reducing, characterized by sulfidic conditions. The lack of Fe oxyhydroxide sorbent for As in the riverbed sediments is countered by the greater concentration of Al oxide surfaces, which can provide the required sorption sites for the lower concentrations of As.

Redox conditions likely vary between the wetland sediments and the riverbed due to hydrologic conditions. Water content of the two sediments is different, as the riverbed is constantly flooded and the upper wetland sediment experiences periods of desaturation. Hydrologic modeling of the wetland and riverbed conducted by Zeeb (*31*) predicted that two flow

regimes occur (upward flow through the peat from the upland, or downward flow during flooding). During periods of little precipitation and maximum plant evapotranspiration (ET), the riverbed was modeled as a losing stream, with upward flow through the peat. ET of water in the wetland was estimated to average 6 mm/day for cattails during the summer and 1-3 mm/day in the winter based on literature-reported values of New England wetlands (*31*). We found that the combination of low rainfall in the summer and high rates of ET lead to a depression in the water table of as much as 27 cm below the surface. The presence of O_2 in the unsaturated sediment can precipitate hydrous ferric oxide phases, which strongly adsorb As. During periods of lower ET (winter to spring) and flooded conditions (typical in spring), dissolution of these (hydr)oxide phases would be expected to release As. The persistence of Fe (hydr)oxides in the wetland would depend on factors affecting microbial reduction rates, including degree of crystallinity (more amorphous is generally more labile), surface area, and the availability of an organic carbon source. Although we did not optimize our experiments to test the persistence of Fe hydroxides, we did not observe variations in As solid phase speciation or porewater Fe for cores obtained during different seasons.

In addition to influencing water table fluctuations, wetland plant roots may contribute to the creation of oxidized microzones in the upper wetland sediment. Cattails (*Typha latifolia*), the dominant species in the area of the wetland investigated, contain a dense root network in the upper 40 cm of sediment. To survive in waterlogged soils, cattails pump oxygen to their roots (*61*). An Fe-rich plaque, reported to be oxidized iron, precipitates on the roots (*62; 63*). Researchers (*64-66*) have suggested that the oxidized iron plaque can be an effective substrate onto which As can adsorb, yielding high concentrations of contaminants in the near-root (rhizosphere) soil. Elevated As concentrations in the rhizosphere may arise from a high flux of As-containing porewater to the roots for ET, enhanced by a preferential precipitation on a high-affinity Fe (hydr)oxide substrate. In the long term, the periods of oxidation by both water table fluctuations and rhizosphere oxidation might be additive and result in the steady state

persistence of more oxidized phases in the wetland compared to the riverbed. The contribution of plants to As immobilization requires further study.

8. CONCLUSIONS

In Wells G & H wetland sediments, most solid phase As was adsorbed onto hydrous ferric oxides or mixed valence Fe phases. Higher concentrations and sorption site densities of hydrous ferric oxide phases, in addition to the strong affinity of As for Fe, support the conclusion that As is controlled by amorphous Fe hydroxides in the wetland rather than other sorbents like goethite, Al oxides, or phyllosilicates. A small fraction of the As in the 30-35 cm maximum contaminant horizon was bound to sulfides, as determined by both extractions and XANES analysis. Since no amorphous sulfide was detected at this depth, the presence of As(III)-S is possibly due to recalcitrant detrital phases or due to microredox zones within the sediments.

The speciation of As in the nearby riverbed sediments includes a large adsorbed component, but also incorporation in more crystalline phases, including sulfides and either As_2O_3 or silicates. In contrast to the Fe-reducing upper 40 cm of the wetland, the riverbed sediments are more reducing. Riverbed sediments are sulfidic throughout and a significant portion of As was coprecipitated in crystalline phases. Unlike in the wetland, adsorbed As in the riverbed may be predominantly adsorbed onto Al oxides, as Al concentrations were ample to provide enough sorption sites for the As concentrations.

While pH-pe diagrams and in-situ measurements were reasonably good at predicting oxic, Fe-reducing, or sulfate-reducing conditions, the modeling exercise did not accurately predict As speciation. Throughout both wetland and riverbed cores, we determined that As(III) and As(V) coexist in the sediments, including both As(V)-O and As(III)-S species. The presence of As(V) in the solid phase at depth was in contrast to geochemical pH-pe equilibrium modeling, particularly under sulfidic conditions. The reason for the recalcitrance of the As(V) solid phase species is not known. More study is required to determine the kinetic and other yet unidentified

limitations on the As(V) reduction in reducing sediments. At this particular wetland site, the possibility of periodic infiltration of oxidizing water, perhaps due to reversals in flow regimes, might maintain the As(V) component, and cannot be ruled out without further study.

In conclusion, the mobility of As currently retained in the wetland is controlled by several factors. The adsorbed As associated with amorphous Fe hydroxides in the wetland is susceptible to release during reduction of the sorbent or competitive desorption by phosphate. In contrast to the riverbed, the relatively more oxidizing conditions of the upper 40 cm in the wetland effectively immobilize the large reservoir of As under the current conditions.

9. REFERENCES

(1) Cullen W. R.; Reimer K. J. (1989) Arsenic speciation in the environment. *Chem. Rev.* **89**, 713-764.

(2) (2001) Arsenic in Drinking Water: 2001 Update. National Research Council.

(3) Kaiser J. (2001) Second look at arsenic finds higher risk. *Science* **293**, 2189.

(4) Lok C. (2001) Plans to reduce acceptable arsenic limit put on hold. *Nature* **410**, 503.

(5) Bhumbla D. K.; Keefer R. F. (1994) Arsenic mobilization and bioavailability in soils. In *Arsenic in the Environment. Part I: Cycling and Characterization*, Vol. 26 (ed. Nriagu, J. O.), pp. 51-82. John Wiley & Sons, Inc.

(6) Sun X.; Doner H. E. (1998) Adsorption and oxidation of arsenite on goethite. *Soil Sci.* **163**(4), 278-287.

(7) Manning B. A.; Fendorf S. E.; Goldberg S. (1998) Surface structures and stability of arsenic(III) on goethite: Spectroscopic evidence for inner-sphere complexes. *Environ. Sci. Technol.* **32**(16), 2383-2388.

(8) Goldberg S.; Johnston C. T. (2001) Mechanisms of arsenic adsorption on amorphous oxides evaluated using macroscopic measurements, vibrational spectroscopy, and surface complexation modeling. *J. Colloid Interf. Sci.* **234**(1), 204-216.

(9) Waychunas G. A.; Rea B. A.; Fuller C. C.; Davis J. A. (1993) Surface chemistry of ferrihydrite: Part 1. EXAFS studies of the geometry of coprecipitated and adsorbed arsenate. *Geochim. Cosmochim. Acta* **57**, 2251-2269.

(10) Mitsch W. J.; Gosselink J. G. (1993) *Wetlands*. Van Nostrand Reinhold.

(11) Moore J. N.; Ficklin W. H.; Johns C. (1988) Partitioning of arsenic and metals in reducing sulfidic sediments. *Environ. Sci. Technol.* **22**, 432-437.

(12) Rochette E. A.; Bostick B. C.; Li G. C.; Fendorf S. (2000) Kinetics of arsenate reduction by dissolved sulfide. *Environ. Sci. Technol.* **34**(22), 4714-4720.

(13) Manning B. A.; Goldberg S. (1997) Adsorption and stability of arsenic(III) at the clay mineral-water interface. *Environ. Sci. Technol.* **31**(7), 2005-2011.

(14) Sadiq M. (1990) Arsenic chemistry in marine environments: a comparision between theoretical and field observations. *Mar. Chem.* **31**, 285-297.

(15) Masscheleyn P. H.; Delaune R. D.; Jr. W. H. P. (1991) Effect of redox potential and pH on arsenic speciation and solubility in a contaminated soil. *Environ. Sci. Technol.* **25**(8), 1414-1419.

(16) Davis A.; De Curnou P.; Eary L. (1997) Discriminating between sources of arsenic in the sediments of a tidal waterway, Tacoma, Washington. *Environ. Sci. Technol.* **31**, 1985-1991.

(17) Seyler P.; Martin J.-M. (1989) Biogeochemical processes affecting arsenic species distribution in a permanently stratified lake. *Environ. Sci. Technol.* **23**, 1258-1263.

(18) Jones C. A.; Langner H. W.; Anderson K.; McDermott T. R.; Inskeep W. P. (2000) Rates of microbially mediated arsenate reduction and solubilization. *Soil Sci. Soc. Am. J.* **64**(2), 600-608.

(19) McGeehan S. L.; Naylor D. V. (1994) Sorption and redox transformation of arsenite and arsenate in two flooded soils. *Soil Sci. Soc. Am. J.* **58**, 337-342.

(20) Zobrist J.; Dowdle P. R.; Davis J.; Oremland R. S. (2000) Mobilization of arsenite by dissimilatory reduction of adsorbed arsenate. *Environ. Sci. Technol.* **34**, 4747-4753.

(21) Munger A. S.; Shutes R. B. E.; Revitt D. M.; House M. A. (1997) An assessment of metal removal by a laboratory scale wetland. *Water Sci. Technol.* **35**(5), 125-133.

(22) Flanagan N. E.; Mitsch W. J.; Beach K. (1994) Predicting metal retention in a constructed mine drainage wetland. *Ecol. Eng.* **3**, 135-159.

(23) Dunbabin J. S.; Bowmer K. H. (1992) Potential use of constructed wetlands for treatment of industrial wastewaters containing metals. *Sci. Tot. Environ.* **111**, 151-168.

(24) Zhang T.; Ellis J. B.; Revitt D. M.; Shutes R. B. E. (1990) Metal uptake and associated pollution control by *Typha latifolia* in urban wetlands. In *Constructed Wetlands for Water Pollution Control*. Pergamon Press.

(25) Brix H.; Schierup H. H. (1989) The use of aquatic macrophytes in water-pollution control. *Ambio* **18**, 100-107.

(26) La Force M.; Hansel C.; Fendorf S. (2000) Arsenic speciation, seasonal transformations, and co-distribution with iron in a mine waste-influenced palustrine emergent wetland. *Environ. Sci. Technol.* **34**, 3937-3943.

(27) Aurilio A.; Durant J. L.; Hemond H. F.; Knox M. L. (1995) Sources and distribution of arsenic in the Aberjona watershed, Eastern Massachusetts. *Water, Air, Soil Poll.* **81**, 265-282.

(28) Spliethoff H. M.; Hemond H. F. (1996) History of toxic metal discharge to surface waters of the Abjerona Watershed. *Environ. Sci. Technol.* **30**(1), 121-128.

(29) Brabander D.; Keon N.; Stanley R.; Hemond H. (1999) Intra-ring variability of Cr, As, Cd, and Pb in red oak revealed by secondary ion mass spectrometry: Implications for environmental biomonitoring. *PNAS* **96**(25), 14635-14640.

(30) Durant J. L.; Zemach J. J.; Hemond H. F. (1990) The history of leather industry waste contamination in the Aberjona Watershed: a mass balance approach. *Civil Eng. Pract.*, 41-65.

(31) Zeeb P. (1996) Piezocone Mapping, Groundwater Monitoring, and Flow Modeling in a Riverine Peatland: Implications for the transport of arsenic. Ph.D. Dissertation, Massachusetts Institute of Technology.

(32) Fifield J. (1981) Peat Hydrology in Two New England Salt Marshes. M.S. Thesis, Massachusetts Institute of Technology.

(33) Andreae M. (1999) Determination of Trace Elements. In *Methods of Seawater Analysis* (ed. Grasshoff, K.;Kremling, K.;Ehrhardt, M.). Wiley-VCH.

(34) Nordstrom D. K.; Wilde F. D. (1998) National field manual for the collection of water-quality data: Reduction-oxidation potential (electrode method). In *U.S. Geological Survey Techniques of Water-Resources Investigations*, Vol. 9, pp. section 6.5.2.

(35) Stumm W.; Morgan J. J. (1996) *Aquatic Chemistry*. John Wiley & Sons, Inc.

(36) Chapelle F. H.; Haack S. K.; Adriaens P.; Henry M. A.; Bradley P. M. (1996) Comparison of Eh and H_2 measurements for delineating redox processes in a contaminated aquifer. *Environ. Sci. Technol.* **30**, 3565-3569.

(37) Christensen T.; Bjerg P.; Banwart S.; Jakobsen R.; Heron G.; Albrechtsen H.-J. (2000) Characterization of redox conditions in groundwater contaminant plumes. *J. Contam. Hydrol.* **45**, 165-241.

(38) Greenberg A. E.; Trussell R. R.; Clesceri L. S. (1985) Standard Methods for the Examination of Water and Wastewater. American Public Health Association, American Water Works Association, Water Pollution Control Federation.

(39) Andreae M. (1977) Determination of arsenic species in natural waters. *Anal. Chem.* **49**(6), 820-821.

(40) Aurilio A. C.; Mason R. P.; Hemond H. F. (1994) Speciation and fate of arsenic in three lakes of the Aberjona Watershed. *Environ. Sci. Technol.* **28**(4), 577-585.

(41) Keon N. E.; Swartz C. H.; Brabander D. J.; Harvey C.; Hemond H. F. (2001) Validation of an arsenic sequential extraction method for evaluating mobility in sediments. *Environ. Sci. Technol.* **35**, 2778-2784.

(42) Rogers C.; Brabander D.; Barbour M.; Hemond H. (2002) Use of physical, chemical, and biological indices to assess impacts of contaminants and physical habitat alteration in urban streams. *Environ. Toxicol. Chem.* **21**(6), 1156-1167.

(43) Jackson M. L.; Lim C. H.; Zelazny L. W. (1986) Oxides, hydroxides, and aluminosilicates. In *Methods in Soil Analysis. Part I- Physical and Mineralogical Methods* (ed. Klute, A.), pp. 101-150. Amer. Soc. Agron. Inc.

(44) Murdoch A.; Azcue J. M. (1995) *Manual of Aquatic Sediment Sampling*. Lewis Publishers.

(45) Bauer C.; Kheboian C. (1988) Response to Comments. *Anal. Chem.* **60**(14), 1477.

(46) Rapin F.; Tessier A.; Campbell P.; Carignan R. (1986) Potential artifacts in the determination of metal partitioning in sediments by a sequential extraction procedure. *Environ. Sci. Technol.* **20**(8), 836-840.

(47) Foster A.; Brown Jr. G.; Tingle T.; Parks G. (1998) Quantitative arsenic speciation in mine tailings using x-ray absorption spectroscopy. *Am. Mineral.* **83**, 553-568.

(48) Foster A.; Brown Jr. G. E.; Parks G. (1998) X-ray absorption fine-structure spectroscopy study of photocatalyzed, heterogeneous As(III) oxidation on kaolin and anatase. *Environ. Sci. Technol.* **32**, 1444-1452.

(49) Ressler T. (2001) WinXAS. http://www.winxas.de/

(50) Huerta-Diaz M. A.; Morse J. W. (1990) A quantitative method for determination of trace metal concentration in sedimentary pyrite. *Mar. Chem.* **29**, 119-144.

(51) Schecher W. D.; McAvoy D. C. (1998) MINEQL+: A Chemical Equilibrium Modeling System. Environmental Research Software.

(52) Eary L. E. (1992) The solubility of amorphous As_2S_3 from 25 to 90°C. *Geochim. Cosmochim. Acta* **56**, 2267-2280.

(53) Smedley P.; Kinniburgh D. (2002) A review of the source, behaviour, and distribution of arsenic in natural waters. *Appl. Geochem.* **17**, 517-568.

(54) Dzombak D. A.; Morel F. M. M. (1990) *Surface Complexation Modeling: Hydrous Ferric Oxide*. John Wiley & Sons, Inc.

(55) Ali M.; Dzombak D. (1996) Competitive sorption of simple organic acids and sulfate on goethite. *Environ. Sci. Technol.* **30**(4), 1061-1071.

(56) Randall S.; Sherman D.; Ragnarsdottir K. (2001) Sorption of As(V) on green rust (Fe4(II)Fe2(III)(OH)12SO4 3H2O) and lepidocrocite (g-FeOOH): Surface complexes from EXAFS spectroscopy. *Geochim. Cosmochim. Acta* **65**(7), 1015-1023.

(57) Manning B.; Goldberg S. (1996) Modeling competitive adsorption of arsenate with phosphate and molybdate on oxide minerals. *Soil Sci. Soc. Am. J.* **60**, 121-131.

(58) Chute N. (1959) Glacial geology of the Mystic Lakes-Fresh Pond area, Massachusetts: Geological Survey Bulletin 1061-F, pp. 187-216. U.S. Government Printing Office.

(59) Myette C.; Olimpio J.; Johnson D. (1987) Area of influence and zone of contribution to Superfund Site Wells G & H, Woburn, Massachusetts. *Water Resources Investigation Report 87-4100*.

(60) (1977) Arsenic. National Research Council.

(61) Armstrong W. (1979) Aeration in higher plants. *Adv. Bot. Res.* **7**, 226-332.

(62) Mendelssohn I.; Kleiss B.; Wakeley J. (1995) Factors controlling the formation of oxidized root channels: a review. *Wetlands* **15**(1), 37-46.

(63) Taylor G. J.; Crowder A. A. (1984) Formation and morphology of an iron plaque on the roots of *Typha latifolia* L. grown in solution culture. *Am. J. Bot.* **71**, 666-675.

(64) Doyle M. O.; Otte M. L. (1997) Organism-induced accumulation of iron, zinc, and arsenic in wetland soils. *Environ. Poll.* **96**, 1-11.

(65) Wang T.; Peverly J. H. (1996) Oxidation states and fractionation of plaque iron on roots of common reeds. *Soil Sci. Am. J.* **60**, 323-329.

(66) Chen C. C.; Dixon J. B.; Turner F. T. (1980) Iron coatings on rice roots: Morphology and models of development. *Soil Sci. Soc. Am. J.* **44**, 1113-1119.

Table 1. Sequential extraction procedure (see Keon et al., 2001 for details).

Step	Extractant	Target phase
Mg	1 M $MgCl_2$, pH 8, 2 h	ionically bound As
PO_4	1 M NaH_2PO_4, pH 5, 16 & 24 h	strongly adsorbed As
HCl	1N HCl, 1 h, 25°C	As coprecipitated with AVS, carbonates, Mn oxides, very amorphous Fe oxyhydroxides & amorphous Al oxides
Ox	0.2 M ammonium oxalate/ oxalic acid, pH 3, 2 h, in dark	As coprecipitated with amorphous Fe oxyhydroxides or crystalline Al oxides
Ti	0.05 M Ti(III)-citrate-EDTA-$NaHCO_3$, pH 7, 2 h	As coprecipitated with crystalline Fe oxyhydroxides; portion of amorphous As_2S_3
HF	10M HF, 1 & 24 h	As_2O_3 & As coprecipitated with silicates
HNO_3	16N HNO_3, 2 h	As coprecipitated with pyrite and amorphous As_2S_3
Hot HNO_3	16N HNO_3 + 30% H_2O_2, EPA method 3050B	orpiment & remaining recalcitrant As minerals

Figure 1. Map of the Aberjona Watershed, including the locations of the two Superfund Sites (Wells G & H wetland and Industri-Plex). In the Wells G & H Superfund Site, we obtained sediment cores from the wetland in a 120 m^2 area shown as the dot in the inset map.

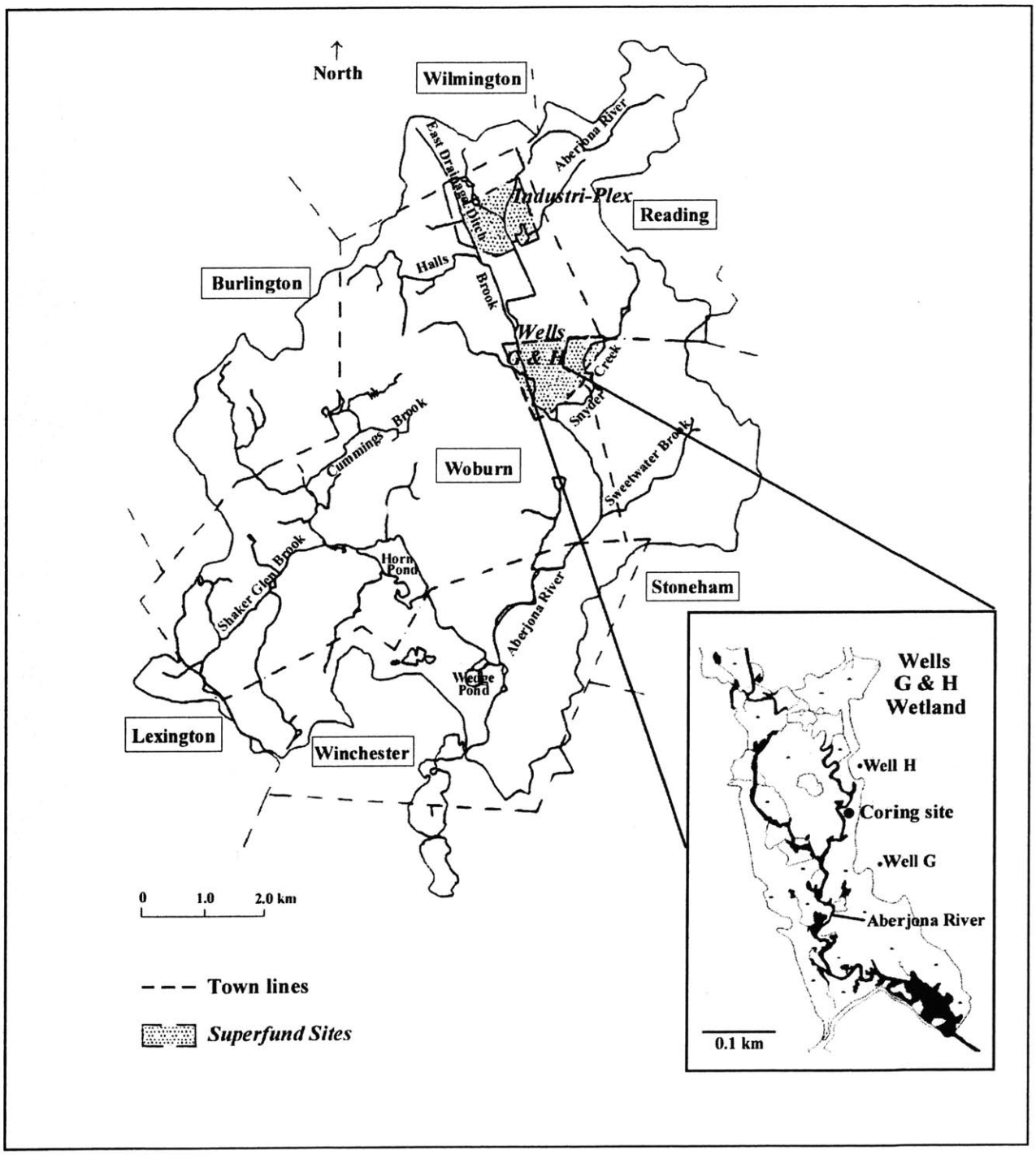

Large map adapted from: Spliethoff & Hemond (1996). Inset map adapted from the EPA website (1998).

Figure 2. Solid phase elemental As concentrations for replicate cores in the wetland (A-*i*) and riverbed (B-*i*). Labels for wetland cores include the distance between the core location and the riverbank. Riverbed cores were obtained from the center of the 3-4 m wide river, within a 6 m stretch of the river. Porewater As concentrations for one wetland core (A-*ii*) and one riverbed core (B-*ii*) are shown. Error bars are 1σ for two subsamples at each porewater depth.

A. Wetland

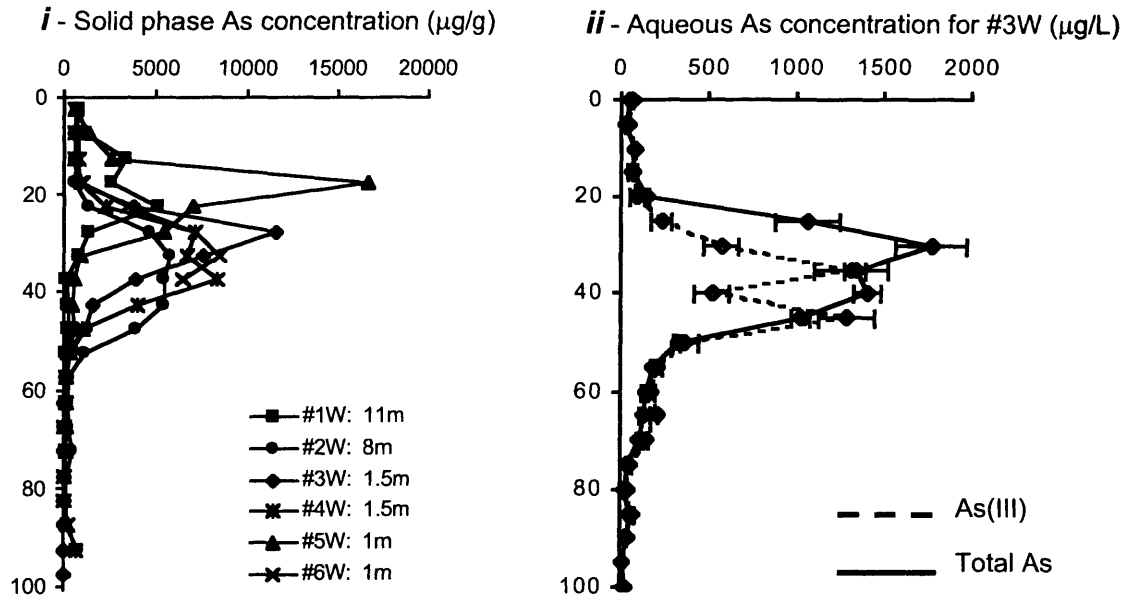

B. Riverbed

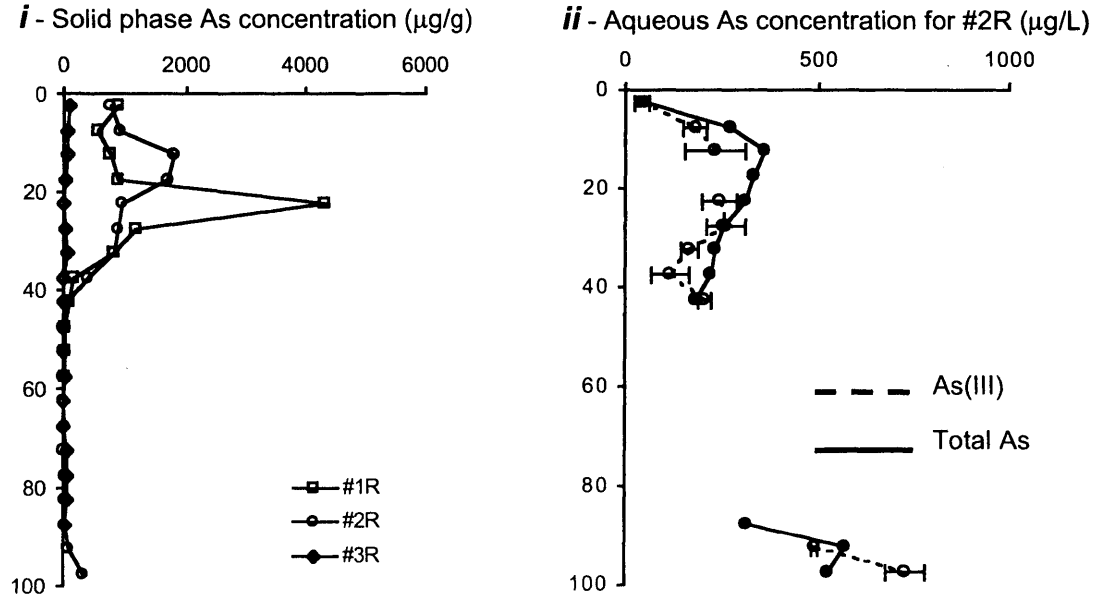

Figure 3. Depth profiles of measured pH (*i*), platinum electrode potential (PEP, *ii*), porewater Fe(II) and solid phase Fe (asterisk symbols) (*iii*), and acid volatile sulfides (AVS; *iv*) for wetland core #3W (A) and riverbed core #2R (B). The pH and PEP data were used in equilibrium modeling (Fig. 4), and the average aqueous Fe concentration was used to construct the pH-pe diagrams.

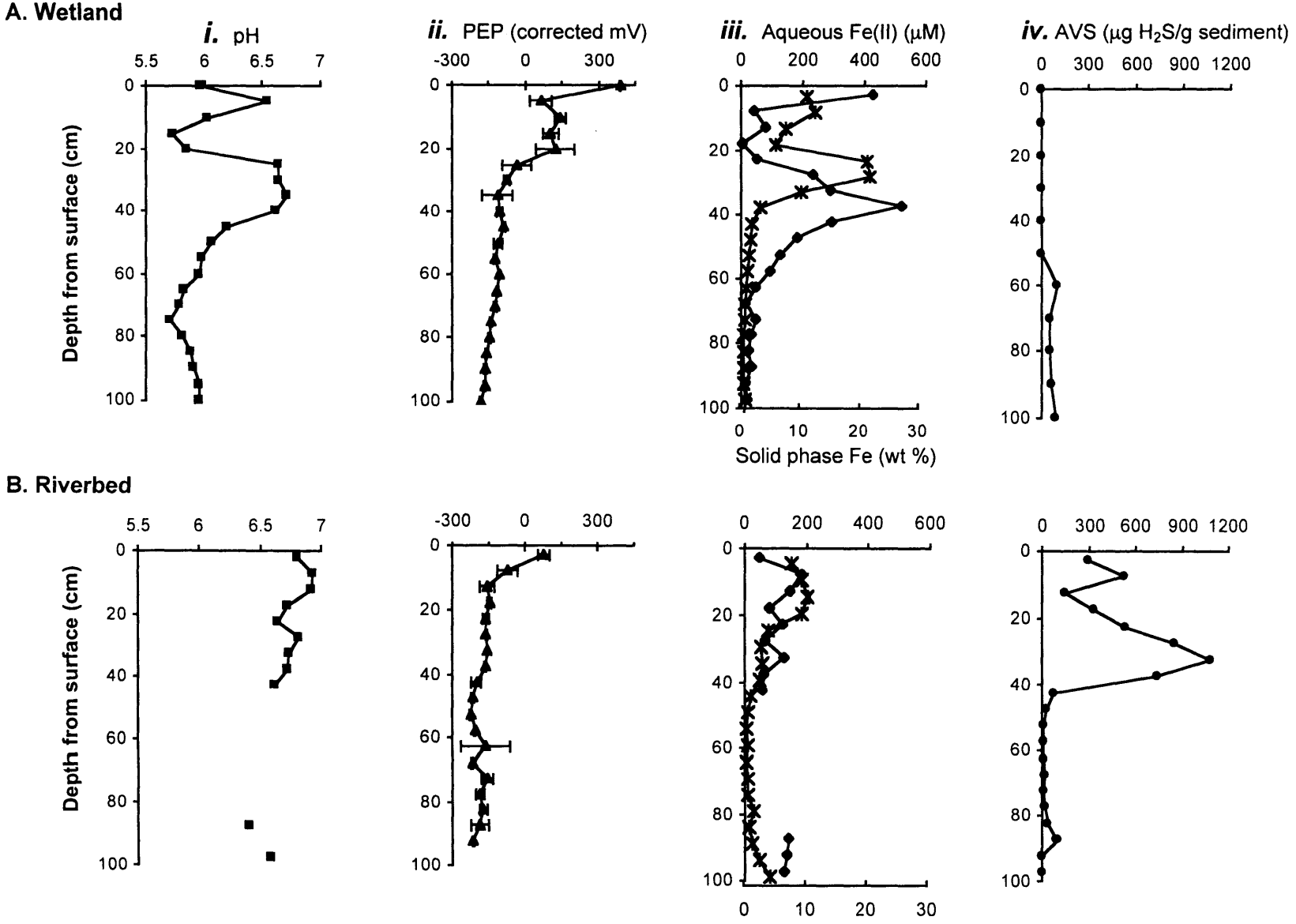

Figure 4A. pH-pe equilibrium modeling of the upper 100 cm of the wetland. In-situ measurements of pH and PEP from sediment core #3W are represented as data points, where the data points are depths in cm. Points on the pe-dependent lines represent the pH and pe where specie on either side of the line are present in equal proportions.

A. Wetland

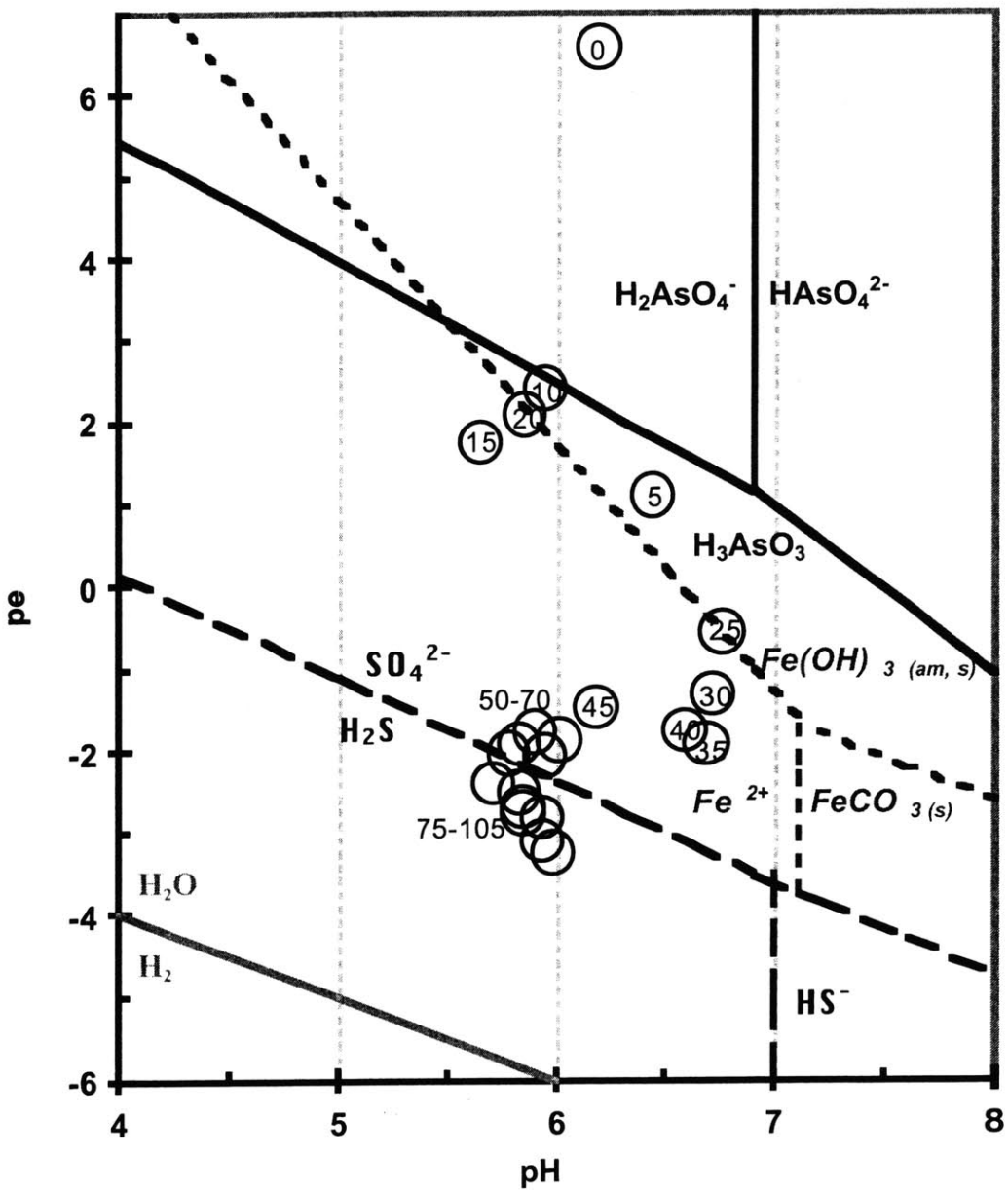

Figure 4B. Riverbed sediment pH-pe equilibrium modeling of the upper 100 cm. In-situ measurements of pH and PEP from sediment core #2R are represented as data points, where the data points are depths in cm. For clarity lost due to overlapping symbols, data points from 48-93 cm are shown as a larger circle on the plot.

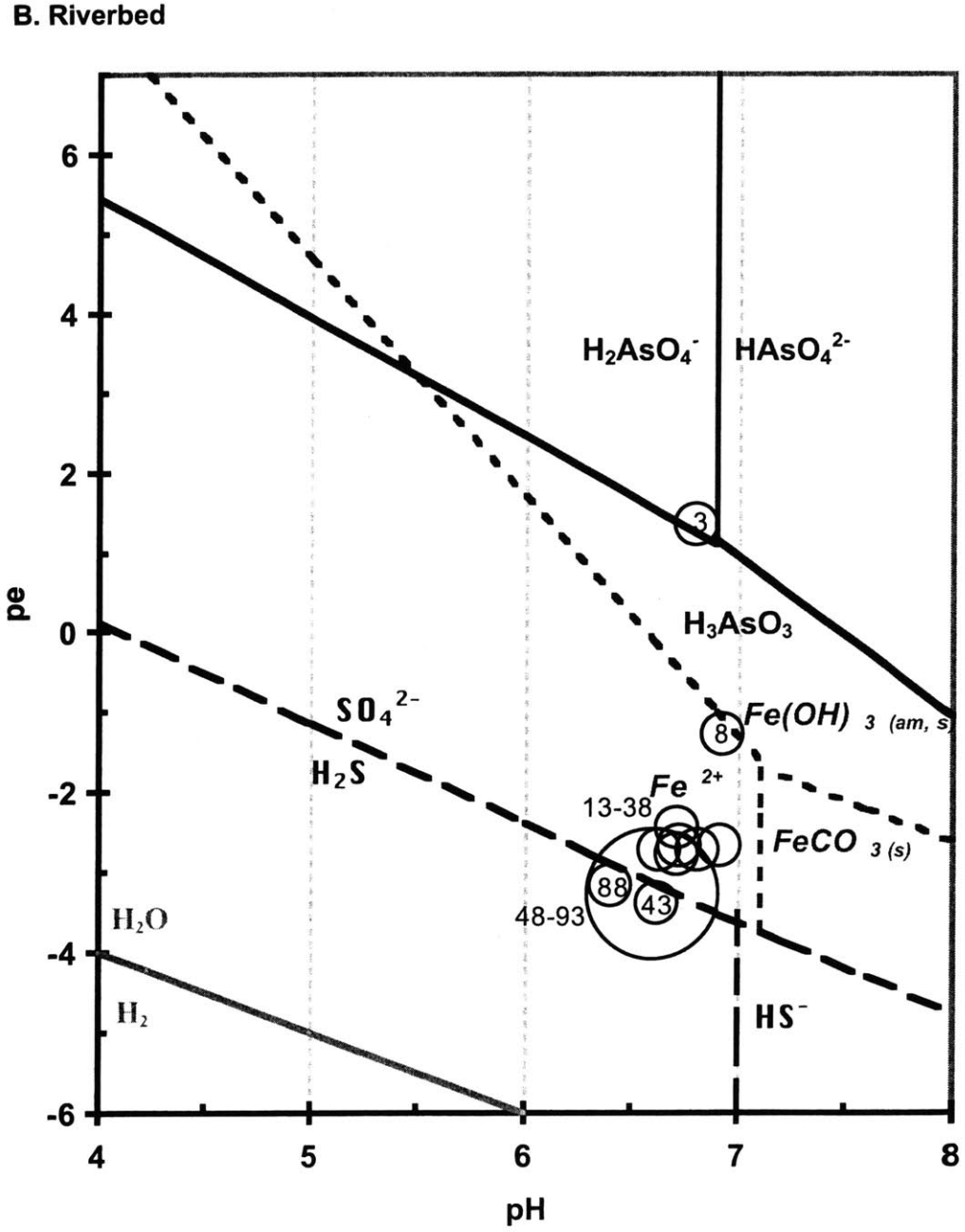

Figure 5. XRF elemental concentrations for wetland core #4W (circles) and riverbed core #2R (crosses), including elements that are possible sorbents or co-precipitated elements with As in various phases.

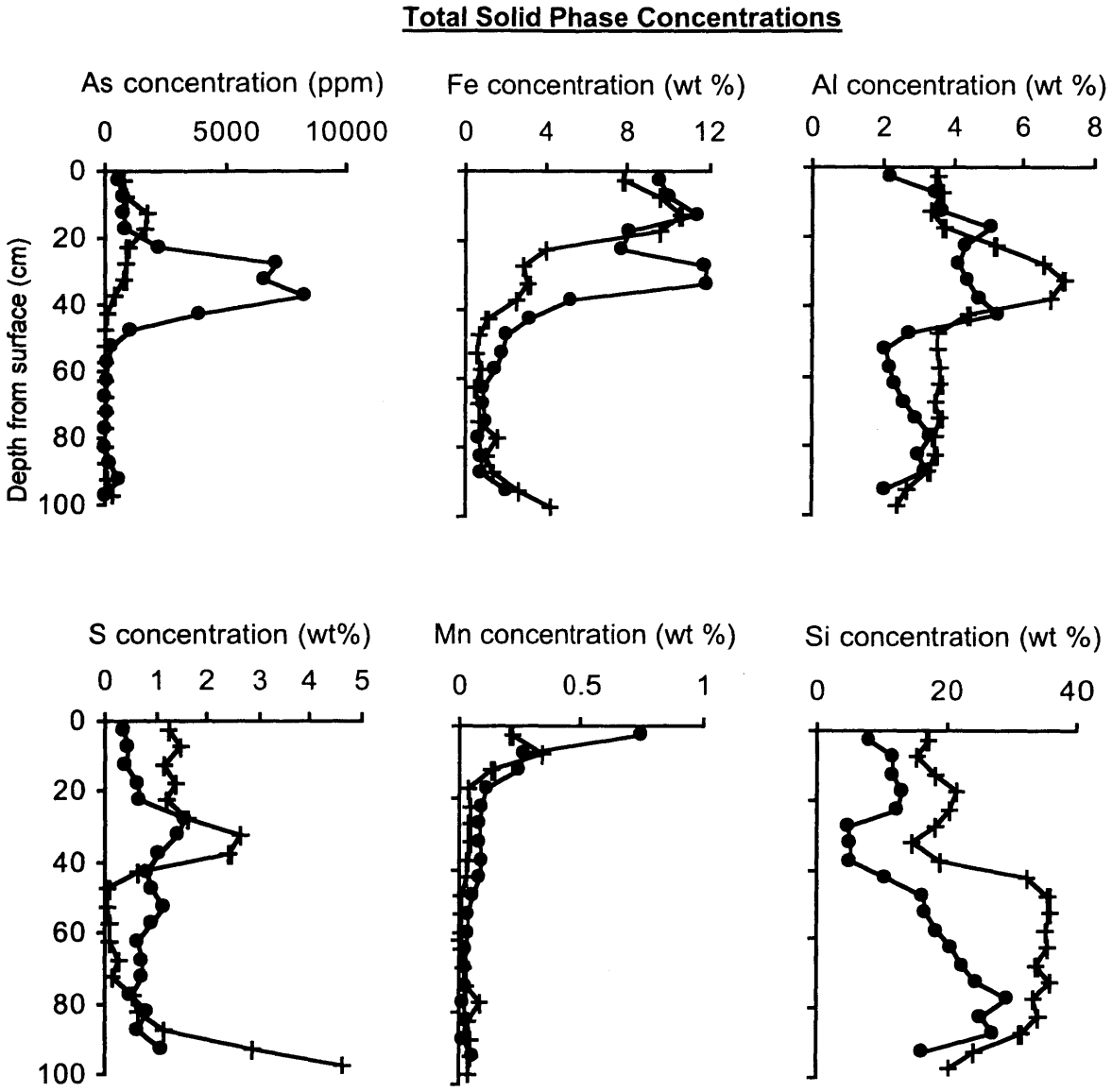

Figure 6. Extraction results of 4 depths for wetland core #4W, including (*i*) As concentrations and (*ii*) percentages in each extractant pool, described in more detail in Table 1. A split scale is used for the y-axis (*i*) to show the distribution of As among extractants for sediments with highly variable concentrations as a function of depth.

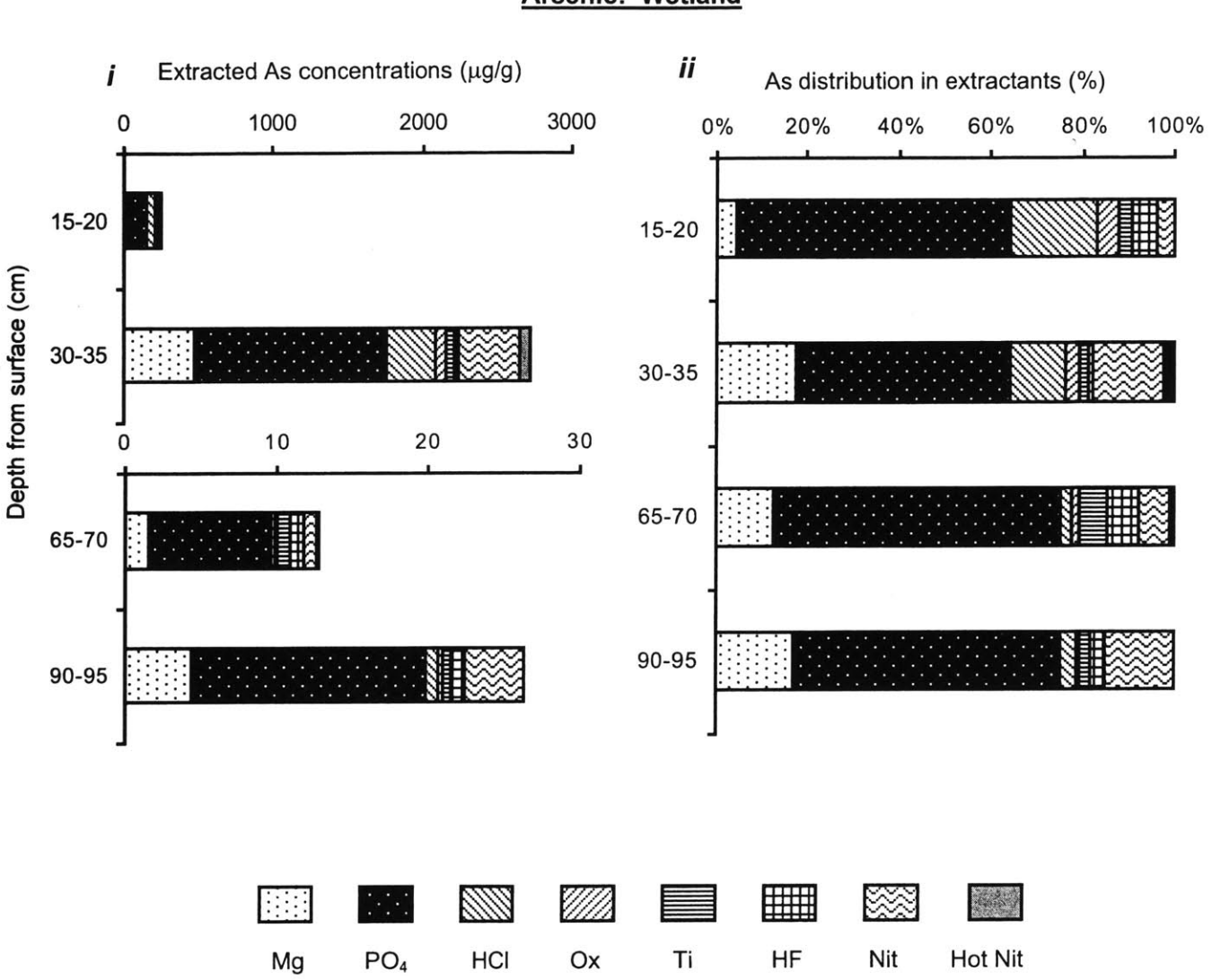

Figure 7. Extraction results of 4 depths for wetland core #2R, (*i*) As concentrations and (*ii*) percentages in each extractant pool.

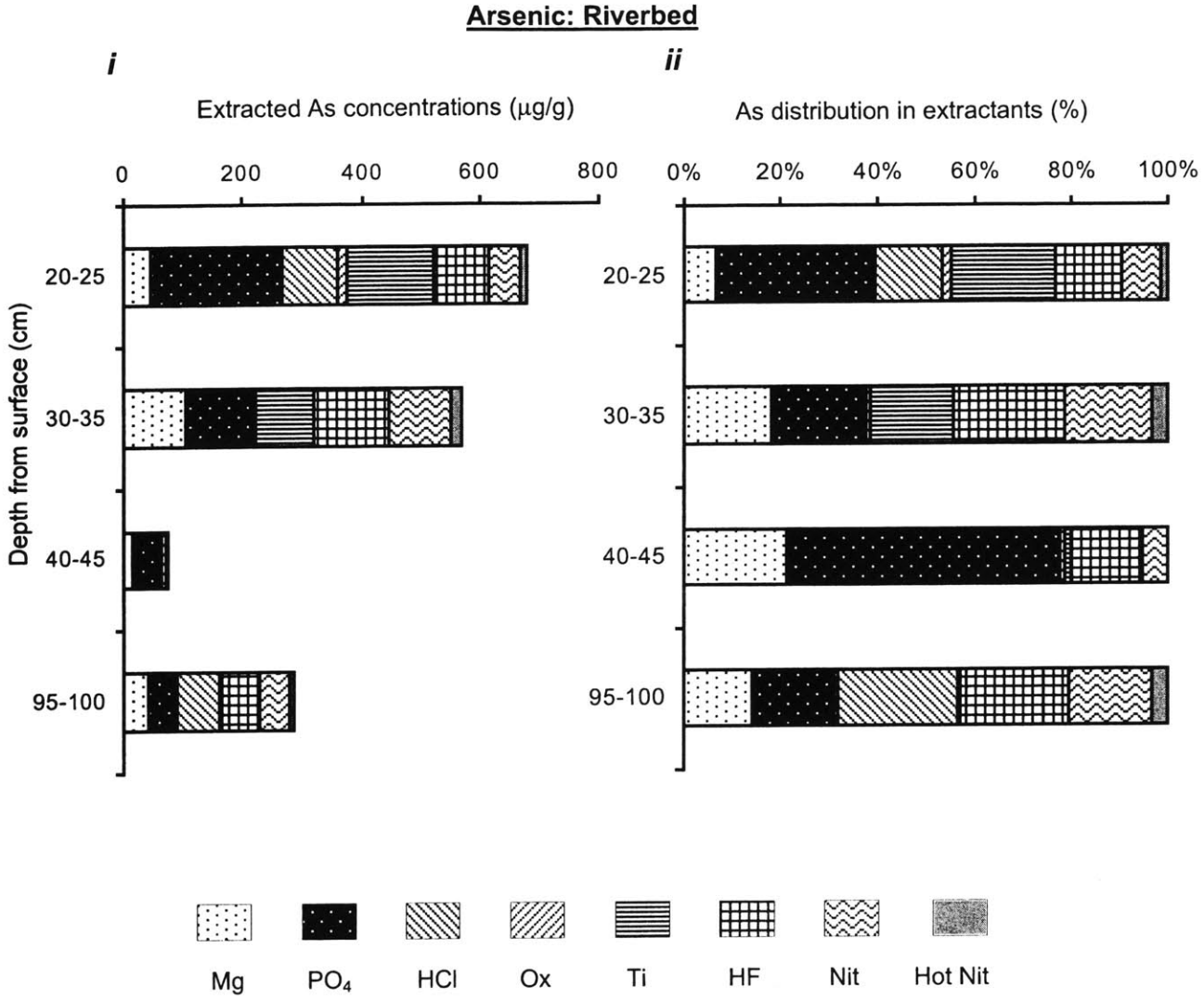

Figure 8. Fe distribution in extraction steps for wetland core #4W, in (*i*) concentration extracted (μg Fe/g sediment) and (*ii*) percentage in each extractant pool. A split scale is used for the y-axis (*i*) to show the distribution of Fe among extractants for sediments with highly variable concentrations as a function of depth.

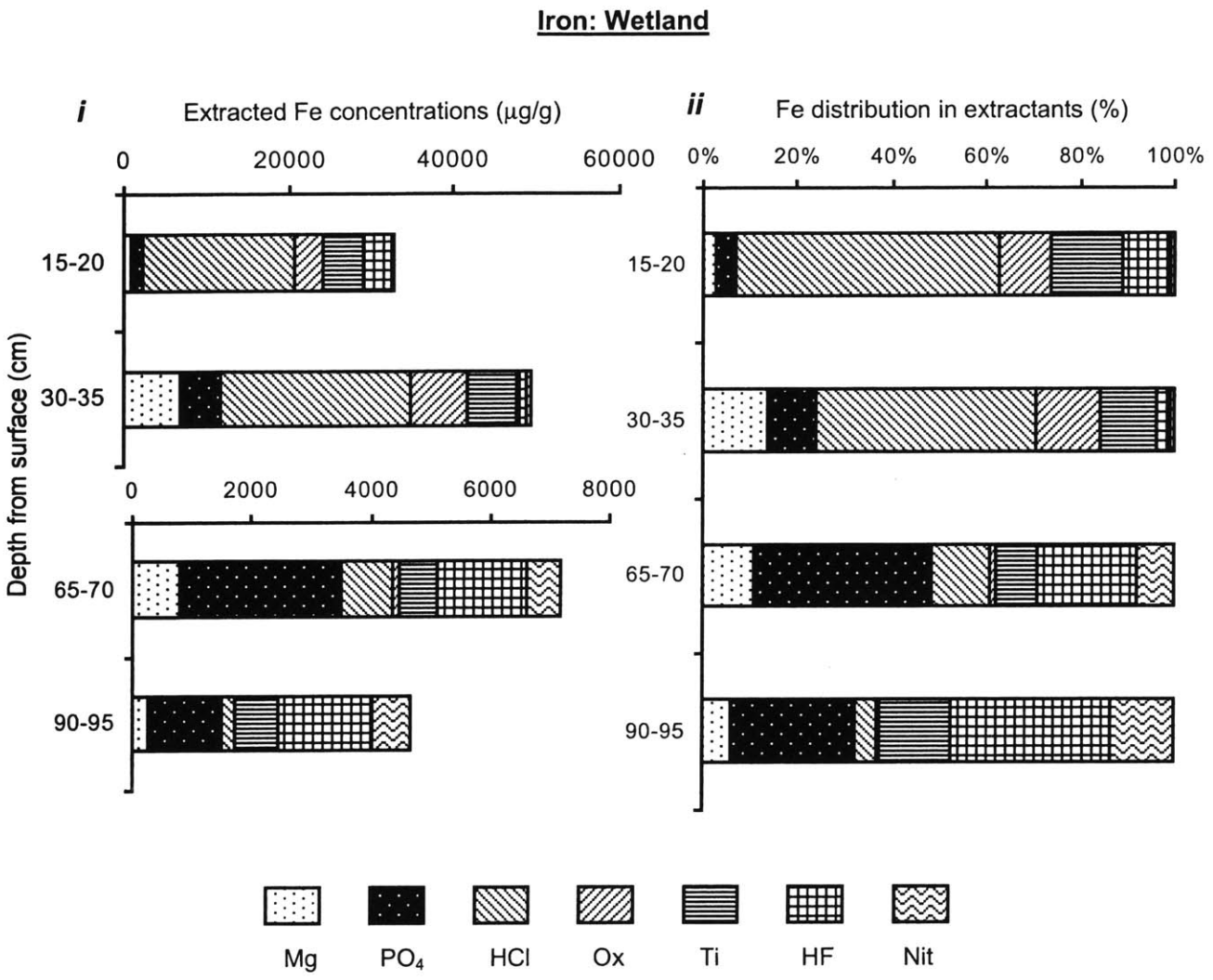

Figure 9. Distribution of Fe in extraction steps from riverbed core #2R as (*i*) concentration extracted (μg Fe/g sediment) and (*ii*) percentage in each extractant pool. A split scale is used for the y-axis (*i*) to show the distribution of Fe among extractants for sediments with highly variable concentrations as a function of depth.

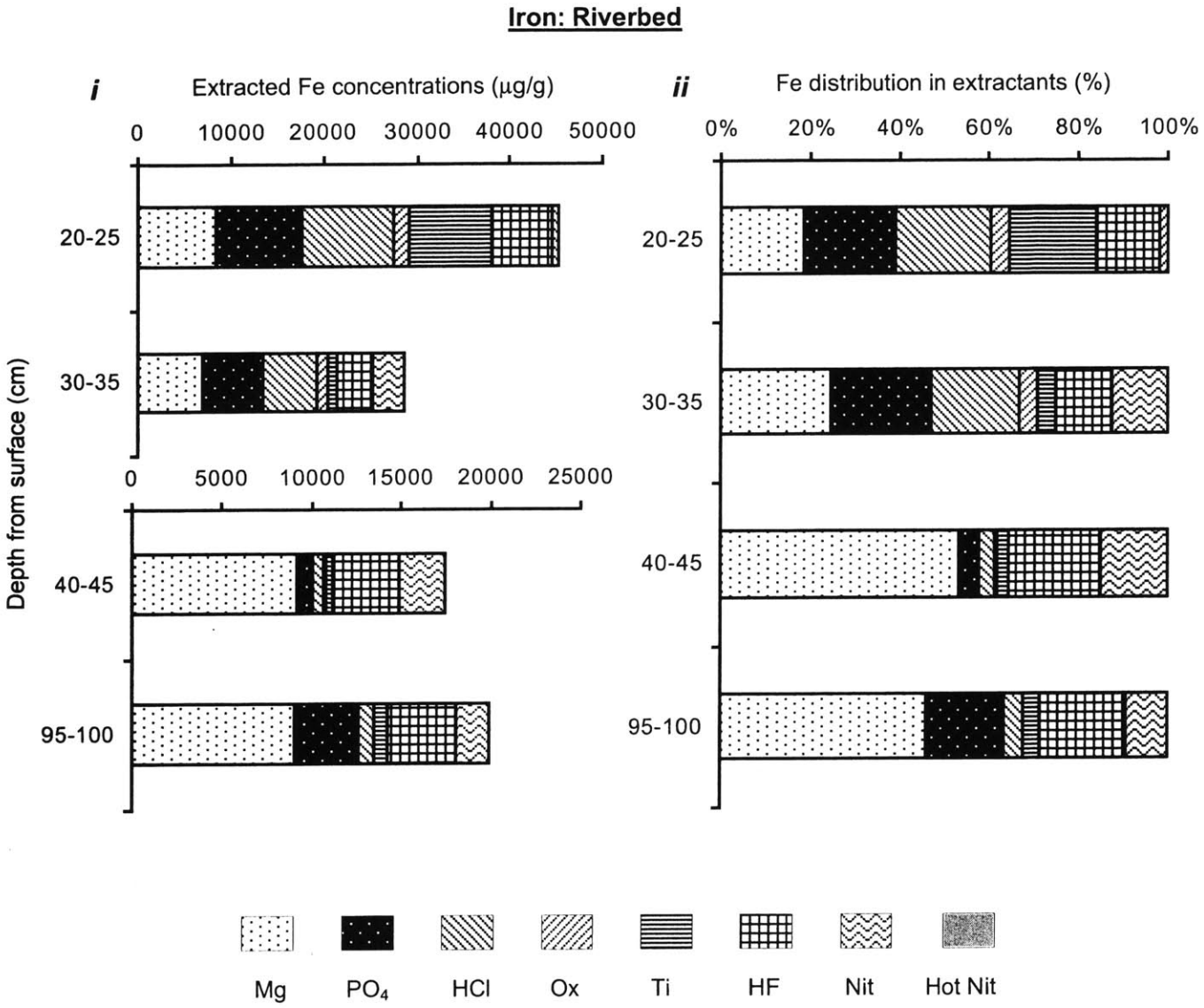

Figure 10. Distribution of Al in extraction steps is shown below for the (*i*) concentration extracted (μg Al/g sediment) and (*ii*) percentage in each extractant pool from (A) a wetland sediment subsample from 30-35 cm depth of core #4W and (B) a riverbed subsample from 40-45 cm depth of core #2R.

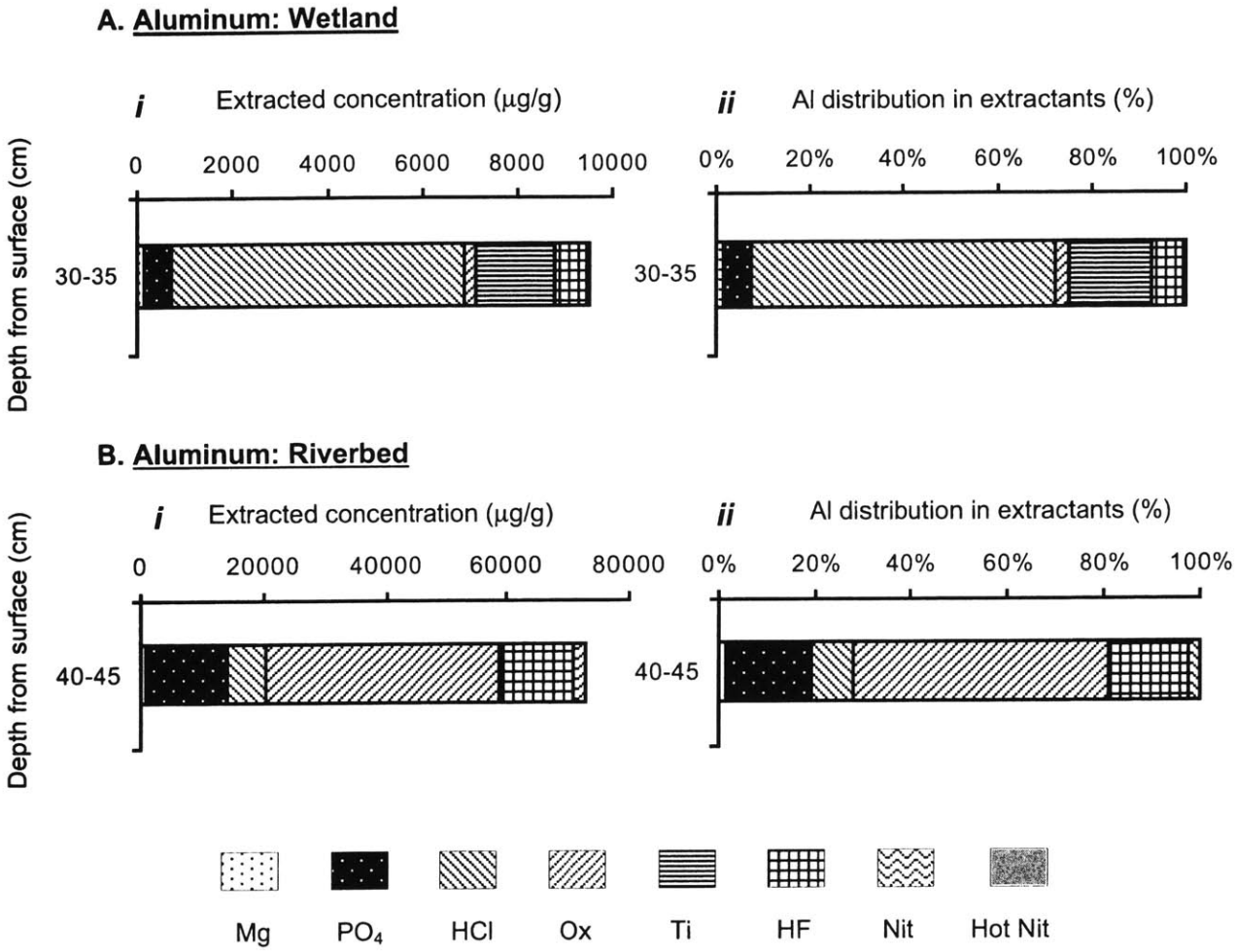

Figure 11. XANES analysis of As solid phase oxidation states for (A) wetland core #4W and (B) riverbed core #2R. Total As concentrations for each depth are listed underneath each stacked bar.

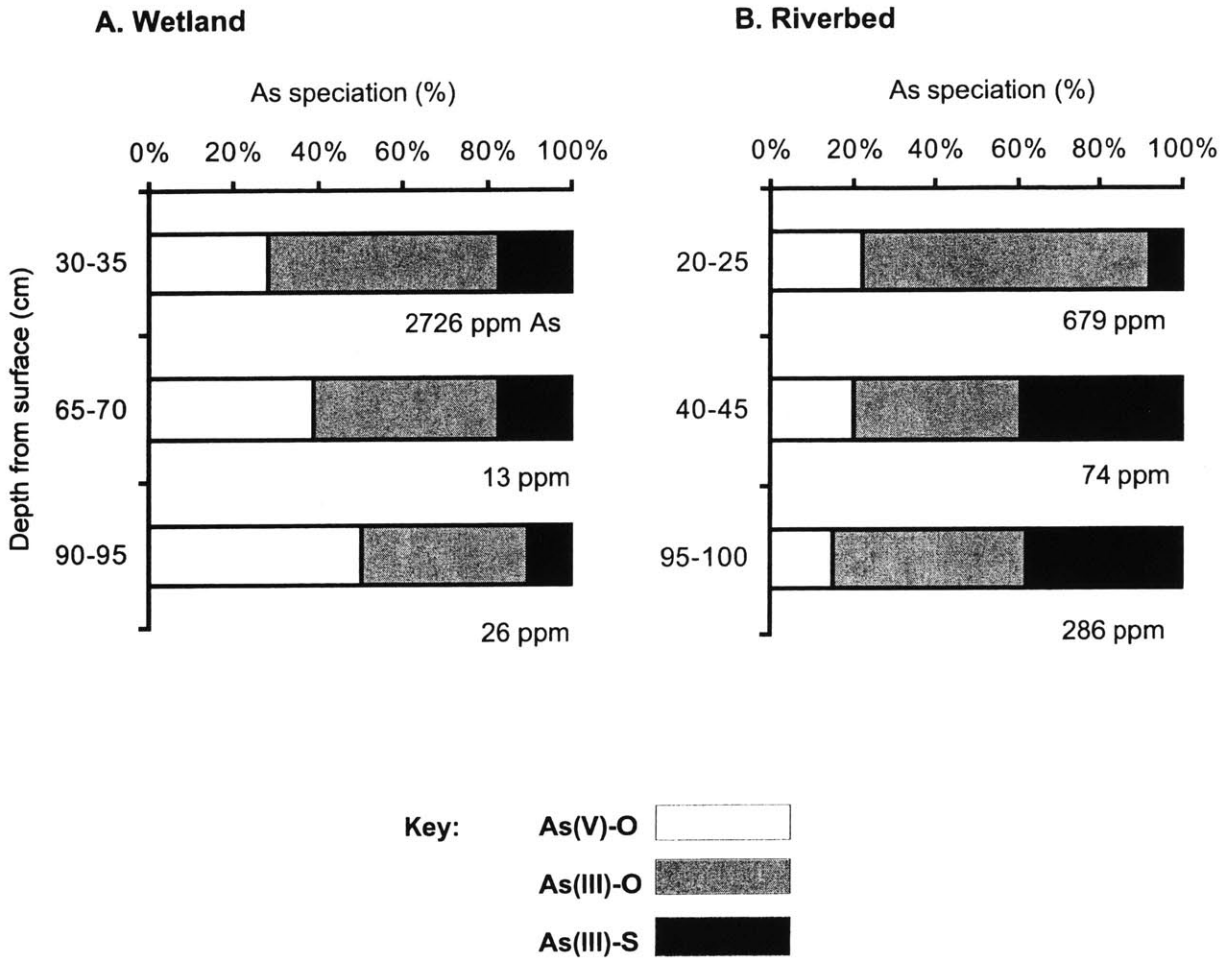

Chapter 4

Arsenic Distribution and Speciation in Iron-Rich Root Plaques: The influence of *Typha latifolia* on arsenic cycling in the Wells G & H Wetland

This chapter is prepared for submission to *Science*. Co-authors on the manuscript include: D.J. Brabander, S. Sutton, M. Newville, and H.F. Hemond.

1. Abstract

Adsorption of arsenic (As) onto iron (hydr)oxide phases is often a dominant mechanism of As retention in oxic sediments. In the root zone of reducing wetland sediments, the plant-induced formation of oxic microzones around roots is hypothesized to impact As mobility. In this study, we characterized the near-root environment of *Typha latifolia* (cattail) roots and investigated the role of As sorption onto Fe plaques and rhizosphere sediment. The plaque was determined to be 15-30 μm thick from XRF microtomographic analysis, comprised predominantly of Fe(III) (evidenced by x-ray near-edge spectroscopy (XANES)). Fe and As were highly correlated (R=0.98) on a spatial scale of 5-10 μm in the root plaque. Extractions of the plaque demonstrated that As was mostly adsorbed, in a molar ratio consistent with hydrous ferric oxides. Oxidation state mapping of the root plaque showed that both As(III) and As(V) were retained in the plaque, which for the first time indicates that the plaque can sequester As(III). Mass balance analysis of root plaque Fe and As revealed that the model of root oxygenation and precipitation of Fe from the trasnspiration stream could explain the observed concentrations of both elements. Arsenic stored in the plaque was determined to be a significant sink of aqueous As, in that dissolution of the plaque could increase the porewater concentration significantly.

2. Introduction

Arsenic (As) mobility in the environment is strongly dependent upon the speciation of As and the solid phases with which As may adsorb or coprecipitate. Redox and pH conditions of sediments play a major role in determining the solid phase associations of As. The mobility of As is maximized under Fe-reducing conditions with insufficient available sulfide for precipitation of As sulfides (*1*). In freshwater wetlands, sediments rapidly become reducing following flooding due to decreased oxygen diffusion through the sediment and abundant organic substrates for microbial respiration (*2*).

Other wetland processes, including the activity of plants in particular, may operate against this model by oxidizing the sediment. In waterlogged sediments deficient in O_2, wetland plants such as *Typha latifolia* (cattails) have specialized, porous aerenchyma tissue to allow maximum, pressurized oxygen transport to the roots (*3*). Oxygen release at the roots is believed to be a protective mechanism for wetland plants in anoxic sediments, in order to reduce the toxicity of reduced organic compounds (e.g. ethylene, lower alcohols, lower fatty acids), as well as inorganic compounds that can be toxic in high concentrations (e.g. H_2S and Fe(II)) (*3*).

T. latifolia may transport more oxygen to the roots in reducing wetland sediments due to an increased root porosity than in oxic sediments (*4*). The extent of oxygen release by *T. latifolia* roots under reducing conditions was estimated between 0.2 and 0.4 mmoles of O_2 per gram of roots (dry weight) per hour (*4; 5*). Oxygen exuded from the root can react with Fe(II) in the porewater, forming an Fe(III) hydroxide plaque on the root surfaces (*6*). In addition to abiotic Fe oxidation by O_2, microbial Fe oxidation at the root-soil interface may occur, enhancing formation of Fe solid phases (*6; 7*). The availability of O_2 released from the root to oxidize Fe(II) and precipitate Fe(III) in the rhizosphere depends on the competition presented by other reduced species, such as methane (*5; 8; 9*).

Root exudation of oxygen and organic compounds as well as the flux of solutes to the root (i.e. in the evapotranspiration stream) occur in the rhizosphere, which may lead to microzones of redox and pH in root-zone that can affect As mobility. The *rhizosphere* of wetland plants is the sediment zone directly affected by root activity (*10*). The extent of oxidizing influence of the *T. latifolia* roots on the rhizosphere is uncertain, which has prompted study of changes in the near root soil compared to bulk soil. Ye et al. (*11*) suggested that the oxidized rhizosphere zone may extend beyond the plaque to a few millimeters. Some studies have shown that rhizosphere soil may experience acidification due to Fe(II) oxidation and exudation of organic acids, in contrast to the general increase in pH observed during reduction of Fe-rich, high organic matter wetland sediments due to the reduction of Fe(III) (*10; 12; 13*). Others report

that the rhizosphere may sufficiently oxidize vegetated sediments to yield a higher measured platinum electrode potential in sediments, a parameter indicative of redox conditions (*5; 14*). One potential consequence of oxidizing rhizosphere conditions is the precipitation of Fe oxyhydroxides and subsequent adsorption of As in the plaque and rhizosphere sediment.

Several studies have conjectured that As retention in plaques might be high, due to the adsorption affinity of As for Fe(III) hydroxides. Before the application of x-ray absorption spectroscopy techniques in studying roots, chemical extractions were the main method of studying As in plaques. An initial investigation using chemical extractions of wetland plant root plaques indicated that As may be concentrated in the plaque along with Fe (*15-17*). The thickness of the Fe plaque, which partially determines the sorption capacity for As, was estimated from solution culture studies and scanning electron microscopy to be around 15 μm, with maximum development 1 cm from the root tip but coverage extending over all root surfaces (*6*). The extent to which As is retained within root plaques was largely unknown.

The As adsorption capacity of an Fe-rich plaque depends on the nature of the Fe phase, including whether the Fe is oxidized or reduced, crystalline or amorphous. The composition of the Fe plaque has been presumed to be Fe(III) hydroxide, such as goethite (α-FeOOH) or lepidocrocite (γ-FeOOH) (*18-20*). Findings of enhanced plaque formation on roots in solution culture with Fe(II) (compared to Fe(III)) have been interpreted as evidence of Fe oxidation as the mechanism of plaque formation (*6*). However, the introduction of O_2 into the solution culture coupled to the rapid oxidation kinetics of Fe(II) to Fe(III) may have caused experimental artifacts. The assumption that the Fe plaque is comprised solely of Fe(III) hydroxides was challenged by Wang and Peverly (*21*), who found that up to a third of the Fe was Fe(II). Wang and Peverly postulated that the Fe(II) in the rhizosphere was predominantly siderite ($FeCO_3$) due to high microbially-produced pCO_2. An earlier report by St-Cyr and Crowder (*22*) hypothesized that $FeCO_3$ was the precursor for Fe hydroxide formation in the plaque, with high concentrations of CO_2 promoting siderite formation, and rapid oxidation kinetics yielding

lepidocrocite (*7*). To our knowledge, the only direct evidence of a mixed Fe oxidation state in plaque has been offered by Wang and Peverly (*21; 23*), which relied on dried, powdered roots for Mossbauer spectroscopy and chemical extractions.

The development of XRF (x-ray fluorescence) microtomography and microXAFS (x-ray absorption fine structure spectroscopy) now allows the spatial resolution of trace-level contaminants on a 5-10 μm scale. These techniques can probe the plaque and interior of the roots directly without extensive destructive, potentially-oxidizing sample preparation. The first studies of metals in roots using XRF microtomography were conducted by Hansel et al. (*24; 25*), who demonstrated that the technique was feasible in metal-rich environments on two wetland plant species (*Phlalaris arundinacea* and *T. latifolia*). In the present study, we probed intact *T. latifolia* (cattail) roots from a contaminated wetland using XRF microtomography to determine (i) the thickness and uniformity of the Fe plaque, (ii) the micro-distribution and correlation of As and other contaminants (Pb, Cu, Zn) with Fe, and (iii) the feasibility of As oxidation state mapping.

We also evaluated the importance of root-associated sediment (i.e. root plaque and rhizosphere sediment) in sequestering aqueous As in a contaminated wetland. We tested the hypothesis that As would be concentrated in the plaque and rhizosphere sediment compared to bulk sediment. To determine the relative proportion of As in roots and rhizosphere sediment, we employed the best available experimental methods with improvements designed for reducing conditions. First, wetland plant roots were separated from sediment by hand, which is tedious and time-intensive but the most accurate method (*26; 27*). Unlike other studies, we maintained an anoxic environment during the root separation procedure and used deoxygenated water washes to remove the rhizosphere soil, in order to prevent experimentally-induced oxidation of Fe or As. Experimental separations of rhizosphere soil are operationally defined as the water-removable soil particles remaining on the roots after agitation of the picked roots (typically less than 1 mm thick), while plaque is classified as the layer remaining after washing (*16; 28*).

We determined the thickness of *T. latifolia* Fe plaques, which was coupled with root dimensional measurements to estimate plaque volume in a sediment core. Using literature-reported *Typha* root oxidation rates, we next determined if the roots could release enough O_2 to oxidize the amount of Fe observed in the plaque. We then investigated whether the estimated Fe and As concentrations in the plaque could be explained by the calculated fluxes, based on the rate of water transport to the roots and porewater concentrations.

Finally, we assessed the potential impact to aqueous As concentrations if the As retained in the root plaque were released. We used the same estimate of plaque volume combined with the concentration of As in the plaque and porewater content of the core to estimate the mass of As in a given core volume in order to determine the importance of the plaque as a reservoir of As contamination.

3. Methods

3.1 Site description

The Wells G & H wetland is a 16 hectare riverine peatland estimated to contain 10 metric tons of As, predominantly in the upper 50 cm of the sediment. Arsenic contamination is attributed to extensive industrial manufacturing processes in which As was a major by-product (*29*). The retention of heavy metals and As in the wetland, at concentrations up to or exceeding 10,000 mg/kg, has stimulated research into the retention of the contaminants and the potential for partitioning into the groundwater at this site. Arsenic solid phase associations in the wetland sediment were investigated previously, using a sequential extraction method (*30*). Arsenic was apportioned into fractions including loosely- and strongly-adsorbed As; As co-precipitated with metal oxides, carbonates, or amorphous monosulfides; As co-precipitated with crystalline iron (oxyhydr)oxides; As oxides; As co-precipitated with pyrite; and As sulfides. This study found that As was predominantly strongly adsorbed (i.e. competitively desorbed by phosphate) and highly correlated to Fe (*31*), which suggests that a fraction of the solid-phase As might be

released into groundwater during Fe reduction and hence be available for transport to plant roots.

The site has been classified as an emergent, persistent herbaceous wetland, containing the wetland macrophyte species *T. latifolia*, *Lythrum salicaria* (purple loosestrife), *Carex stricta* (tussock sedge), and *Phragmites australis* (common reed) (*32*). An initial investigation of the distribution of the species throughout the wetland showed that *T. latifolia*, *C. stricta*, and *L. salicaria* are dominant and co-exist, whereas *P. australis* occurs in monoculture stands in some areas of the wetland (App. E, Fig. I). The Aberjona river flows through the wetland via several meandering channels. For this study, we selected the area between the east channel and the upland, about midway between Wells G and H. This region was most accessible for sampling and predominantly contained *T. latifolia*, which was chosen for closer study due to its extensive root zone and prevalence in the wetland as well as around the world.

3.2 Root imaging and microtomography

Fresh *T. latifolia* root samples were obtained from the Wells G & H wetland several days prior to analysis. Using a flat shovel, a 0.27 m^3 block of sediment was transferred into a N_2-purged glove bag in the field and transported to the lab, where the roots were separated from the soil the same day.

Cattail root systems are comprised of a rhizome, or underground stem approximately 2 cm in diameter, from which roots of about 1 mm diameter propagate. Root hairs stem from the 1 mm diameter roots, and range between 100-700 μm in diameter. Live roots attached to *T. latifolia* rhizomes were hand separated from the sediment in a N_2-purged glove bag to prevent oxidation, induced by exposure to O_2, of ferrous iron on the roots. A portion of the roots was washed with deoxygenated (< 0.3 mg O_2/L) Milli-Q water and the rest of the roots were left with adhering sediment. In early XRF microtomography tests of elemental distribution in roots, we found that wet roots dried during the analysis time and did not maintain structural integrity; yet

elemental mapping required stability around the longitudinal axis. Thus, for early analyses we freeze-dried roots to maintain structure during analysis for total-element distribution in the roots (as done by *25*). For As oxidation state mapping and other speciation analyses, we later developed a methodology to impregnate the roots with oil, both to minimize the potential oxidation during freeze-drying and to maintain structural integrity of the roots during analysis. For this procedure, wet roots were first immersed in isopropyl alcohol for 24 h to replace the water, under a N_2-purged atmosphere. Increasing amounts of mineral oil were added into the alcohol over a 48 h period until nearly 100% of the solution was oil (due to alcohol evaporation).

Elemental distributions were determined through a cross-sectional root slice (without physically cutting the root) at beamline 13-ID-C, Advanced Photon Source, Argonne National Laboratory. The APS ring was operated at 7 GeV, with the beamline using APS Undulator A (158 poles). The x-ray beam was passed through a Si(111) cryogenic double crystal monochromator, which was detuned by approximately 50%. The beam size was then reduced from 300 μm to 3 μm using Kirkpatrick Baez micro-focusing optics (*33*). XRF data was collected simultaneously for several elements using a solid state, multi-channel germanium detector. For tomograms, roots were mounted on a computer-controlled platform, translated at 5-10 μm steps through the stationary 2-3 μm pencil beam operated in fluorescence mode, rotated by 5° around the vertical axis, followed by repeated translation and rotation for a total of 180° root rotation. Tomogram reconstructions were generated by filtered backprojection (*34*).

Plaque concentrations for data points that were above background for As and Fe (approximately 10 μg/g) were calculated by comparison with the standard reference material thin film. Maximum concentrations and averages were calculated using a density estimate of 4 g/cm^3 (Fe hydroxide).

Arsenic oxidation state maps were produced by measuring fluorescence intensities at the As(III) white line energy (11,869.2 eV), at an energy above the edge for total As (12,000

eV), and at an energy below the edge for background. We attempted to also obtain As(V) data directly, but the beam was not stable for the long period of time (> 12 hr) necessary to obtain all four data sets.

Arsenic x-ray absorption near-edge spectra (XANES) were collected using a defocused (400 μm height x 400 μm width) x-ray beam through the entire 300 μm root. As XANES were energy-calibrated to a Standard Reference Material foil at 11,867 eV. Fe XANES data was obtained on a different part of the root using the same defocused beam. XANES data analysis was performed using WinXAS v. 2.1 (*35*).

3.3 Core sampling and root separation from bulk and rhizosphere sediment

To obtain root material, four sediment cores 40 cm in length were retrieved from the Wells G & H wetland using a 7.6 cm diameter Lexan™ piston corer (*31; 36*). Previous studies showed that between three to six root cores is typically sufficient to characterize root systems with relatively uniform root density (*26; 27*). The cores were capped immediately with plastic caps in a N_2-purged glove bag, sealed with parafilm and duct tape, and transported back to the laboratory. Holes predrilled in the Lexan at 5 cm increments were used as ports for microelectrodes, which were uncovered in the glove box to measure pH and platinum electrode potential. Prior to sediment core sectioning, pH and PEP were measured in triplicate for each 5 cm depth increment by inserting microelectrode probes (Microelectrodes, Inc.) into the core through the predrilled holes. The pH microelectrode was an exposed-tip MI-4144 (1.7 mm needle diameter) glass combination probe calibrated with pH buffers before each analysis. PEP was measured with an exposed-tip MI-800 (1.7 mm diameter) Pt/KCl, Ag/AgCl combination microelectrode calibrated with ZoBell's solution before analysis. PEP measurements were converted to the standard hydrogen potential scale by adding +209 mV to the measured value (*37*). PEP data was used to assess the relative changes in redox conditions as a function of depth, and to determine if Fe-reducing conditions were expected. Following microelectrode

measurements, the core was divided into 10 cm increments by manually slicing through the Lexan and sediment using a hacksaw in the glove box. Each sediment increment was capped, weighed, sealed, and stored at 4°C until root separation, which was completed within a week.

Roots were separated from the sediment in each core section (0-10 cm, 10-20 cm, 20-30 cm, and 30-40 cm) and classified as detailed in Table 1. We performed the separation, sieving, and washing in a N_2- purged glove bag to prevent oxidation of reducing phases. The 0.25 mm^2 sieve mesh size for separating rhizosphere sediment from roots was selected to minimize losses of fine roots (*27*). The metric of Valiela (*38*) and Boehm (*27*) to separate live and dead roots was used (briefly, live roots are rigid, whole, and often connected to larger, more easily identifiable live roots). No dyes or other indicators were used to confirm the classification due to the desire to avoid chemical contaminants.

Wet weights of each pool were measured after separation. Subsamples from each pool were digested by concentrated hot nitric acid and hydrogen peroxide (EPA method 3050B) to obtain total As concentrations. In addition to total digestions, sequential extractions of live root subsamples (between 2-44 g, depending on availability in an increment) were performed to determine if As was adsorbed, and if the plaque Fe could contain sufficient sorption sites to adsorb the observed As (Table 2). Aqueous As in digestates was measured by graphite-furnace atomic absorption spectrometry (GFAAS) or hydride generation atomic fluorescence (HGAF) (*31*).

3.4 Measurements for mass balance calculations

For the mass balance calculations of As and Fe, we measured root lengths and diameters for a 0.27 g subsample of roots separated from the 10-20 cm depth of maximum root density using a magnifying glass. In the 0.27 g root subsample, roots ranged in diameter from 0.1-1.5 mm. We measured the dimensions of each of the 530 small roots (typically 0.3 mm diameter and 2 mm length), calculated each root's surface area and volume, and summed the

results of the individual roots. Based on the sums, we estimated a root surface area = 1,400 mm^2 and root volume = 150 mm^3 for the 0.27 g subsample. In addition to the small roots, 6 large roots (typically 10 mm diameter and 70 mm length) were contained in the 0.27 g subsample. The sum of each large root's surface area and volume calculated from individual measurements yielded an a root surface area = 1,300 mm^2; root volume = 400 mm^3. Total root surface area was calculated for the sum of the large and small roots (including root hairs) in the subsample using the formula for cylinder surface area, which yielded an estimate of 2,700 mm^2. Surface area for the whole 450 cm^3 soil increment was therefore 270,000 mm^2 by extrapolation to the whole increment. Total root volume in a 10 cm core increment was calculated to be 55,000 mm^3 by extrapolating the subsample mass to the total root mass of 27 g. Plaque volume was estimated by multiplying surface area of roots in the increment by a plaque thickness of 0.03 mm (determined by XRF microtomography; Fig. 3) to yield an estimated volume of plaque of 8,200 mm^3.

4. Results and Discussion

4.1 Potential plant-induced changes in sediment pH and redox

The 0-20 cm plant root zone was typically characterized by lower pH and higher platinum electrode potential compared to the 20-40 cm depths (Fig. 1), which had fewer live roots. The PEP values between 20-40 cm in Fig. 1 are consistent with Fe-reducing conditions in the sediments, whereas the upper 20 cm are in the stability region characterized by oxidized Fe (App. B).

To evaluate whether the recorded PEP measurements are more likely to be a bulk measurement or indicative of conditions in the root rhizosphere, we used estimates of root density. Based on the volume of the 10-20 cm soil increment (450 cm^3) and the estimated root volume in the increment (55 cm^3), approximately 1/8 of the increment volume is comprised of roots. First, we assumed that the roots are evenly distributed and the diameter of the roots

averages 5 mm. If roots comprise 1/8 of the increment volume, then there would be a distance between roots of approximately 40 mm (i.e. 5 mm x 8, which is based on the assumption that a unit length of core would have an 8:1 ratio). Given the microelectrode tip diameter of 1.7 mm, the likelihood of probing rhizosphere sediment (assuming the rhizosphere extends out to 1 mm from the root) is around 4%. Measurements were obtained at 3 locations in a core section for each depth, yet we found that it is still more likely that the PEP is a bulk measurement rather than a measure of the rhizosphere. The higher PEP found in the upper sediments may be due to a larger rhizosphere influence than previously reported or possibly evapotranspiration-driven air entry into the upper 20 cm of the sediments. The lower pH observed in the upper sediments may reflect the presence of iron hydroxides whose reduction at lower depths increases the pH compared to that of the upper sediments.

4.2 Plaque imaging, thickness, and elemental distribution

Initial studies using scanning electron microscopy (SEM, Fig. 2) revealed that plaque was fairly uniform on live root surfaces. Energy-dispersive spectroscopic analysis by SEM showed that the plaque contained up to 18% Fe. Arsenic, Pb, Cu, and Zn were below the detection limits of the SEM energy dispersive detector (approximately 0.1%). The high photon flux and brightness available at the Advanced Photon Source (APS, Argonne, IL), however, were capable of imaging the distribution of these elements and determining the spatial distribution of As in the plaque.

XRF microtomography of roots at APS provided direct cross-sectional elemental mapping through uncut, intact live roots. The tomograms produced for roots of varying sizes (100-500 μm) showed an Fe ring around all cattail roots tested (n = 9, Fig. 3 for 300 μm root, smaller root shown in App.E, Fig.VII). The Fe plaque of the 100-500 μm root hairs examined in this experiment was approximately 30 μm in thickness, for both unwashed roots and roots

washed with deoxygenated distilled water. No Fe or As was observed within the roots tested, which implies that the root surface concentrates elements in the plaque.

XRF tomographic maps of Fe, As, Pb, Cu, and Zn show that Fe and As form a plaque ring around the roots, whereas measurable Pb, Cu, and Zn occur only at discrete locations (Fig. 3A-E). All of these elements are contained in the arsenian Iberian pyrite source material used for past sulfuric acid manufacturing processes upstream (*39*), and Pb, Cu, and Zn are also co-contaminants from tannery processing that occurred in this watershed (*29; 40*). The processes transporting the elements to and immobilizing them in the plaque appear to differ for As compared to Cu, Zn, and Pb. Fe and As are highly correlated in the plaque (Fig. 4, R = 0.98) at the resolution of 10 μm data points.

Average concentrations and the ratio of Fe and As in the root plaque were determined from XRF microtomography data. For Fe, the average plaque concentration was calculated as 2.5%, with a maximum of 14.7% detected. Average As content of the plaque was 105 μg/g, with a maximum of 780 μg/g. Thus, the average ratio of As/Fe in the plaque was 3 mmoles As/mole Fe. Approximately a 10-fold lower As/Fe concentration was observed by XRF microtomography compared to extraction data for root plaque, indicating some heterogeneity exists on the small scale of a root cross-section determined by microtomography. The discrepancy in the ratio between the two methods arises mostly from 10-fold lower extractable-Fe concentrations in the plaque compared to as measured by XRF microtomography.

4.3 As & Fe speciation in root plaque

Both As(III) and As(V) coexist in approximately equal proportion in the porewater of the root zone (*31*). We questioned whether As(III) is oxidized in the plaque before precipitation, or if both are sequestered in the plaque. Speciation of As in root sections (n = 2) by XANES analysis yielded an average of approximately 20% As(III) and 80% As(V) (Figure 5), which provides evidence that both are retained in the plaque. Fe XANES results (Fig. 6) showed that

the *T. latifolia* root plaque was mainly Fe(III), which agrees with most literature reports of a predominantly Fe(III)-rich plaque on *T. latifolia* (*25*) and contradicts the finding of Ye et al (*11*).

The micro-scale distribution of As oxidation states in the root plaque was probed to evaluate possible patterns, such as a potentially increased concentration of As(V) near the root due to root oxygenation. Arsenic oxidation state microtomograms (Figure 7) shows that both As(III) and A(V) are present in the plaque in a fairly heterogeneous distribution. Similarly, bulk XANES through a two-dimensional root cross-section (Fig. 5) confirmed that a mixture of As(III) and As(V) existed. The presence of As(III) within the plaque is plausible based on the mixed oxidation states found in the porewater, but may suggest that As in the rhizosphere is not completely oxidized by the roots like Fe.

A few small, localized patches suggest that As(III) may be concentrated near the interior of the plaque and As(V) in the exterior (Fig. 7, e.g. upper right corner). Several potential explanations might explain a trend toward higher As(III) in the plaque interior. The possible accumulation of As(III) in the interior of the plaque may occur if As(III) is able to diffuse into the plaque and adsorb to Fe in the plaque interior. Slower kinetics of adsorption for As(III) to amorphous Fe hydroxide, compared to As(V), may enhance the distance As(III) travels in the plaque (*41*). Alternately, As(V) may outcompete As(III) for sorption sites in the outer region of the plaque, resulting in further transport of As(III) into the plaque. Although our data is far from conclusive about distribution patterns in the plaque, our main finding is that oxidation state maps demonstrate that the plaque adsorbs both oxidation states, removing As from the porewater.

4.4 Quantification of root-associated As

4.4.1 Mass of biomass and sediment fractions. Biomass (in mass of live and dead roots per core increment volume, or g/ 450 cm^3) and the proportion of rhizosphere soil, decaying rhizome, and bulk soil were estimated for 10 cm increments of four sediment cores (Figure 8). The uppermost increments, 0-10 and 10-20 cm, contained the greatest proportion of live roots,

with an average of 34 ± 27 and 47 ± 21 g live roots/ 450 cm^3, respectively. By comparison, the 20-30 cm depth contained 6 ± 5 g live roots/ 450 cm^3, and at 30-40 cm depth, only one of the four cores showed any live roots (0.97 g). For dead roots, twice as much biomass was found for the 20-30 and 30-40 cm depths (119 ± 22 and 145 ± 40 g dead roots/ 450 cm^3) compared to the upper 0-10 and 10-20 cm increments (59 ± 38 and 38 ± 17). From these results, we concluded that the depth of maximum live root density was between 10-20 cm, and dead root density was greatest between 30-40 cm. Unlike live roots, decaying rhizome pieces were relatively uniform at 20% of the mass (200 g/ 450 cm^3). Of the sediment components, rhizosphere sediment accounted for 58-118 g sediment/ 450 cm^3, or 5-12% of total mass. Bulk sediment made up the largest fraction of the mass, ranging from 500-600 g/ 450 cm^3, or about half of the total mass in each increment.

4.4.2 Proportion of As in roots and rhizosphere soil. To determine the percentage of As sequestered by roots and rhizosphere sediment in an increment depth, we multiplied the concentration of As found in each separated fraction by the mass of that fraction, which yielded the As content in milligrams. The upper 20 cm from several cores contained elevated rhizosphere As concentrations compared to the bulk As concentrations. When the concentrations were multiplied by the mass fraction (5-12%), total As in the rhizosphere sediment was between 15-57% (Fig. 9). The 10-20 cm depth from Core 1 contained 8 times higher As concentrations compared to the bulk sediment and comprised 56% of the As in the increment with only 10% of the total mass. In Cores 3 and 4, the 20-30 cm depth contained 13% and 18% of the total As within the rhizosphere sediment.

For core depths within the maximum-density root zone (0-10 and 10-20 cm), washed live roots contributed between 0.3-6% of total As. Core 4, however, contained a live root fraction that comprised 24% of the As to the 10-20 cm depth increment, as the roots contained 0.78% As by weight. Dead roots did not contribute more than 5% of As to any depth increment, except in two core increments from 30-40 cm in which 9% (Core 2) and 31% (Core 3) of As was

associated with dead roots. The result of 31% of As in the dead root pool for a single core depth arose from a combination of high As concentrations (0.55%, or 5,500 mg/kg) with a relatively high concentration of dead roots in this depth.

Decaying rhizome comprised 2-30% of core increment mass, but contributed less than 8% of As within the upper 20 cm. One 20-30 cm depth had a decaying rhizome component that made up 18% of total As. In both dead roots and decaying rhizome segments, we might expect to find elevated concentrations of metals (*42-44*). Chen (*19*) suggested that, in decomposing root cells, the cells may act as 'casts' in which metals can accumulate. Conversely, Fe(III) in root plaque might be reduced to Fe(II) when the plant dies and the source of O_2 to the sediment is removed. Further work into the stability of metals in decomposing peat litter would improve our understanding of the ultimate fate of metals concentrated in peat.

4.4.3 Sorption capacity of Fe in plaque and rhizosphere sediment. We investigated the proportion of As to Fe in the root plaque and rhizosphere sediment to determine whether Fe controls As by an adsorptive mechanism. Table 3 displays both the distribution of As and Fe among the extractant pools and the ratio of adsorbed As to total extracted Fe in mmol As/ mol Fe. More than 90% of the As was PO_4-extractable (i.e. strongly adsorbed). The range of As/Fe ratios found in the plaque (42-125 mmoles As/mole Fe) and rhizosphere sediment of live roots (35-218 mmoles As/mole Fe) could be accounted for by the surface site density of hydrous ferric oxides (HFO, $Fe(OH)_3$). HFO is estimated to adsorb 250 mmoles adsorbate per mole of Fe (*45*). Crystalline Fe oxides, such as goethite (α-FeOOH), contain a lesser sorption site density, at approximately 16 mmoles of sorption sites per mole of Fe; as a result, goethite could not account for more than half of the observed adsorbed As (*46*).

Several pieces of evidence are consistent with the hypothesis that aqueous As is transported to the root and adsorbed to predeposited Fe phases in the plaque, rather than being coprecipitated with Fe phases during plaque formation. First, the ratio of As/Fe in ferrihydrite with coprecipitated As is typically higher (~ 700 mmoles As/ mole Fe) than As adsorbed on

ferrihydrite (250 mmoles As/mole Fe) (*47*). Second, sequential extractions of rhizosphere sediment extractions showed that most of the As in the plaque was strongly adsorbed. Despite this evidence, we were surprised that the buildup of plaque on root surfaces over time does not lead to occlusion of adsorbed As previously immobilized, and subsequently appear to be coprecipitated As by the extraction method. This suggests that continual Fe plaque formation after As becomes sorbed to plaque Fe phases does not occur to a great extent.

4.4.4 Experimental uncertainties in quantifying proportions of root-associated As. We have attempted to overcome the experimental challenges inherent to the study of root systems. Significant experimental error may have been introduced by the methods used to separate roots and classify the five pools within each depth increment. The positive findings of high root-associated As in some core sections support the hypothesis that *T. latifolia* roots affect As within the contaminated root zone. The finding of elevated rhizosphere As was detected for one core (Fig. 9, Core #1, 10-20 cm). The lack of elevated rhizosphere As concentrations for other cores might not reflect higher concentrations of As due to experimental error, such as: (i) underestimation of root As contribution from small roots with a relatively high surface area (which would have been erroneously included in the bulk soil component if the method was not sufficient to separate them) or (ii) uneven removal of rhizosphere soil when roots were picked from the soil (i.e. which would also add to the bulk soil As). Thus, the results of high As concentrations in rhizosphere soil and live and dead roots provide only a lower bounds of actual root-associated As, but are useful nonetheless as a constraint on the system.

4.5 Mass balance of Fe & As in root plaques

4.5.1 Iron oxidation of plaque. To determine if oxidation of Fe(II) to Fe(III) in the plaques could be explained by literature-reported O_2 release rates from *T. latifolia* roots, we performed a mass balance calculation. The plaque volume of 8.2 cm^3 per 450 cm^3 of peat calculated in Section 3.3 was used, which corresponded to 27 g wet weight (equivalent to 4.0 g

dry weight) of roots. Assuming an oxygen release rate of 0.2 mmoles/ g dry weight roots per hour (*4; 5*), 4.0 g of dry weight roots, and the stoichiometry of 1 mole of O_2 required to oxidize 4 moles of Fe(II) to $Fe(OH)_3$, we calculated a maximum Fe(II) oxidation rate of 3.2 mmoles/hr if all of the O_2 was used to oxidize Fe(II). This rate of oxidation assumes the limiting reagent is O_2.

To consider the availability of Fe for forming the root plaque, we found that the Fe(II) concentrations in the porewater ranged from 2 to 27 mg/L between 0-20 cm depth (Ch. 3, Fig. 3). A previous study estimated that water drawdown by ET is approximately 6 mm/day in the summer (*48*). For a 450 cm^3 core section (radius of 3.81 cm), the volume of water uptake was calculated by considering the diameter and volume in a cylinder with 6 mm height and accounting for the effective porosity of 0.56 (*49*), which yielded 15 cm^3/ day of water transported to the roots. We calculated the amount of Fe in water pulled to the roots by multiplying the range of porewater Fe(II) concentrations (2-27 mg/L) by the volume of water taken up (15 cm^3/day), which yielded an estimate of between 0.03-0.41 mg Fe/day. Oxidation of this amount of Fe requires only up to 0.5% of the available daily O_2. At a minimum, the roots produced during the growing season of one year would be expected to be actively taking up water in the transpiration stream and precipitating Fe plaque. Gill and Jackson (*50*) reported that an average turnover rate (annual belowground production/ maximum belowground standing crop) of temperate wetland plant roots is 55% (high compared to non-wetland plants), which includes one species of cattail (*Typha glauca*). We assumed that the root production terms in the root turnover rate are directly proportional to the plaque production term. To approximate the concentration of Fe in the plaque that could be produced in one year, we used Eqn 1:

$$\text{Concentration in plaque } \frac{(ug)}{(g\ plaque)} = \frac{M_{increment} \times 1/T_{wetland\ roots}}{V_{plaque} \times p_{plaque}} \qquad \textit{(Eqn. 1)}$$

where,

M = mass of Fe pulled to roots in transpiration stream per year (11,000-150,000 μg/yr),

$T_{wetland\ roots}$ = root turnover (55% per yr),

V_{plaque} = plaque volume calculated for a 450 cm^3 increment of sediment (8.2 cm^3), and

p_{plaque} = plaque density, approximated as 2 g/cm^3 for plant material mixed with ferrihydrite.

The calculation yielded a range of 1,200-17,000 μg Fe/ g plaque produced in one year, or 0.12-1.7% by weight.

In comparison, the average concentration of Fe in plaque measured by XRF microtomography was 2.5% and by extractions was 0.2% Fe. Given all of the assumptions in the Fe plaque concentration calculation and the order-of-magnitude range reported in concentrations, the estimate is in surprisingly good agreement with the measured Fe in the plaque. It is worth mentioning the constraints on and uncertainties associated with a number of variables to more closely evaluate the relative agreement of the calculation and measured concentrations. One of the largest possible sources of error in the calculation is the estimation of plaque volume, particularly because only 1% of the roots were sampled and the results were extrapolated to the whole increment. Another potential source of error is that accumulation of Fe may occur over longer periods than one year for roots that do not turn over (i.e. die) that year. In addition, although the 55% per year turnover rate implies that 55% of the roots are produced every year, the rate is an estimate based on different *Typha* species.

4.5.2 Arsenic stored in plaque The expected As plaque concentration from one year's accumulation due to transpiration uptake of water was calculated, also using Eqn 1. The same parameters were used as for Fe, except with M = 180-1,000 μg/yr (from a porewater As concentration range of 32-190 μg/L and transpiration rate of 15 cm^3/ day). From this calculation, we estimated an As concentration range of 19-110 μg As/g plaque. In comparison, measured As plaque concentrations ranged from 100 μg/g (by XRF microtomography) to 200 μg/g (by extractions of root plaques). Thus, the As plaque concentration can be reasonably

explained from this simple model using root water uptake rates, porewater As concentrations, and root density estimates.

The importance of As sequestered in root plaques compared to the porewater As concentration was estimated using Eqn 2:

$$\text{As porewater concentration if plaque is dissolved } \left(\frac{\text{ug As}}{\text{L}}\right) = \frac{[As]_{plaque} \times V_{plaque} \times p_{plaque}}{V_{porewater\ in\ increment}} \qquad \text{(Eqn. 2)}$$

where,

$[As]_{plaque}$ = average plaque As concentration (100 μg As/ g plaque, from XRF microtomography),

V_{plaque} = plaque volume in the 450 cm^3 core volume, (8.2 cm^3),

p_{plaque} = plaque density (2 g/cm^3), and

$V_{porewater\ in\ increment}$ = porewater volume (0.3 L).

The new As concentration of the porewater, if all of the As in the plaque was dissolved, would therefore be estimated at 5.5 mg As/L. In comparison, porewater in the 0-20 cm depth was measured to be 0.032-0.19 mg/L. Thus, the plaque appears to retain a significant amount of As compared to the aqueous concentration. Sequestration of this As concentration in the plaque would require approximately 100 ± 70 pore volumes of water. Similarly, release of plaque As to the porewater could result in a 100-fold increase in porewater As concentrations, in the absence of As redistribution into solid phases.

5. Conclusions

Arsenic and Fe were highly correlated in the 30 μm thick Fe plaque encircling *T. latifolia* roots from the Wells G & H wetland. Arsenic-to-iron ratios in the plaque ranged from 3 to 125 mmoles As/ mole Fe, determined by both XRF microtomography and chemical extractions. The combination of the molar ratios, the finding that the plaque arsenic was adsorbed, and the

confirmation of predominantly Fe(III) in the plaque support the hypothesis that As is sorbed to amorphous Fe phases such as ferrihydrite in the plaque.

For the first time, the feasibility of oxidation state mapping using XRF microtomography was demonstrated for plant roots. A mixture of As(III) and As(V) phases was observed in all roots tested. Similarly, a previous study showed that the root zone porewater contains a mixture of As oxidation states (*31*). These findings indicate that the plaque plays a role in sorbing both species from the porewater. The possibility that As(III) may be located preferentially in the interior of the root plaque was suggested by our data but needs to be explored further with the analysis of additional roots.

The assessment of the magnitude of As sequestration on roots and in rhizosphere sediment showed that As was concentrated in these pools for two cores in the 10-20 cm depth increment. In the live root zone of one core, the rhizosphere sediment accounted for a significant proportion of the total As corresponding to only a small fraction of the total sediment mass. In another core, live roots (including the plaque) similarly comprised a significant proportion of the total As due to elevated concentrations of As in the roots. In general, with the exceptions noted, most As in the sediment was associated with the bulk sediment. We surmise that the large quantities of As contained in the solid phase is strongly retained in the sediment matrix and thus may not be bioavailable for transport to the roots under these environmental conditions. However, the ability to consistently discern the actual contribution of roots and root-associated sediment to As retention is limited by the methodologies available to separate roots from sediment. A more efficient protocol and a better understanding of the influence of roots on the rhizosphere sediment would be required to more conclusively determine the magnitude of wetland plant-induced retention of As in wetlands.

The concentration of Fe precipitated in the plaque could be reasonably explained using a model of Fe transport to the roots (given the transpiration rate), with oxidation and precipitation as ferrihydrite at the root surface. Analysis of literature values of *T. latifolia* O_2

release compared to Fe(II) available for plaque precipitation revealed that Fe is the limiting factor in determining plaque concentrations, as O_2 should be greatly in excess.

Like Fe, As concentrations in the plaque were in good agreement with the modeled concentrations, indicating that flux of porewater to the roots for transpiration could explain the elevated concentrations observed in the plaque. Modeling of plaque volume with observed As concentrations was supportive of the hypothesis that Fe plaque formation on *T. latifolia* plants in contaminated sediments can impact As cycling in the near-root environment by sequestering As in the plaque.

6. References

(1) Smedley P.; Kinniburgh D. (2002) A review of the source, behaviour, and distribution of arsenic in natural waters. *Appl. Geochem.* **17**, 517-568.

(2) Mitsch W. J.; Gosselink J. G. (1993) *Wetlands*. Van Nostrand Reinhold.

(3) Armstrong W. (1979) Aeration in higher plants. *Adv. Bot. Res.* **7**, 226-332.

(4) Kludze H. K.; DeLaune R. D. (1996) Soil redox intensity effects on oxygen exchange and growth of cattail and sawgrass. *Soil Sci. Soc. Am. J.* **60**, 616-621.

(5) Jespersen D. N.; Sorrell B. K.; Brix H. (1998) Growth and root oxygen release by *Typha latifolia* and its effects on sediment methanogenesis. *Aquat. Bot.* **61**, 165-180.

(6) Taylor G. J.; Crowder A. A. (1984) Formation and morphology of an iron plaque on the roots of *Typha latifolia* L. grown in solution culture. *Am. J. Bot.* **71**, 666-675.

(7) Mendelssohn I.; Kleiss B.; Wakeley J. (1995) Factors controlling the formation of oxidized root channels: a review. *Wetlands* **15**(1), 37-46.

(8) van der Nat F.; Middelburg J. (1998) Effects of two common macrophytes on methane dynamics in freshwater sediments. *Biogeochem.* **43**, 79-104.

(9) Gerard G.; Chanton J. (1993) Quantification of methane oxidation in the rhizosphere of emergent aquatic macrophytes: defining upper limits. *Biogeochem.* **23**, 79-97.

(10) Hinsinger P. (1998) How do plant roots acquire mineral nutrients? Chemical processes involved in the rhizosphere. In *Adv. Agron.*, Vol. 64, pp. 225-265. Academic Press.

(11) Ye Z. H.; Baker A. J. M.; Wong M. H.; Willis A. J. (1997) Copper and nickel uptake, accumulation, and tolerance in *Typha latifolia* with and without iron plaque on the root surface. *New Phytol.* **136**, 481-488.

(12) Dunbabin J. S.; Pokorny J.; Bowmer K. H. (1988) Rhizosphere oxygenation by *Typha domingensis* Pers. in miniature artificial wetland filters used for metal removal from wastewaters. *Aquat. Bot.* **29**, 303-317.

(13) Hill B. M.; Siegel D. I. (1991) Groundwater-flow and the metal content of peat. *J. Hydrol.* **123**(3-4), 211-224.

(14) Shotyk W. (1988) Review of the inorganic geochemistry of peats and peatland waters. *Earth-Sci. Rev.* **25**, 95-176.

(15) Doyle M. O.; Otte M. L. (1997) Organism-induced accumulation of iron, zinc, and arsenic in wetland soils. *Environ. Poll.* **96**, 1-11.

(16) Otte M. L.; Kearns C. C.; Doyle M. O. (1995) Accumulation of arsenic and zinc in the rhizosphere of wetland plants. *Bull. Environ. Contami. Toxicol.* **55**, 154-161.

(17) Otte M. L.; Dekkers M. J.; Rozema J.; Broekman R. A. (1991) Uptake of arsenic by *Aster tripolium* in relation to rhizosphere oxidation. *Can. J. Bot.* **69**, 2670-2677.

(18) Taylor G. J.; Crowder A. A. (1983) Uptake and accumulation of copper, nickel, and iron by *Typha latifolia* L. grown in solution culture. *Can. J. Bot.* **61**, 1825-1830.

(19) Chen C. C.; Dixon J. B.; Turner F. T. (1980) Iron coatings on rice roots: Morphology and models of development. *Soil Sci. Soc. Am. J.* **44**, 1113-1119.

(20) Bacha R.; Hossner L. (1977) Characteristics of root coatings formed on rice roots as affected by iron and manganese additions. *Soil Sci. Soc. Am. J.* **41**, 931-935.

(21) Wang T.; Peverly J. H. (1996) Oxidation states and fractionation of plaque iron on roots of common reeds. *Soil Sci. Am. J.* **60**, 323-329.

(22) St-Cyr L.; Crowder A. (1988) Iron oxide deposits on the roots of Phragmites australis related to the iron bound to carbonates in the soil. *J. Plant Nutr.* **11**, 1253-1261.

(23) Wang T.; Peverly J. (1999) Iron oxidation states on root surfaces of a wetland plant (*Phragmites australis*). *Soil Sci. Soc. Am. J.* **63**, 247-252.

(24) Hansel C. M.; Fendorf S. (2001) Characterization of Fe plaque and associated metals on the roots of mine-waste impacted aquatic plants. *Environ. Sci. Technol.* **35**, 3863-3868.

(25) Hansel C.; LaForce M.; Fendorf S.; Sutton S. (2002) Spatial and temporal association of As and Fe species on aquatic plant roots. *Environ. Sci. Technol.* **36**(9), 1988-1994.

(26) Caldwell M. M.; Virginia R. A. (1989) Root Systems. In *Plant Physiological Ecology: Field methods and instrumentation* (ed. Pearcy, R. W.;Ehleringer, J.;Mooney, H. A.;Rundel, P. W.), pp. 432. Chapman and Hall.

(27) Boehm W. (1980) *Methods of Studying Root Systems*. Springer-Verlag.

(28) Curl E. A.; Truelove B. (1986) *The Rhizosphere*. Springer-Verlag.

(29) Aurilio A.; Durant J. L.; Hemond H. F.; Knox M. L. (1995) Sources and distribution of arsenic in the Aberjona watershed, Eastern Massachusetts. *Water, Air, Soil Poll.* **81**, 265-282.

(30) Keon N. E.; Swartz C. H.; Brabander D. J.; Harvey C.; Hemond H. F. (2001) Validation of an arsenic sequential extraction method for evaluating mobility in sediments. *Environ. Sci. Technol.* **35**, 2778-2784.

(31) Keon N.; Swartz C.; Brabander D.; Myneni S.; Hemond H. (2002) Geochemical controls on arsenic speciation in contaminated wetland peat and riverbed sediments. Chapter 3.

(32) Orson R. A. (1996) The Aberjona River Marsh System: A paleoecological investigation of wetland development in the vicinity of Well H. Orson Environmental Consulting.

(33) Eng P.; Newville M.; Rivers M.; Sutton S. (1998) Dynamically figured Kirkpatrick Baez X-ray microfocusing optics. In *X-Ray Microfocusing: Applications and Technique, SPIE Proc. 3449* (ed. McNulty, I.), pp. 145.

(34) Rivers M.; Sutton S.; Eng P. (1999) Geoscience applications of x-ray computed microtomography. In *Developmens in X-Ray Tomography II, SPIE Proc. 3772*, pp. 78-86.

(35) Ressler T. (2001) WinXAS. http://www.winxas.de/

(36) Fifield J. (1981) Peat Hydrology in Two New England Salt Marshes. M.S. Thesis, Massachusetts Institute of Technology.

(37) Nordstrom D. K.; Wilde F. D. (1998) National field manual for the collection of water-quality data: Reduction-oxidation potential (electrode method). In *U.S. Geological Survey Techniques of Water-Resources Investigations*, Vol. 9, pp. section 6.5.2.

(38) Valiela I.; Teal J.; Persson N. (1976) Production and dynamics of experimentally enriched salt marsh vegetation: Belowground biomass. *Limnol. Oceanogr.* **21**(2), 245-252.

(39) Leistel J.; Marcoux E.; Thieblemont D.; Quesada C.; Sanchez A.; Almodovar G.; Pascual E.; Saez R. (1998) The volcanic-hosted massive sulphide deposits of the Iberian Pyrite Belt. *Miner. Deposita* **33**, 2-30.

(40) Brabander D.; Keon N.; Stanley R.; Hemond H. (1999) Intra-ring variability of Cr, As, Cd, and Pb in red oak revealed by secondary ion mass spectrometry: Implications for environmental biomonitoring. *PNAS* **96**(25), 14635-14640.

(41) Pierce M. L.; Moore C. B. (1982) Adsorption of arsenite and arsenate on amorphous iron hydroxide. *Water Res.* **16**, 1247-1253.

(42) Dunbabin J. S.; Bowmer K. H. (1992) Potential use of constructed wetlands for treatment of industrial wastewaters containing metals. *Sci. Tot. Environ.* **111**, 151-168.

(43) Orson R. A.; Simpson R. L.; Good R. E. (1992) A mechanism for the accumulation and retention of heavy metals in tidal freshwater marshes of the upper Delaware River estuary. *Estuar. Coast. Shelf Sci.* **34**, 171-186.

(44) Gallagher J. L.; Kibby H. V. (1980) Marsh plants as vectors in trace metal transport in Oregon tidal marshes. *Am. J. Bot.* **67**(7), 1069-1074.

(45) Dzombak D. A.; Morel F. M. M. (1990) *Surface Complexation Modeling: Hydrous Ferric Oxide*. John Wiley & Sons, Inc.

(46) Ali M.; Dzombak D. (1996) Competitive sorption of simple organic acids and sulfate on goethite. *Environ. Sci. Technol.* **30**(4), 1061-1071.

(47) Fuller C. C.; Davis J. A.; Waychunas G. A. (1993) Surface chemistry of ferrihydrite: Part 2. Kinetics of arsenate adsorption and coprecipitation. *Geochim. Cosmochim. Acta* **57**, 2271-2282.

(48) Zeeb P. (1996) Piezocone Mapping, Groundwater Monitoring, and Flow Modeling in a Riverine Peatland: Implications for the transport of arsenic. Ph.D. Dissertation, Massachusetts Institute of Technology.

(49) Gill R.; Jackson R. (2000) Global patterns of root turnover for terrestrial ecosystems. *New Phytol.* **147**, 13-31.

Table 1. Classification and separation methodology of wetland core 10 cm increments. After roots were separated from the sediment by hand in a N_2-purged glove bag, they were washed with a fine spray of deoxygenated water over a 0.25 mm mesh size, 25 cm diameter polyethylene sieve. Sediment particles (<0.25 cm) washed from the roots was classified as *rhizosphere sediment*. Sediment remaining after roots were picked out of the core increment was placed in a 2.5 mm mesh size, 25 cm diameter sieve and washed. Sediment that passed through the sieve was classified as *bulk sediment*, and material that remained on the sieve were termed *decomposing rhizome*.

Pool	Separation method & description of pool
Live roots	> 0.25 mm roots; cylindrical; white or orange-colored
Dead roots	> 0.25 mm roots; flattened; black; apparently decomposing roots
Rhizosphere sediment	< 0.25 mm sediment washed from live & dead roots
Decaying rhizome	> 2.5 mm pieces of decomposing rhizome; flat ~ 1-5 cm pieces of dead rhizome
Bulk sediment	< 2.5 mm sediment particles washed from peat after removal of roots

Table 2. Sequential extraction procedure used to remove plaque from live roots. The method is an abbreviated version of that described by Keon et al. (2001), wherein As is differentiated into soluble, adsorbed and co-precipitated pools. This shortened method does not attempt to separate amorphous from crystalline Fe phases, as the method was used here to determine whether As was adsorbed or co-precipitated to Fe phases in the plaque.

Step	Extractant	Target phase	Possible mechanism
DI	Deoxygenated Milli-Q water, pH 5, 25°C one repetition	Soluble As	
Mg	1 M $MgCl_2$, pH 8, 2 h, 25°C one repetitions + one water wash	ionically bound As	anion exchange of Cl for As; possible Mg-As complex
PO_4	1 M NaH_2PO_4, pH 5, 16 & 24 h, 25°C one repetition of each time duration + one water wash	strongly adsorbed As	anion exchange of PO_4 for AsO_4 & AsO_3
Ti	0.05 M Ti(III)-citrate-EDTA-bicarbonate, pH 7, 2 h, 25°C one repetitions + one water wash	As coprecipitated with Fe hydroxides (amorphous & crystalline), Al oxides, Mn oxides, carbonates, and acid volatile sulfides	reduction of Fe(III) to Fe(II); partial oxidation of amorphous As sulfides by Fe(III)-citrate complexes

Table 3. A. Fe and As concentrations (μg As or Fe/ g wet roots) in extractants of live root plaques (except 30-40 cm, where dead roots were used for lack of live roots) from 10 cm depth increments. Percentages of Fe and As in extractants compared to totals extracted are listed in italics. **B.** Ratio of extractable As to Fe in root plaque (results shown in A, normalized for As and Fe molecular weights). Ratios of As/Fe are also shown for rhizosphere soil (extractions not shown).

A	DI	%	Mg	%	PO_4	%	TiCEB	%	Total
As									
0-10 cm	4	*1*	4	*1*	326	*95*	7	*2*	342
10-20 cm	2	*2*	2	*2*	73	*95*	1	*1*	78
20-30 cm	21	*6*	12	*3*	331	*91*	1	*0*	365
30-40 cm	18	*6*	25	*9*	240	*83*	5	*2*	287
Fe									
0-10 cm	124	*6*	50	*3*	877	*45*	916	*47*	1968
10-20 cm	22	*2*	165	*12*	847	*63*	318	*24*	1352
20-30 cm	101	*2*	116	*2*	916	*19*	3791	*77*	4924
30-40 cm	52	*2*	331	*12*	981	*34*	1515	*53*	2880

B	**Plaque** (mmol As/ mol Fe)	**Rhizosphere Sediment** (mmol As/ mol Fe)
0-10 cm	125	35
10-20 cm	42	30
20-30 cm	53	88
30-40 cm	72	218

Figure 1. *In-situ* measurements of pH and platinum electrode potential for 3 wetland sediment cores with 1σ standard deviation (Core 1, x; Core 2, circles; Core 3, squares). Each plant core depth is the average of 3 measurements. Platinum electrode potential is corrected by +209 mV to reference to a standard H_2 electrode. The data profiles show that pH is typically more acidic in the root zone (upper 20 cm) and redox conditions are more oxidizing.

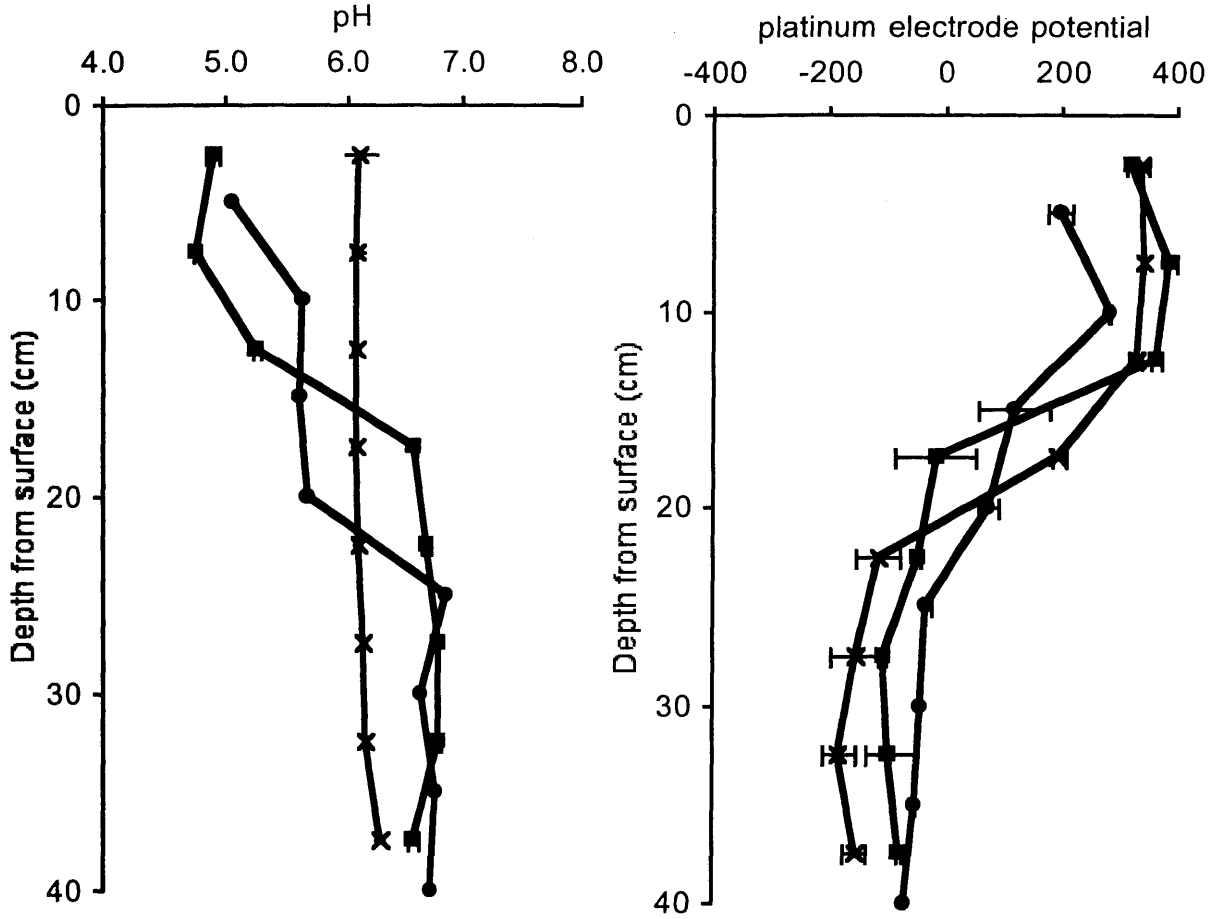

Figure 2. Unwashed (A,B) and distilled-water washed (C,D) live *T. latifolia* roots imaged by backscatter SEM using variable pressure to image uncoated, unimpregnated samples. Washed roots are devoid of the adhered particles (Fig. 2C,D), although the particles in Fig. 2A & B did not appear to contribute significantly to the Fe plaque thickness determined by microtomography. Bright areas correspond to high atomic mass unit (AMU) elements such as Fe. Using energy-dispersive x-ray analysis, we found that Fe comprised approximately 18% of the plaque.

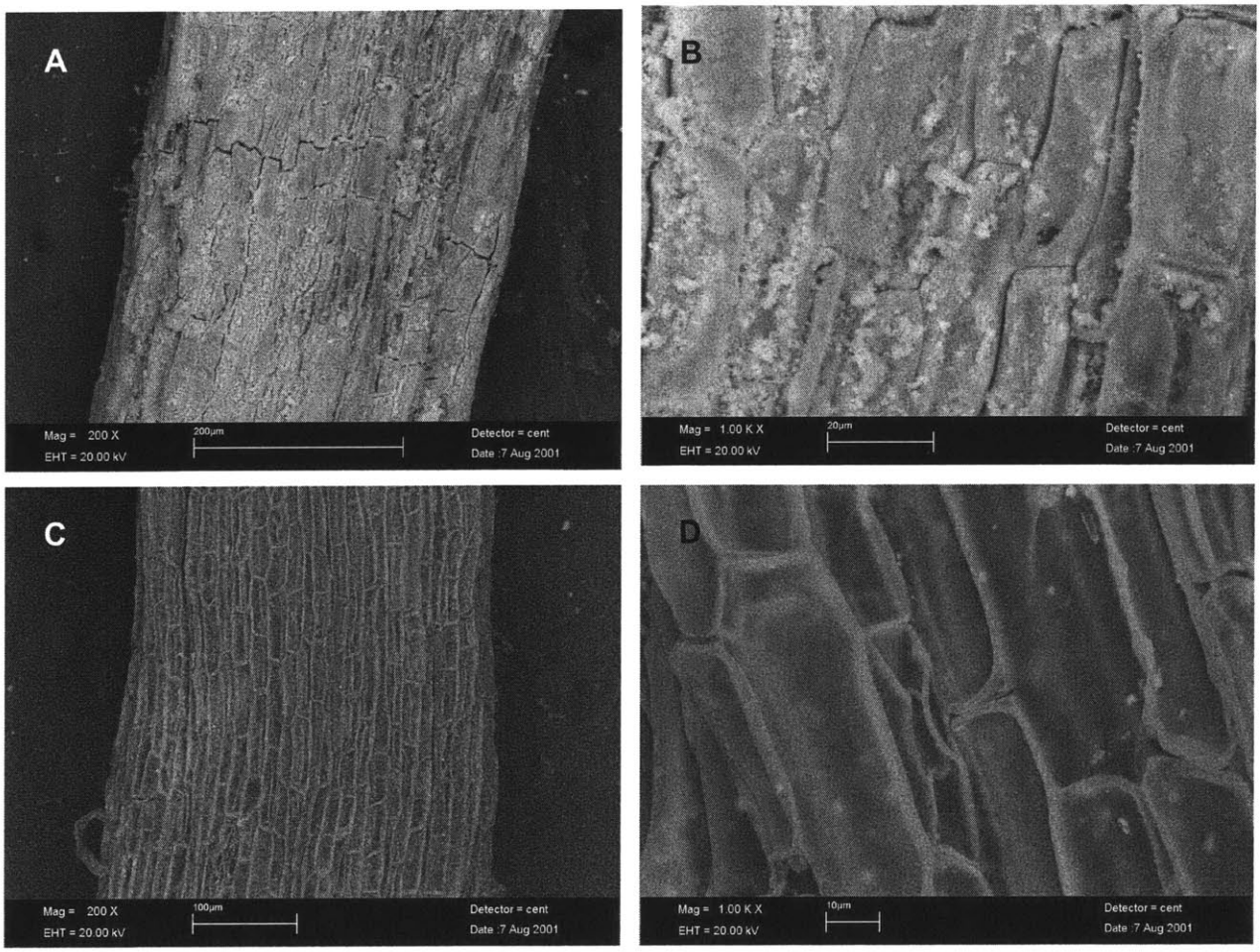

Figure 3A-E. Fluorescence microtomography images of a cross section through a 300 μm diameter *T. latifolia* root, shown in Fig. 2A. Fluorescence data were obtained using a 16.3 keV x-ray beam. The root was translated in 10 μm steps through the 3 μm x-ray beam, followed by rotation of 5 degrees through the z-axis, repeating this sequence for a total of 180 degrees rotation. Dwell time on each element s white line energy was 1 second per step. Higher intensities of fluoresence corresponding to higher concentrations are nearer to the hot end of the color spectrum (white then red, orange, etc). Color spectra was optimized to show the range for each element, thus the elemental maps are not comparable in concentration.

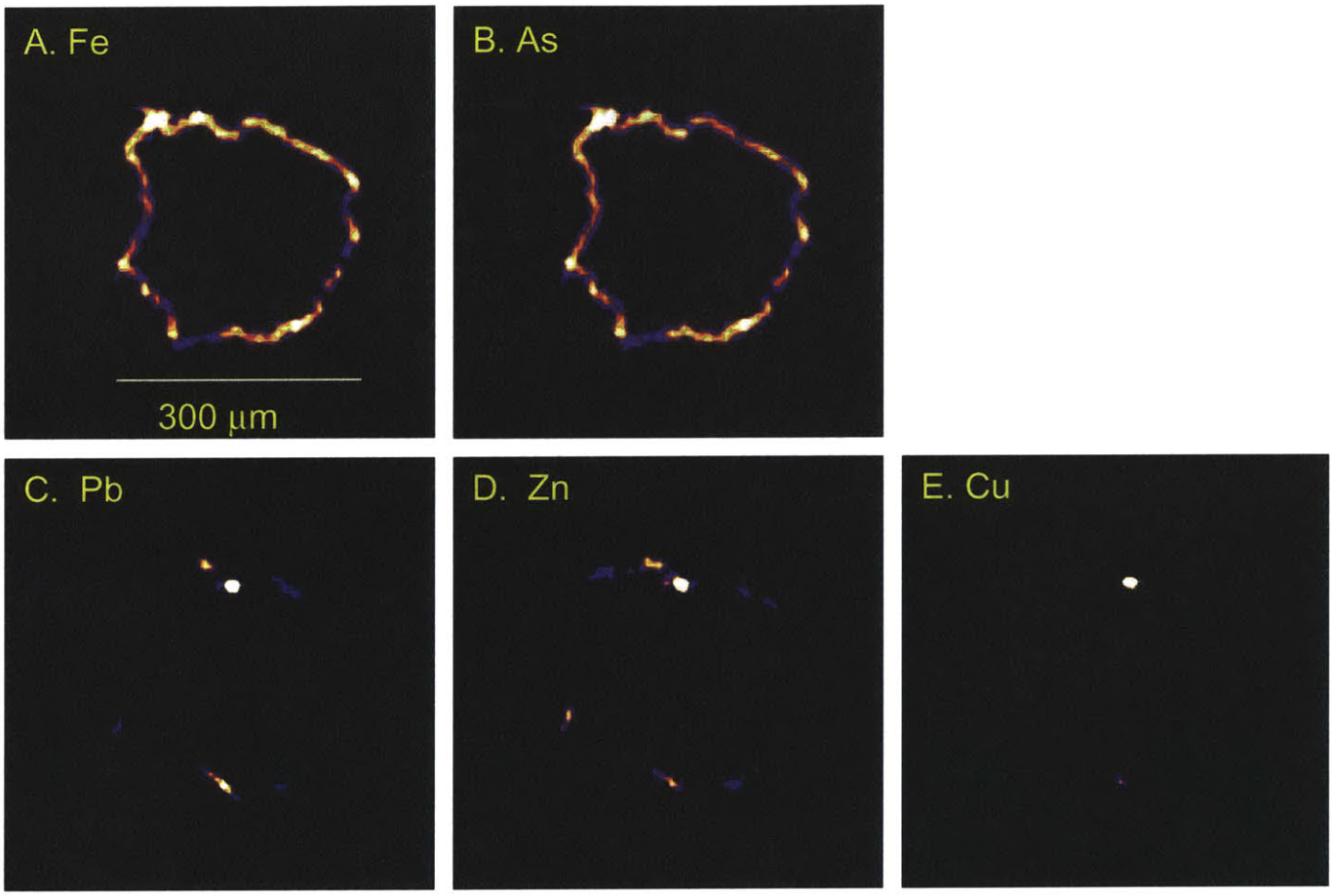

Figure 4. Correlation plot of As versus Fe for the 300 μm root shown in Figure 3A-E. Each point is the fluorescence intensity for a 10 μm step, with a 3 μm beam width. Intensity is directly proportional to the additive count rate for all detectors. The correlation between As and Fe is excellent on a scale of 10 μm steps.

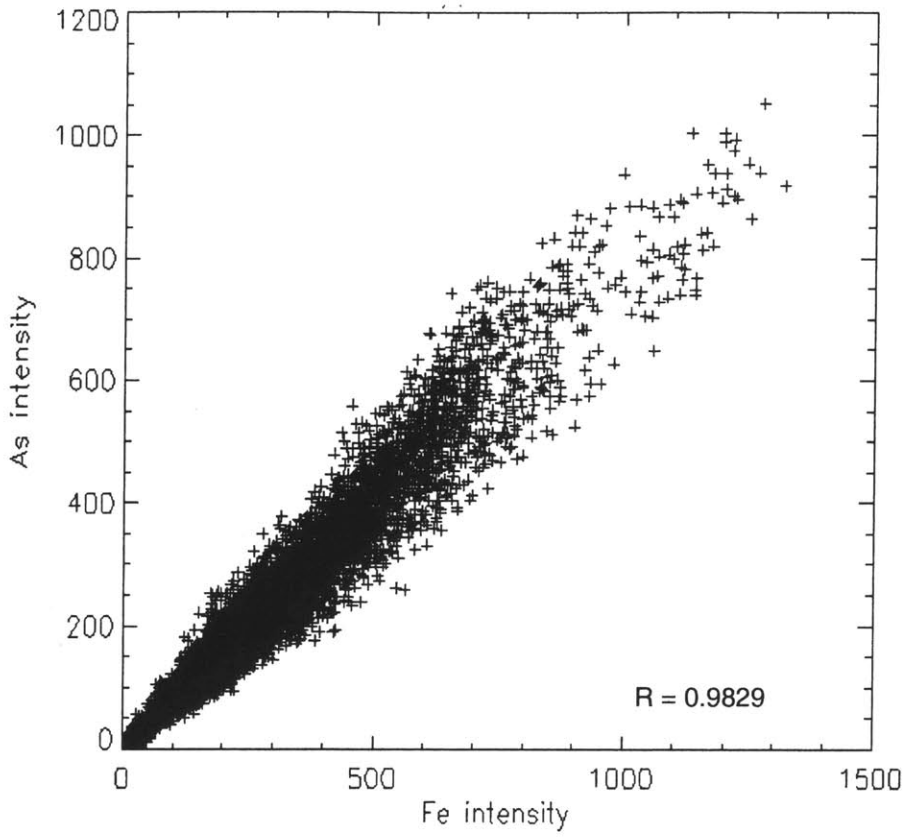

Figure 5. As K-edge x-ray fluorescence averaged spectrum (n = 19) of a 300 μm diameter root cross-section using a defocused 400 μm beam width and height. To prevent oxidiation during analysis, the root was preserved in oil and flushed with He during the run. Data points are represented by circles. The solid line is the data curve fit using As(III) and As(V) on FeOOH as model compounds, which shows that the plaque is comprised of approximately 20% As(III) and 80% As(V).

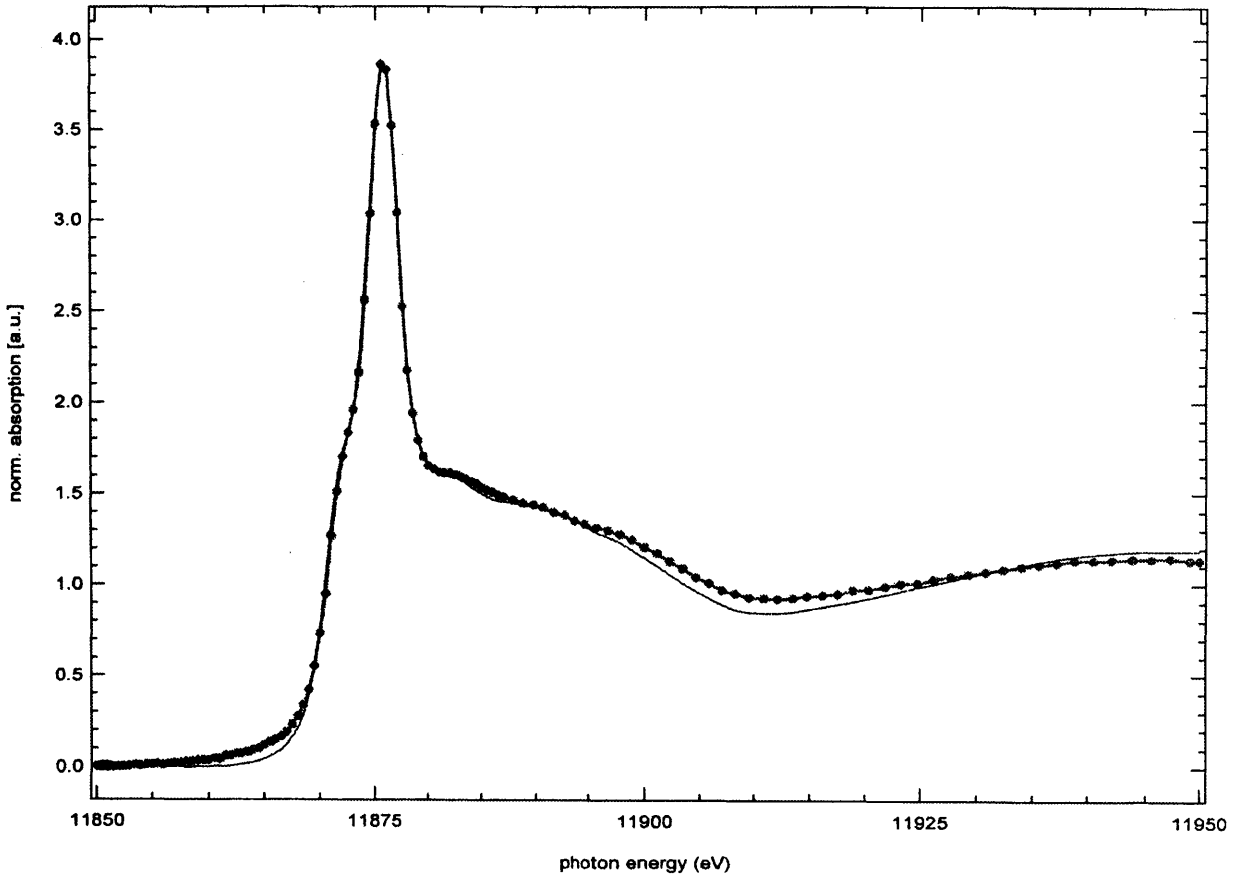

Figure 6. Iron XANES averaged spectrum (n = 7) of the same 300 μm root analyzed in Fig. 5 using a defocused 400 μm beam width and height. In this figure, the sample curve is shown with the XANES spectra for model compounds, including siderite ($FeCO_3$), green rust ($Fe_{6-x}(II)Fe_x(III)(OH)_{12}[(SO_4)_{x/2}\cdot 3H_2O]$), magnetite ($Fe(II)Fe(III)_2O_4$), ferrihydrite ($Fe_2O_3\cdot nH_2O$), and goethite (α-FeOOH). The dotted and solid lines show where the Fe(II) and Fe(III) edges are, respectively.

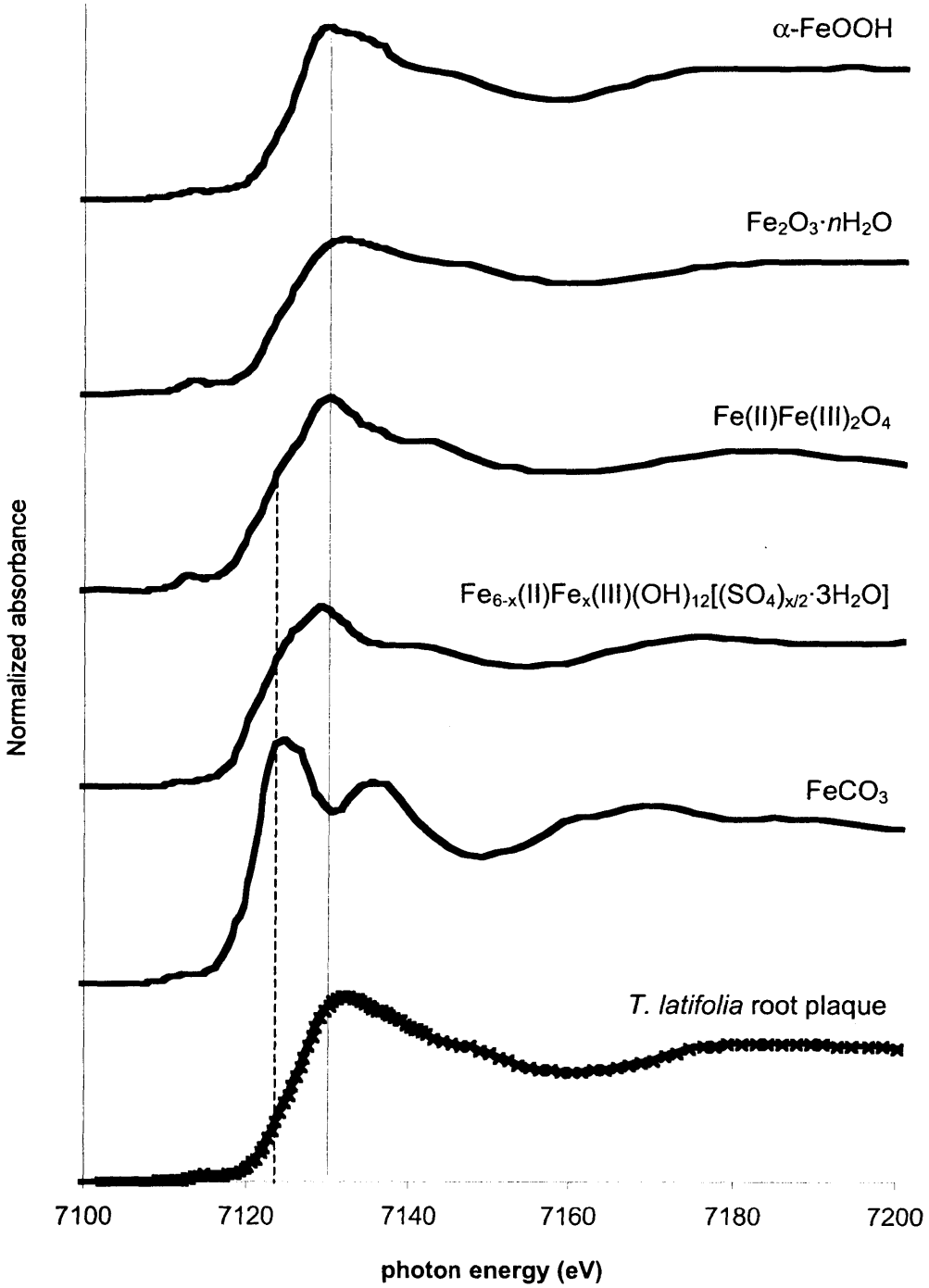

Figure 7. Oxidation state map of As in the root plaque. Weighted redox means are As^{3+} = 43%, As^{5+} = 57%. As^{3+}/ As^{5+} is generally heterogeneous, although there appears to be a tendency for As^{3+} to be in the interior (e.g., circled area). For the As(III) map, the color bar reflects the proportion of As(III) compared to total As. Total As (in μg/g) is shown in the color bar next to image (B). The average As concentration was found to be 105 μg/g, with isolated hotspots as high as 785 μg/g.

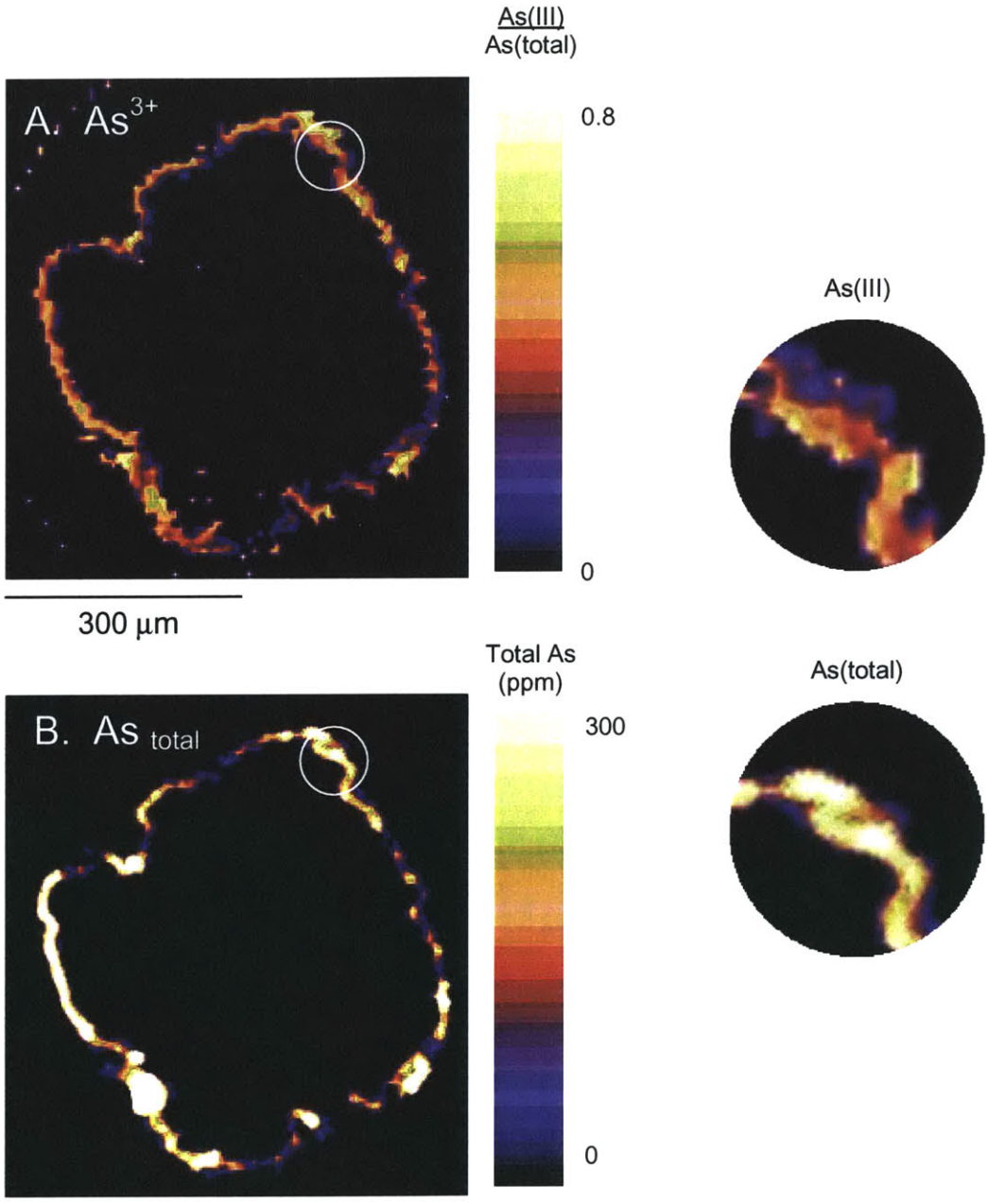

Figure 8. (A) Distribution of different core pools in 10 cm depth increments, in grams of biomass or sediment per core increment. Each depth increment is the average of four cores with 1σ standard deviation shown as error bars. Most of the core mass is bulk sediment, followed by decaying rhizome, and either roots or rhizosphere sediment. (B) Enlarged region of the x-axis to show the variation in live and dead root biomass as a function of depth. Live roots are concentrated in the upper 20 cm, whereas dead roots are greatest below the live root zone at 20-40 cm.

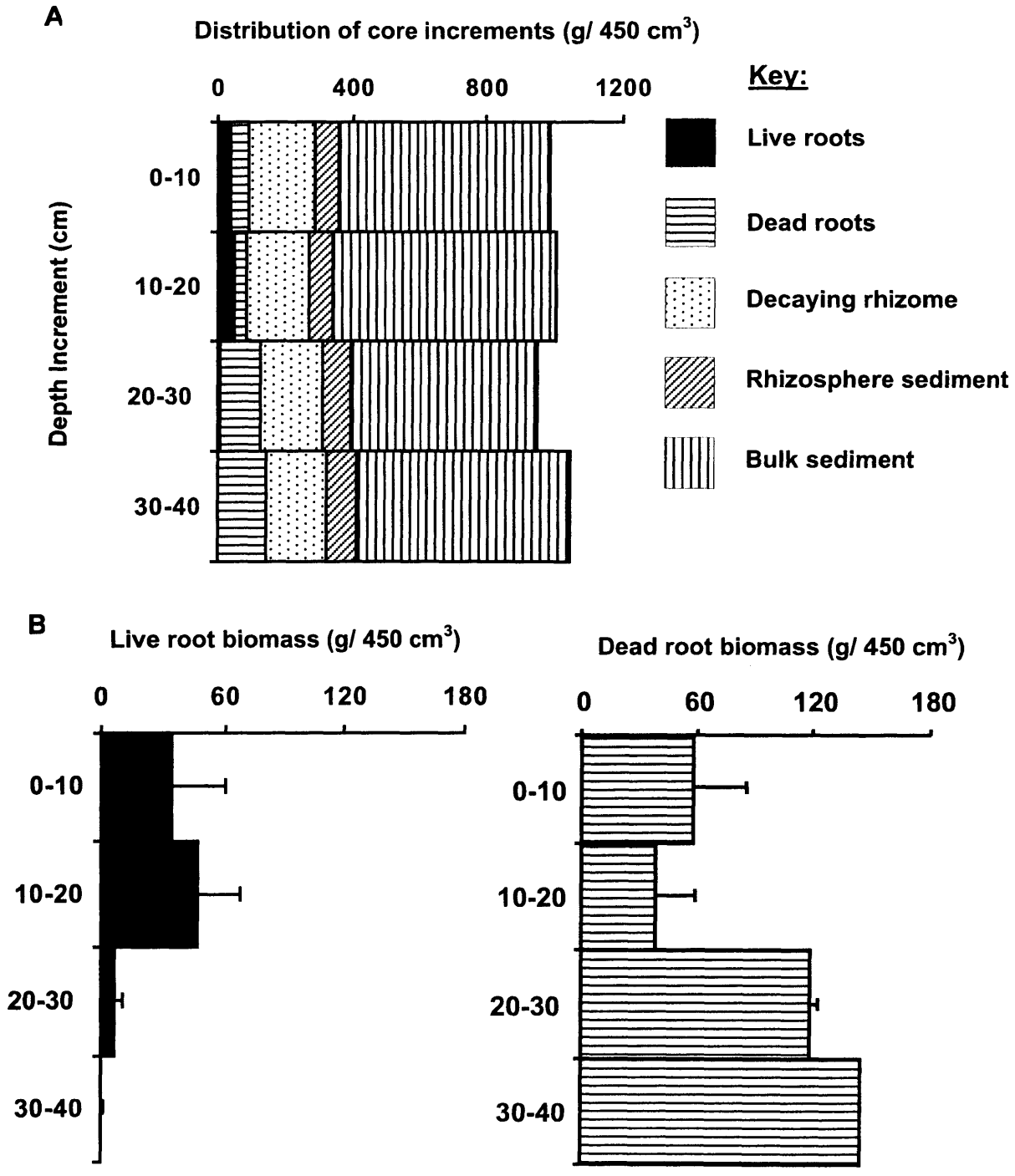

Figure 9. A. Arsenic concentrations for 10-cm depth increments for four sediment cores. B. Fraction of As found in each of the following 5 classifications: live roots, dead roots, decaying rhizomes, rhizosphere sediment, and bulk sediment. Arsenic concentrations shown in (A) were normalized by the fraction of biomass calculated from Figure 8 to give the proportion of As made up by each pool.

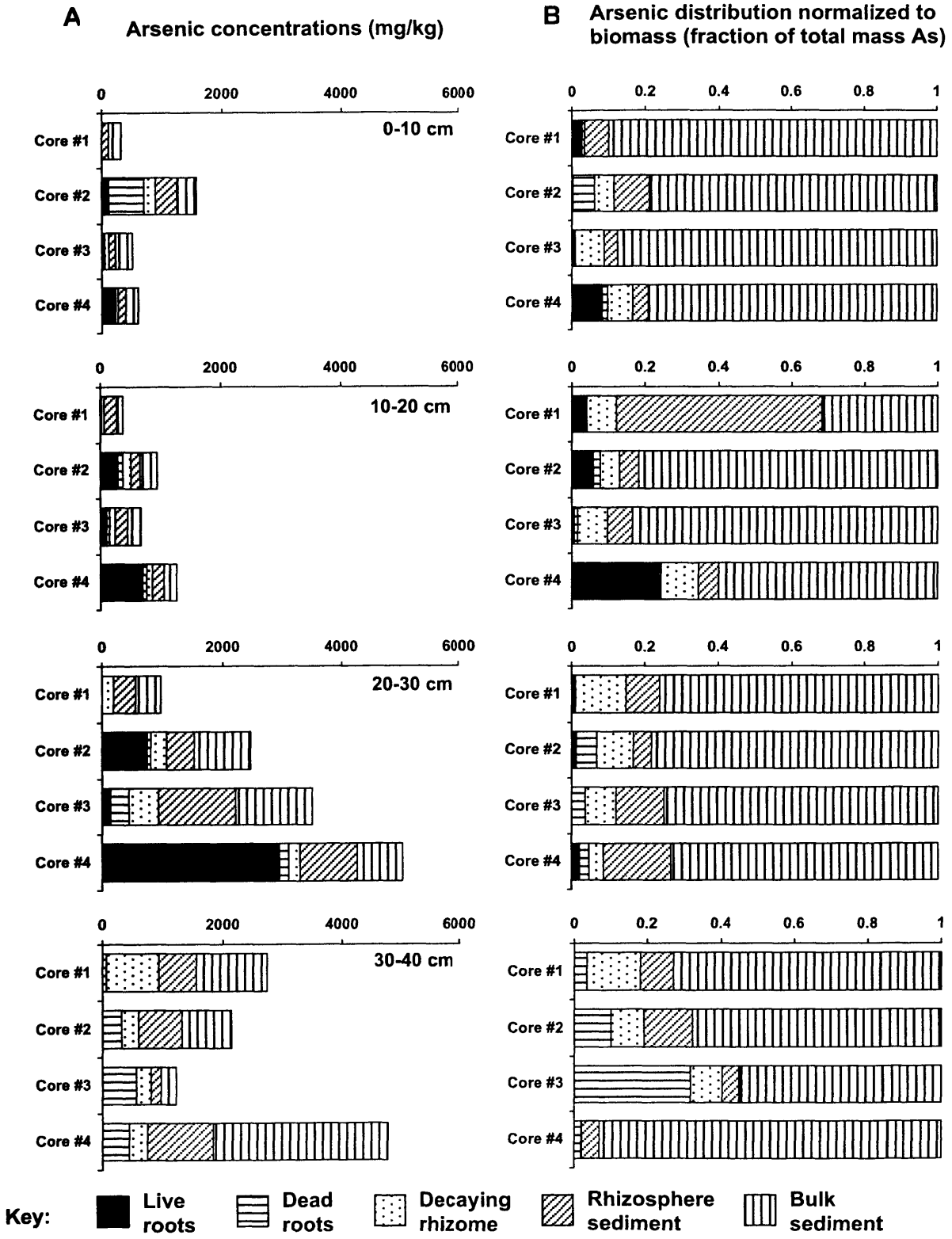

Appendices

Appendix A. Sediment Cores

Appendix B. Construction of pH-pe Diagrams

Appendix C. Mineral Identification in Sediment Cores

Appendix D. X-Ray Absorption Spectroscopy Data Fitting

Appendix E. *T. latifolia* SEM Images & Elemental Maps

Appendix A. Sediment Cores.

Table I. Sediment cores for geochemical analysis were retrieved from a 120 m^2 area of the Wells G & H wetland, to the east of the Aberjona River between the river and the upland. Core IDs are labeled "W" for wetland and "R" for riverbed. Locations of the cores are shown in Figure I. Cores were taken when fresh sediment was required for experimental procedures, in different seasons and during both dry and flooded periods. No discernable pattern in extractable or porewater As was found for the different conditions. Different core lengths resulted from variable recoveries of sediment in the corer, which led to the corer modifications discussed in Chapter 3 and shown in Figure II.

Date collected	**Core ID #** (Ch. 3, Fig. 2)	**Archived sample ID**	**Length of core**	**Reason for collection**	**Notes**
8/4/97	#1W	C1-97	54 cm	Testing piston corer; determination of elemental profiles	Flooded wetland
8/12/97	#5W	C2-97	92 cm	Determination of elemental profiles	No standing water
8/19/97	#2W	C3-97	90 cm	Determination of elemental profiles	
12/10/98	#6W	C8-98	43 cm	Extractions & method development	Comprehensive geochemical analyses
6/23/99	#1R	C1-99	53 cm	Long core for extractions	Poor sediment recovery in meter-long core
7/7/99	#2R	C2-99	100 cm	Long core for extractions	Dry year; Shallow river ~1 ft deep
9/2/99	#3W	C4-99	105 cm	Long core for extractions	Water table low between about 35-40cm
5/29/00	#4W	C1-00	95 cm	Fresh sediment for XAS analysis	
5/29/00	#3R	C2-00	85 cm	Fresh sediment for XAS analysis	River was high & wide, difficulty sampling

Figure I. Wells G & H wetland map. Inset depicts the location of the cores retrieved from the wetland for geochemical analysis.

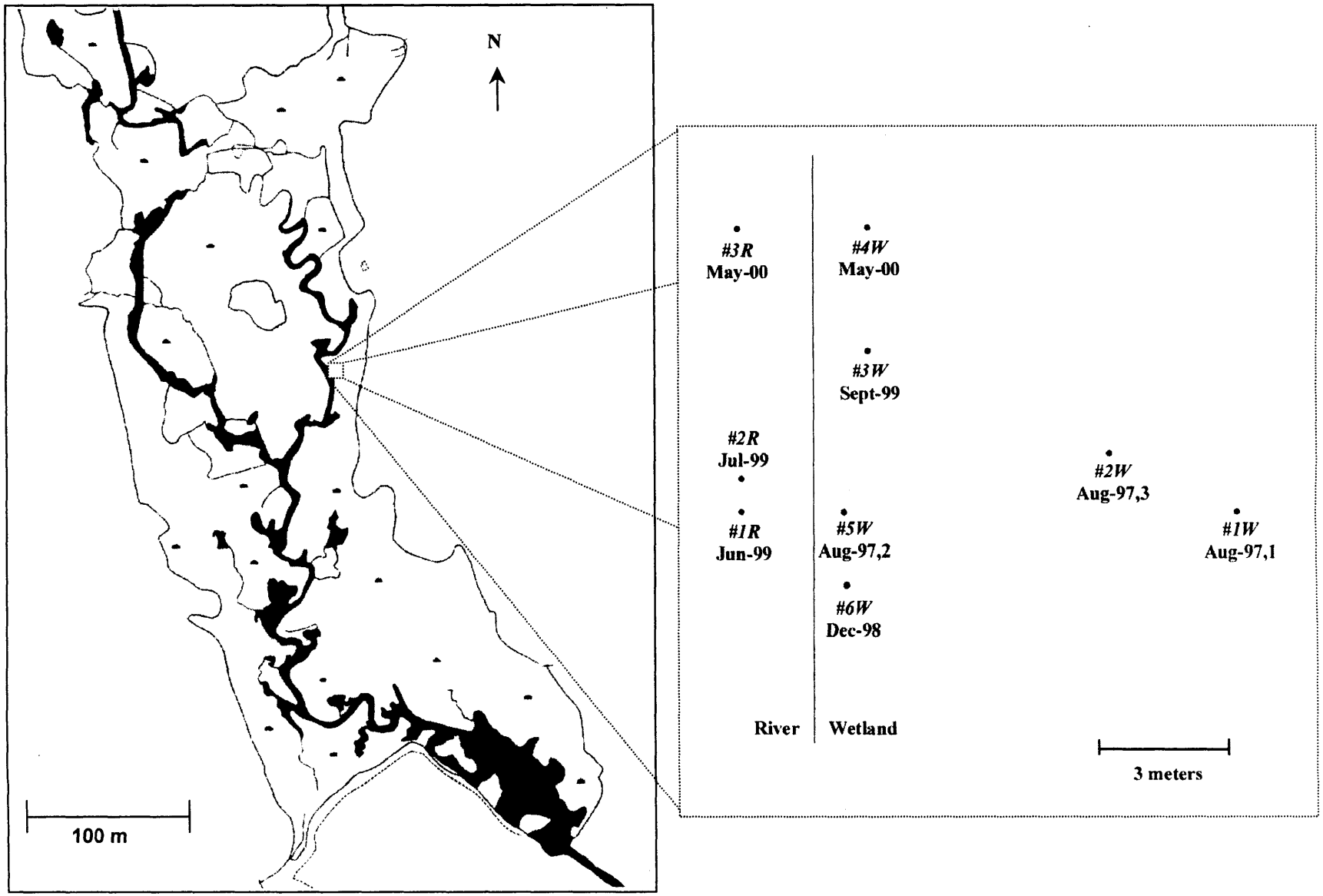

Figure II. Corer design (modified from Fifield, 1981).

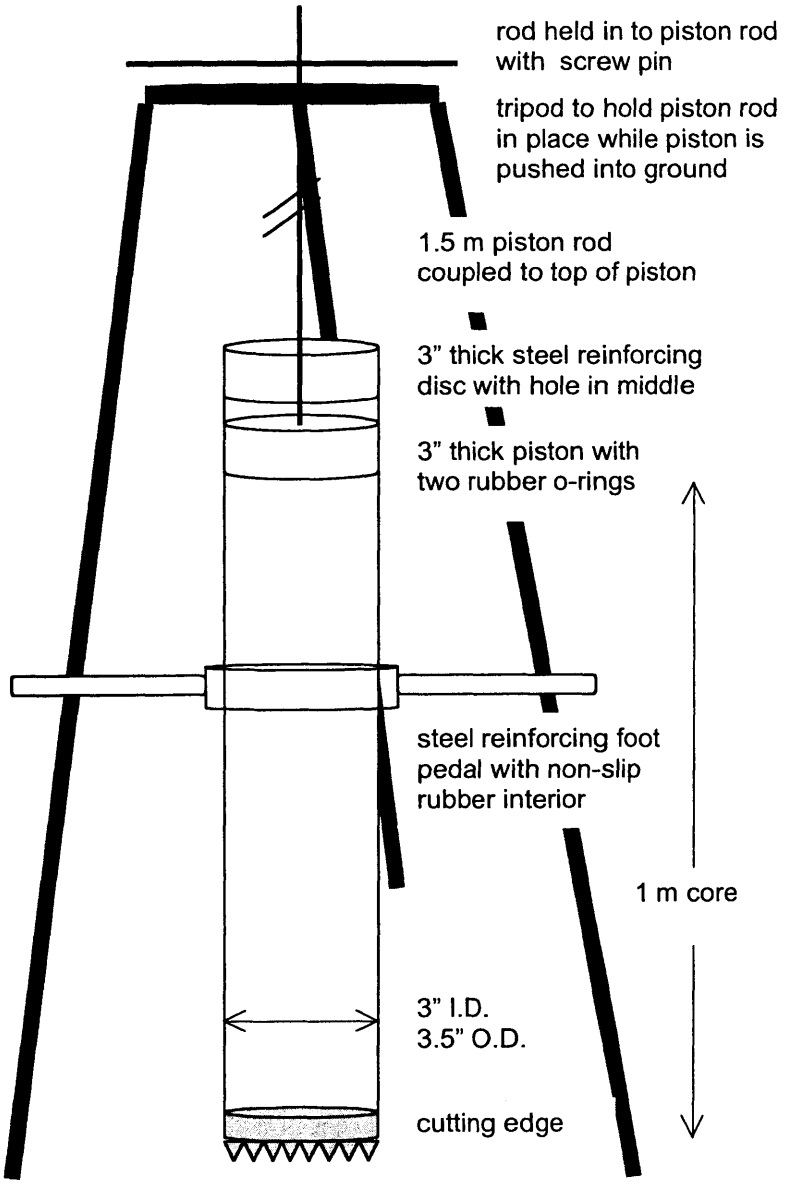

Appendix B. Construction of pH-pe diagrams

B.1. Geochemical reactions. Geochemical modeling of measured pH and redox values was used to predict the porewater and solid phases expected in the wetland and riverbed sediments. pH-pe diagrams were constructed from porewater measurements, according to the method of Stumm and Morgan (*1*). The typical pH range of 4-8 found in these environments was used to limit the reactions selected for consideration in the diagrams. Table I includes the redox reactions considered in Ch. 3-Fig. 4, and Table II contains the reactions dependent on pH.

Table I.

Redox reaction:	Function of pe:
$Fe^{3+} + e^- = Fe^{2+}$	$pe = 13 + \log[Fe^{3+}]/[Fe^{2+}]$
$Fe(OH)_{3\,(amorph,\,s)} + 3H^+ + e^- = Fe^{2+} + 3H_2O$	$pe = 16 - \log[Fe^{2+}] - 3pH$
$Fe(OH)_{3\,(amorph,\,s)} + 2H^+ + HCO_3^- + e^- = FeCO_3 + 3H_2O$	$pe = 16.2 - 2\,pH + \log[HCO_3^-]$
$HAsO_4^{2-} + 4H^+ + 2e^- = H_3AsO_3 + H_2O$	$pe = 14.95 - 2pH + 0.5\,\log[HAsO_4^{2-}]/[H_3AsO_3]$
$H_2AsO_4^- + 3H^+ + 2e^- = H_3AsO_3 + H_2O$	$pe = 11.45 - 1.5pH + 0.5\log[H_2AsO_4^-]/[H_3AsO_3]$
$SO_4^{2-} + 9H^+ + 8e^- = 8HS^- + 4H_2O$	$pe = 4.25 - 1.125pH + 0.125\,\log\,[SO_4^{2-}]/[HS^-]$

Table II.

Reaction:	Function of pH:
$Fe(OH)_3 + H_2O = Fe(OH)_4^- + H^+$	$pH = 19.2 + \log\,[Fe(OH)_4^-]$
$Fe^{2+} + HCO_3^- = FeCO_{3\,(s)} + H^+$	$pH = 0.25 - \log\,[Fe^{2+}] - \log\,[HCO_3^-]$
$H_2AsO_4^- = HAsO_4^{2-} + H^+$	$pH = 6.9 + \log\,[HAsO_4^{2-}]/[H_2AsO_4^-]$
$H_2S = HS^- + H^+$	$pH = 7 + \log\,[HS^-]/[H_2S]$
$H_2CO_3 = HCO_3^- + H^+$	$pH = 6.3 + \log\,[HCO_3^-]/[H_2CO_3]$

Table III. List of formation reactions for common minerals (disordered and crystalline), including the equilibrium constants (I=0; 25°C). All constants are from the Mineql+ v.4.0 database, except amorphous As_2S_3[‡], which was obtained from Eary (*2*). Note that the formation constants are shown here; solubility products K_{sp} used in calculating oversaturation have the opposite sign as formation constants.

Formation Reaction	log K	Solid species	Color
$Fe^{3+} + 3H_2O = Fe(OH)_{3\,(amorph,\,s)}$	-4.891	ferrihydrite	red-brown
$Fe^{3+} + 2H_2O = FeOOH_{\,(s)} + 3H^+$	-0.500	goethite	yellow-brown
$Fe^{3+} + 2H_2O = FeOOH_{\,(s)} + 3H^+$	-1.371	lepidocrocite	orange
$2Fe^{3+} + 3H_2O = Fe_2O_{3\,(s)} + 6H^+$	4.008	hematite	red
$2Fe^{3+} + 3H_2O = Fe_2O_{3\,(s)} + 6H^+$	-6.386	maghematite	red-brown
$Fe^{2+} + 2Fe^{3+} + 4H_2O = Fe_3O_{4\,(s)} + 8H^+$	-3.737	magnetite	grey to black
$Fe^{2+} + 2H_2O = Fe(OH)_{2\,(amorph,\,s)}$	-12.10	amorphous $Fe(OH)_2$	
$Fe^{3+} + 2H_2O + AsO_4^{3-} = FeAsO_4{\cdot}2H_2O_{\,(s)}$	20.197	scorodite	varies
$Fe^{2+} + HS^- = FeS_{\,(amorph,\,s)} + H^+$	3.915	amorphous FeS	black
$Fe^{2+} + HS^- = FeS_{\,(s)} + H^+$	4.648	mackinawite	black
$Fe^{2+} + 2HS^- + 2H^+ = FeS_{2\,(s)} + 2e^-$	18.479	pyrite	gold to black
$Fe^{2+} + CO_3^{2-} = FeCO_{3\,(s)}$	10.55	siderite	white to brown
$2H_3AsO_3 + 3H_2S = As_2S_{3\,(s)} + 6H_2O$	39.99	orpiment	yellow
$2H_3AsO_3 + 3H_2S = As_2S_{3\,(amorph,\,s)} + 6H_2O$	23.8	amorphous As_2S_3[‡]	yellow
$4AsO_3^{3-} + 12H^+ = 2As_2O_{3\,(s)} + 6H_2O$	141.78	arsenolite	white to yellow-brown
$4AsO_3^{3-} + 12H^+ = 2As_2O_{3\,(s)} + 6H_2O$	142.04	claudetite	white
$2AsO_4^{3-} + 6H^+ = As_2O_{5\,(s)} + 3H_2O$	34.50	arsenic pentoxide	white
$AsO_3^{3-} + HS^- + 5H^+ + e^- = AsS_{\,(s)} + 3H_2O$	54.491	realgar	yellow to red

B.2. Ksp's versus IAP's of Fe and As sulfides

To determine whether As sulfides are predicted in the wetland and riverbed sediments, we compared the solubility products of the phases (Ksp) with ion activity products (IAP) for porewater concentrations. Aqueous sulfide was below detection limits of 1 μm for all depths in the wetland and riverbed. Since AVS was observed between 60-100 cm depth in the wetland and 0-40 cm in the riverbed, we calculated the aqueous sulfide concentration if amorphous FeS controls free sulfide (likely, due to high Fe concentrations, and the presence of AVS) (Eqn. 1). Porewater Fe concentrations between 60-100 cm were between 10-30 μM (wetland) and 50-180 μM (riverbed).

$$Fe^{2+} + H_2S = FeS_{(amorph,\ s)} + 2H^+ \qquad \text{Eqn. 1}$$

For pH 5.5-6 in the wetland, the concentration of H_2S plus HS^- would range from 0.3 nM to 0.03 nM if the porewater is in equilibrium with solid phase FeS (porewater $[Fe^{2+}]$ = 30 μM). For pH 6.6 to 7.0 in the riverbed, total aqueous sulfide may be between 4×10^{-13} M and 9×10^{-14} M (for porewater $[Fe^{2+}]$ = 180 μM.

Next, we used the aqueous sulfide predictions to determine if As_2S_3 was expected to precipitate. If the ion activity product (IAP) exceeds the solubility product (K_{sp}), the solid is considered oversaturated. For As_2S_3, the equilibrium equation is shown as Eqn. 2:

$$2H_3AsO_3 + 3H_2S = As_2S_{3\ (s)} + 6H_2O \qquad \text{Eqn. 2}$$

Amorphous As_2S_3 is characterized by a log K_{sp} of –23.8, whereas crystalline As_2S_3 has a log K_{sp} of –40.0. To calculate the IAP for the porewater, we considered the sulfide concentrations calculated above and measured As(III) concentrations (40-150 μM in the wetland, 40-260 μM in the riverbed). For the pH range of 5.5 to 6 in the wetland, the IAP was between –36.3 and

–40.4, which is undersaturated with respect to amorphous As_2S_3. Crystalline As_2S_3 is oversaturated except when the pH is at the high end of the measurements (pH of 6) and the H_3AsO_3 concentration is low (40 μM), which occurs at the lowest depths (90-100 cm). In the riverbed, both amorphous and crystalline As_2S_3 are undersaturated for the pH and As ranges.

B.3. pH-pe Diagrams

Table IV. Measurements of pH and platinum electrode potential (includes correction for H_2 potential) for a wetland core, along with the theoretical conversion of PEP to pe. Plotting pH and pe on the constructed stability diagrams provides a prediction of the expected aqueous and solid phases.

Depth (cm)	pH	Corrected PEP (mV)	pe	Description of stability region
0	6.19	389	6.58	$Fe(OH)_3$, As(V)
5	6.44	65	1.10	$Fe(OH)_3$, As(III)
10	5.96	142	2.40	$Fe(OH)_3$, As(III)-As(V)
15	5.65	104	1.76	Fe(II), As(III)
20	5.86	124	2.09	Fe(II)-Fe(III), As(III)
25	6.75	-33	-0.55	Fe(II)-Fe(III), As(III)
30	6.72	-78	-1.31	Fe(II), As(III)
35	6.69	-114	-1.92	Fe(II), As(III)
40	6.59	-103	-1.75	Fe(II), As(III)
45	6.18	-87	-1.47	Fe(II), As(III)
50	6.02	-110	-1.86	Fe(II), As(III)
55	5.95	-122	-2.07	Fe(II), As(III)
60	5.90	-106	-1.79	Fe(II), As(III)
65	5.83	-114	-1.93	Fe(II), As(III)
70	5.78	-121	-2.05	Fe(II), As(III), SO_4-H_2S
75	5.72	-142	-2.39	Fe(II), As(III), H_2S
80	5.82	-149	-2.52	Fe(II), As(III), H_2S
85	5.85	-159	-2.69	Fe(II), As(III), H_2S
90	5.85	-164	-2.77	Fe(II), As(III), H_2S
95	5.94	-167	-2.82	Fe(II), As(III), H_2S
100	5.94	-183	-3.09	Fe(II), As(III), H_2S

Table V. Measurements of pH and platinum electrode potential (includes correction for H_2 potential) for a riverbed core, along with the theoretical conversion of PEP to pe. Plotting pH and pe on the constructed stability diagrams provides a prediction of the expected aqueous and solid phases.

Depth (cm)	pH	Corrected PEP (mV)	pe	Description of stability region
2.5	6.80	80	1.35	$Fe(OH)_3$, As(III), SO_4
7.5	6.93	-74	-1.26	$Fe(OH)_3$ - Fe(II), As(III), SO_4
12.5	6.92	-158	-2.67	Fe(II), As(III), SO_4
17.5	6.72	-145	-2.45	Fe(II), As(III), SO_4
22.5	6.64	-160	-2.71	Fe(II), As(III), SO_4
27.5	6.81	-160	-2.70	Fe(II), As(III), SO_4
32.5	6.73	-157	-2.65	Fe(II), As(III), SO_4
37.5	6.72	-163	-2.76	Fe(II), As(III), SO_4
42.5	6.62	-201	-3.40	Fe(II), As(III), SO_4-H_2S
47.5		-216	-3.65	Fe(II), As(III), SO_4-H_2S
52.5		-223	-3.77	
57.5		-207	-3.50	
62.5		-163	-2.75	
67.5		-218	-3.68	
72.5		-158	-2.66	
77.5		-186	-3.14	
82.5		-172	-2.91	
87.5	6.41	-187	-3.17	Fe(II), As(III), H_2S
92.5		-214	-3.61	Fe(II), As(III), H_2S
97.5	6.58			

B.4. References

(1) Stumm W.; Morgan J. J. (1996) *Aquatic Chemistry*. John Wiley & Sons, Inc.

(2) Eary L. E. (1992) The solubility of amorphous As_2S_3 from 25 to 90°C. *Geochim. Cosmochim. Acta* **56**, 2267-2280.

Appendix C. Iron mineral identification in Wells G & H Wetland sediments

C.1 Methodology and Results

In Chapter 3, sequential extractions found that As in contaminated Wells G & H wetland sediment was mostly adsorbed strongly, likely onto Fe phases. Iron distribution among the extractant pools revealed that most of the Fe was amorphous (1N HCl or 0.2 M oxalate), with approximately 10% crystalline (Ti-extractable). The amorphous Fe solid phase is discussed in the text of Ch. 3, whereby we concluded that the Fe is most likely hydrous ferric oxide or siderite. The character of the crystalline Fe component remained largely unknown, however. Due to the much greater quantity of the Fe compared to As in the sediment, the 10% of Fe in mineral phases could be important in retaining As. In addition, identification of Fe minerals present could improve our understanding of the redox conditions and Fe cycle in the sediments.

To investigate the crystalline iron phases present in the wetland sediments, we employed several traditional geological methods to characterize the dominant iron minerals. First, minerals with a high density (> 2.96 g/cm^3) were separated from bulk sediment by heavy-liquid density separations. The dense minerals recovered were investigated using the following methods to determine the identity of Fe phases among the dense minerals: optical microscopy to investigate characteristic color (Fig. I), magnetic separation for identifying ferrimagnetic minerals (Fig. II) (iii) x-ray diffraction microscopy for analyzing the identity of major crystalline Fe phases (Fig. III), and (iv) electron microprobe analysis for determining the prevalence of Fe phases (Fig. IV).

Optical microscopy images in Figure I show the wide range of high density minerals found in the 35-40 cm sediment depth. Of particular note are the phases characterized by the morphology of Fe-hydroxide-filled root fragments. The stability of Fe and As in roots after senescence remains an interesting question, as some researchers have suggested that cells can fill in with Fe when outer cell walls decompose (*1; 2*).

Figure II shows the minerals that harbor a lasting applied magnetic force after the magnetic force has been removed, the strongest of which are termed ferrimagnetic phases. Typical ferrimagnetic phases found in the environment include magnetite ($Fe^{2+}(Fe^{3+})_2O_4$, silver to black), pyrrhotite ($Fe_{1-x}S$, $0<x<0.2$, bronze to dark brown), and maghemite (γ-Fe_2O_3, dark brown), and greigite ($Fe^{2+}(Fe^{3+})_2S_4$, blue to black, bronze, or pink color), all of which have a metallic luster (*3; 4*). Antiferromagnetic phases, including hematite (α-Fe_2O_3, reddish gray to black, metallic) and goethite (α-FeOOH, brown or reddish to yellowish brown, nonmetallic luster), exhibit a large range of magnetic susceptibilities from near zero to slightly lower than ferrimagnetic minerals (*3; 5*).

In sediment environments with fluctuating periods of oxidation and reduction, predominant Fe phases may cycle between different forms. Maghemite formation and stability has been suggested in such environments (*5*). Maghemite is formed when most of the Fe^{2+} in magnetite is oxidized to Fe^{3+}, but the mineral maintains its spinel form (unlike hematite, α-Fe_2O_3). Magnetite formed either abiotically or as a result of iron-reducing bacteria liberating Fe^{2+} into their environment is larger in size than that produced by magnetotactic bacteria and may contain more trace elements. Magnetotactic bacteria have been isolated that internally precipitate either magnetite (in low sulfide environments) or greigite (Fe_3S_4, in high sulfide sediments) for use in navigation to microaerobic horizons. The size of these magnetosomes are typically between 35 and 120 nm (*6*).

In Figure II, the dominant magnetic phases appear to be larger than 100 μm, which indicates that the phases were not formed by magnetotactic bacteria. The silver color and high magnetic susceptibility suggests that the phases are magnetite. Orange-reddish phases that also exhibit magnetism in Fig. II appear to be goethite or hematite. The role of magnetic mineral phases such as magnetite in adsorbing As is unknown. Research on the sorptive capacity of

these phases for As may show that the phases provide an important reduced-Fe substrate for As sorption in wetland sediments.

Figure III shows the x-ray diffraction patterns revealing the oxidized Fe phases in the sediments for whole sediment (A) and on the dense mineral fractions (B). We have some reservations about the accuracy of the XRD data since we did not have access to an anoxic XRD instrument, as the air-drying procedure most likely oxidized amorphous reducing Fe. However, we air-dried to not induce goethite formation by oven-drying (*7*), which implies that goethite is an important sediment constituent in the whole sediment fraction. Of the dense mineral fraction, we observed an XRD pattern consistent with Fe or Zn sulfides, goethite, and hematite. The dense fraction comprises only a small percentage of the total mass of the sediment. The separation of dense minerals was useful to be able to identify other potentially important mineral phases by removing organic matter and concentrating the mineral phases. All three of these phases are potential sorbents of As.

Figure IV includes backscatter EMPA images of a sediment subsample from the wetland contaminant zone. Backscatter images in (A) confirms the wide variety of phases present in the sediment, and (B) shows the widespread occurrence of Fe in many different morphological phases. We searched extensively for As phases but were unable to locate any in this sample, most likely due to the presence of As at sub-percent levels (i.e. below EMPA detection limits) in surface coatings rather than in mineral precipitates. Two interesting findings noted in (A) were a small, 5 μm particle containing only Cu and S, and a small particle of gold. Both of these would be consistent with the Iberian source material roasted upstream from the Industri-Plex site (*8; 9*). An investigation of contaminant source attribution in the Wells G & H wetland may better our understanding of the original transport an deposition of As to the wetland, as well as the source of more recalcitrant crystalline phases observed in the riverbed sediments.

Together, the methods used to identify Fe minerals in the 35-40 cm depth of the wetland revealed that a mixture of Fe minerals co-occur. In bulk (unseparated) sediment, goethite

appears to be the predominant Fe mineral (Fig. IIIA) amidst a wide range of Fe-containing solid phases (Fig. IV). Density separations enabled the identification of other less prominent phases, including hematite and Fe or Zn sulfide (Fig. IIIB), and magnetite (Fig. II). The prevalence of Fe-laden root fragments (Fig. I) suggests that roots can retain, and possibly accumulate, Fe following senescence.

References

(1) Mendelssohn I.; Kleiss B.; Wakeley J. (1995) Factors controlling the formation of oxidized root channels: a review. *Wetlands* **15**(1), 37-46.

(2) Chen C. C.; Dixon J. B.; Turner F. T. (1980) Iron coatings on rice roots: Morphology and models of development. *Soil Sci. Soc. Am. J.* **44**, 1113-1119.

(3) Klein C.; Hurlbut Jr. C. (1993) *Manual of Mineralogy*. John Wiley and Sons.

(4) Barthelmy, David. (2002) Website:. http://webmineral.com

(5) Butler R. F. (1992) *Paleomagnetism: Magnetic domains to geologic terranes*. Blackwell Scientific Publications.

(6) Bazylinski D. (1996) Controlled biomineralization of magnetic minerals by magnetotactic bacteria. *Chem. Geol.* **132**, 191-198.

(7) Schwertmann U.; Cornell R. (1991) *Iron Oxides in the Laboratory: Preparation and characterization*. VCH.

(8) Aurilio A.; Durant J. L.; Hemond H. F.; Knox M. L. (1995) Sources and distribution of arsenic in the Aberjona watershed, Eastern Massachusetts. *Water, Air, Soil Poll.* **81**, 265-282.

(9) Leistel J.; Marcoux E.; Thieblemont D.; Quesada C.; Sanchez A.; Almodovar G.; Pascual E.; Saez R. (1998) The volcanic-hosted massive sulphide deposits of the Iberian Pyrite Belt. *Mineral. Deposita* **33**, 2-30.

(10) Sundby B.; Vale C.; Cacador I.; Catarino F.; Madureira M.-J.; Caetano M. (1998) Metal-rich concretions on the roots of salt marsh plants: Mechanism and rate of formation. *Limnoll. Oceanogr.* **43**(2), 245-252.

C.2. Figure I. Optical microscope images of minerals and plant root fragments (density > 2.96 g/cm^3) separated from wetland core 35-40 cm depth. Figure A shows the variety of dense minerals found in this sediment depth. Minerals and phases in B, C, and D vary greatly with no visibly dominant phase, except the presence of phases that look like Fe-hydroxide-filled root fragments. The stability of Fe and As in roots after senescence remains an interesting question, as some researchers have suggested that cells can fill in with Fe when outer cell walls decompose (*1; 2*).

3 mm

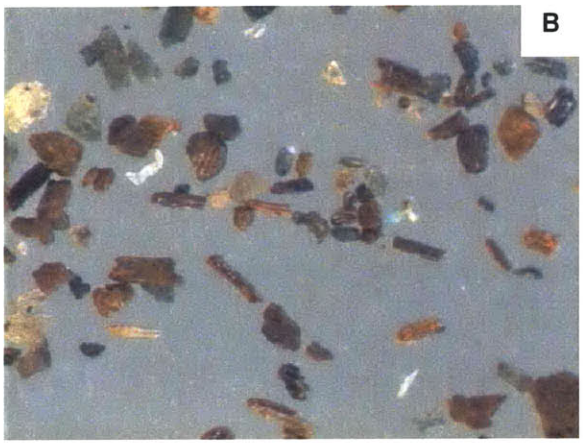

1 mm

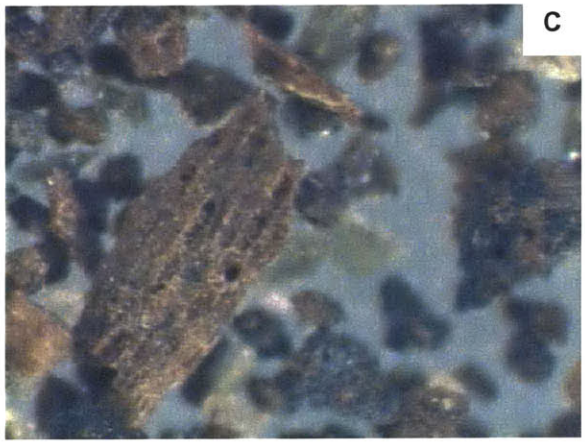

1 mm

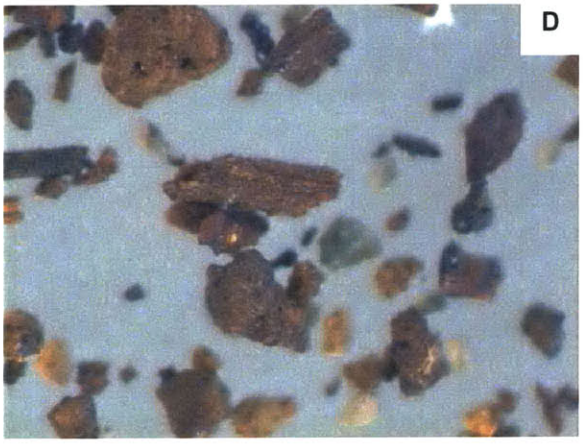

1 mm

C.2. Figure II. Optical microscope images of between 1-5% of the dense minerals ($\rho > 2.96$ g/cm^3) that were separated by a hand magnet from wetland core 35-40 cm depth. Refer to the discussion of the likely phases. Figures B and C contain bright orange phases besides the metallic silver minerals. Figure D shows a mineral (arrow) that may have been precipitated around a root as an Fe concretion (*10*).

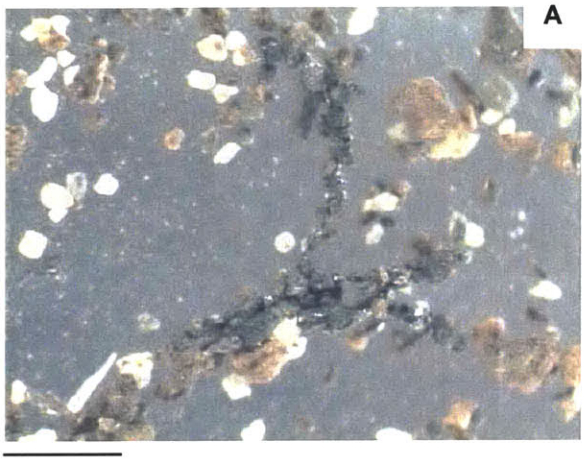

1 mm

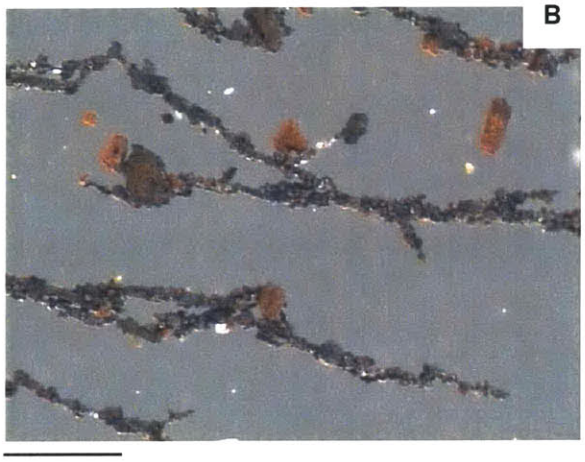

1 mm

1 mm

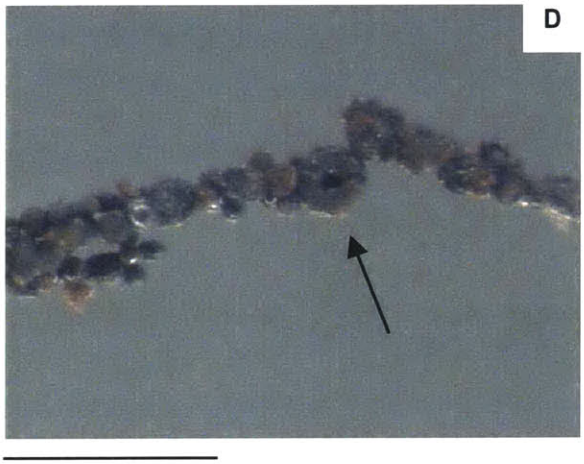

1 mm

C.2. Figure III. X-ray diffraction scan of (A) unseparated sediment and (B) dense minerals (> 2.96 g/cm^3) from wetland core depth 30-40 cm. G = goethite, H = hematite, Q = quartz, S = Zn or Fe sulfide. The densities of goethite (3.3-4.3), hematite (5.3), Zn and Fe sulfides (4-4.3) are greater than the liquid used to separate the minerals from the bulk matrix. Interestingly, goethite is not the dominant fraction among the dense minerals (B), perhaps because it is associated with less dense organic matter (e.g. roots).

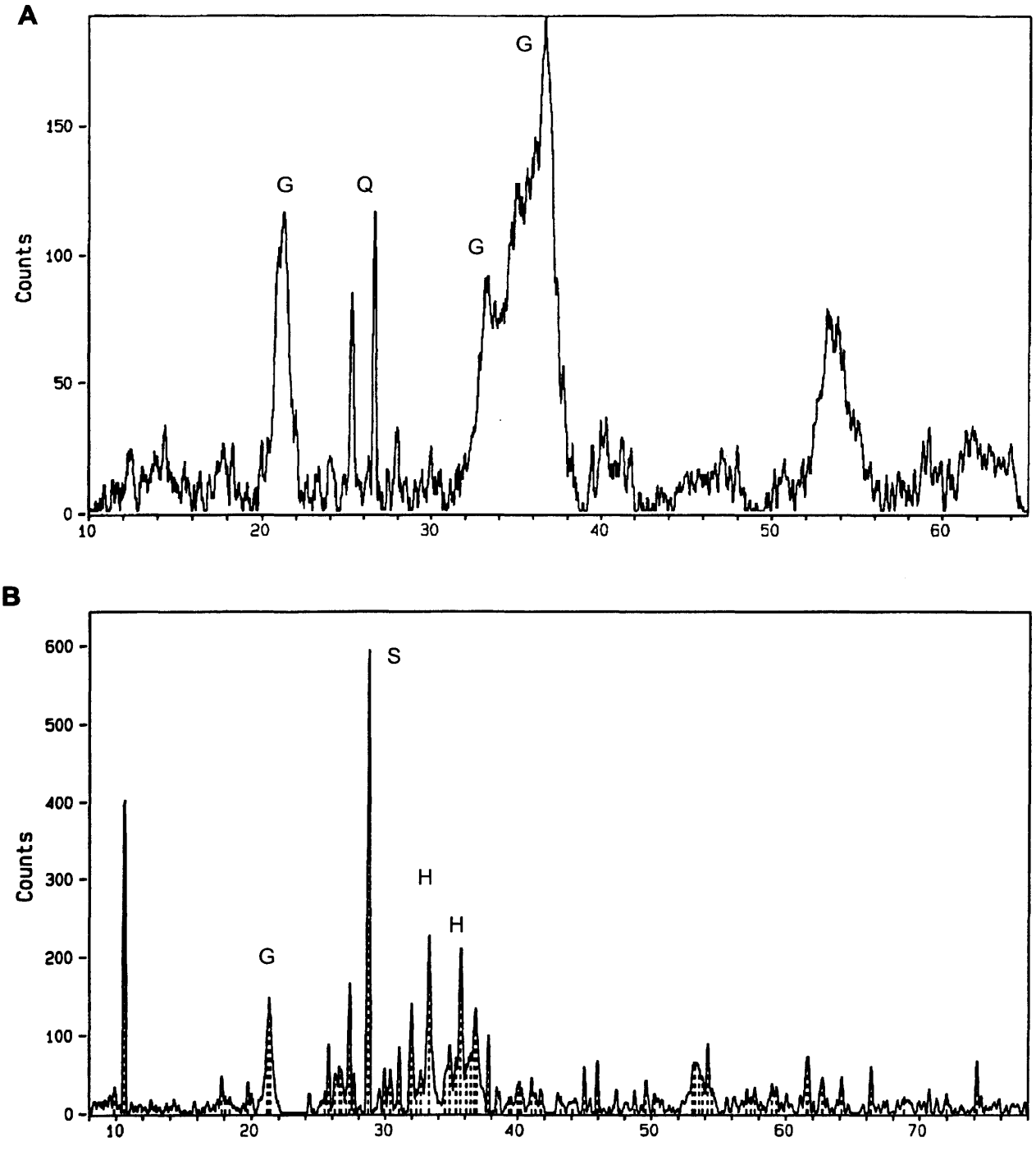

C.2. Figure IV. Electron microprobe analysis (EMPA) image of sediment from 35-50 cm depth, including (A) the backscatter image and (B) Fe map determined by wavelength-dispersive x-ray fluorescence (WD-XRF). Most bright, high atomic number grains in (A) appear to be largely Fe. The larger circled region is an exception as the 5 μm particle contains only Cu and S. The smaller circle appears to be a particle of gold, a trace element consistent with Iberian pyrite source material.

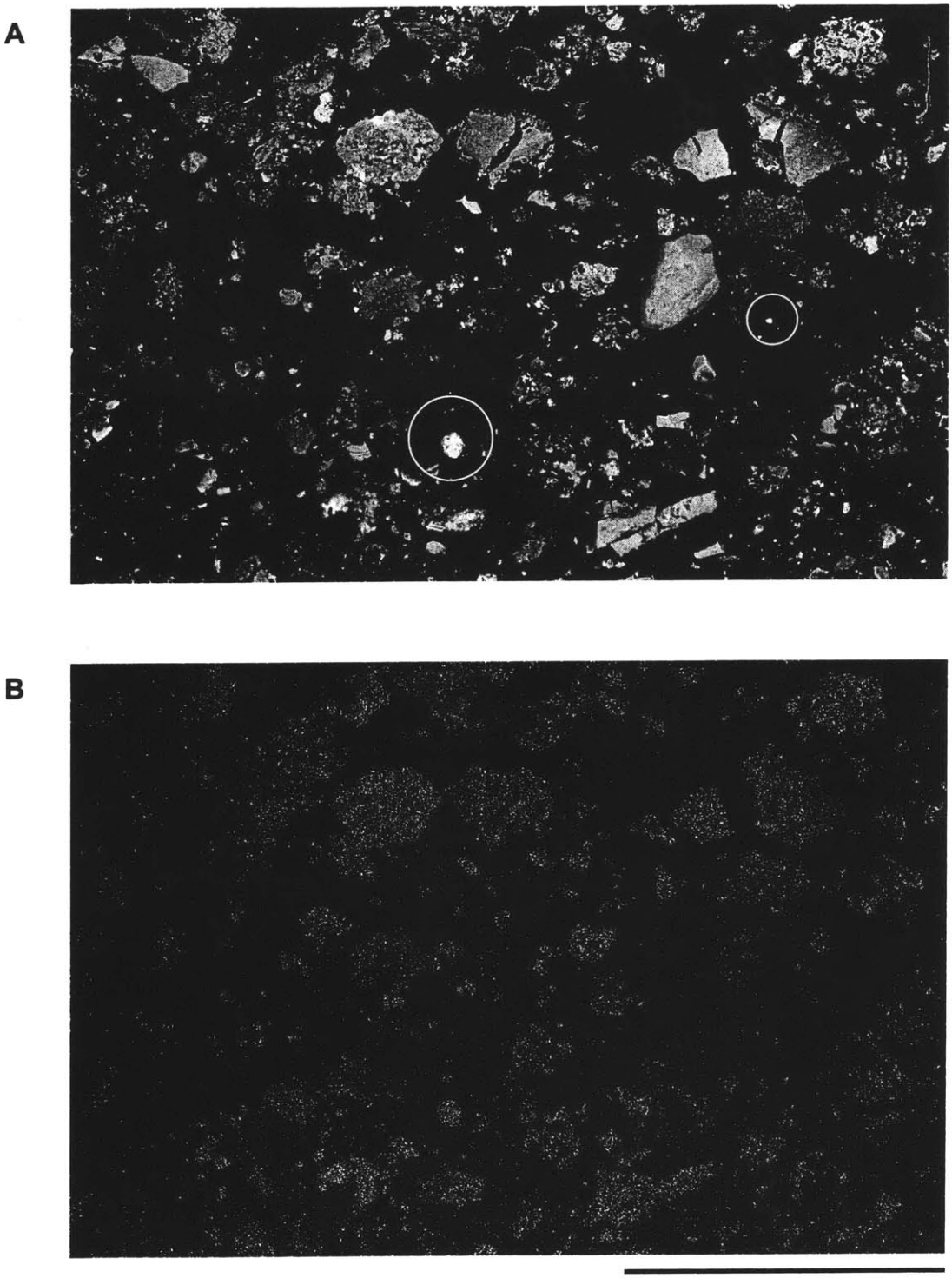

Appendix D. X-ray absorption spectroscopy data fitting

D.1. Figure I. Spectrum of the XANES region of the energy spectrum for the wetland core, with curve fit performed with WinXAS v.2.1 using a linear combination of standards, including NaH_2AsO_4 (As(V)-O), As_2O_3 (As(III)-O), and amorphous As_2S_3 (As(III)-S). The edge positions of all of the samples indicated that FeAsS is not a major component of the sediments, so it was not used in the curve fits. For the 30-35 cm depth, the As oxidation state distribution was determined to be 28% As(V)-O and 72% As(III) (55% As(III)-O + 17% As(III)-S). The As concentration for this depth averaged 2730 μg As/ g sediment. The spectrum below is the average of 12 scans run at a resolution of 0.2 eV in the XANES region.

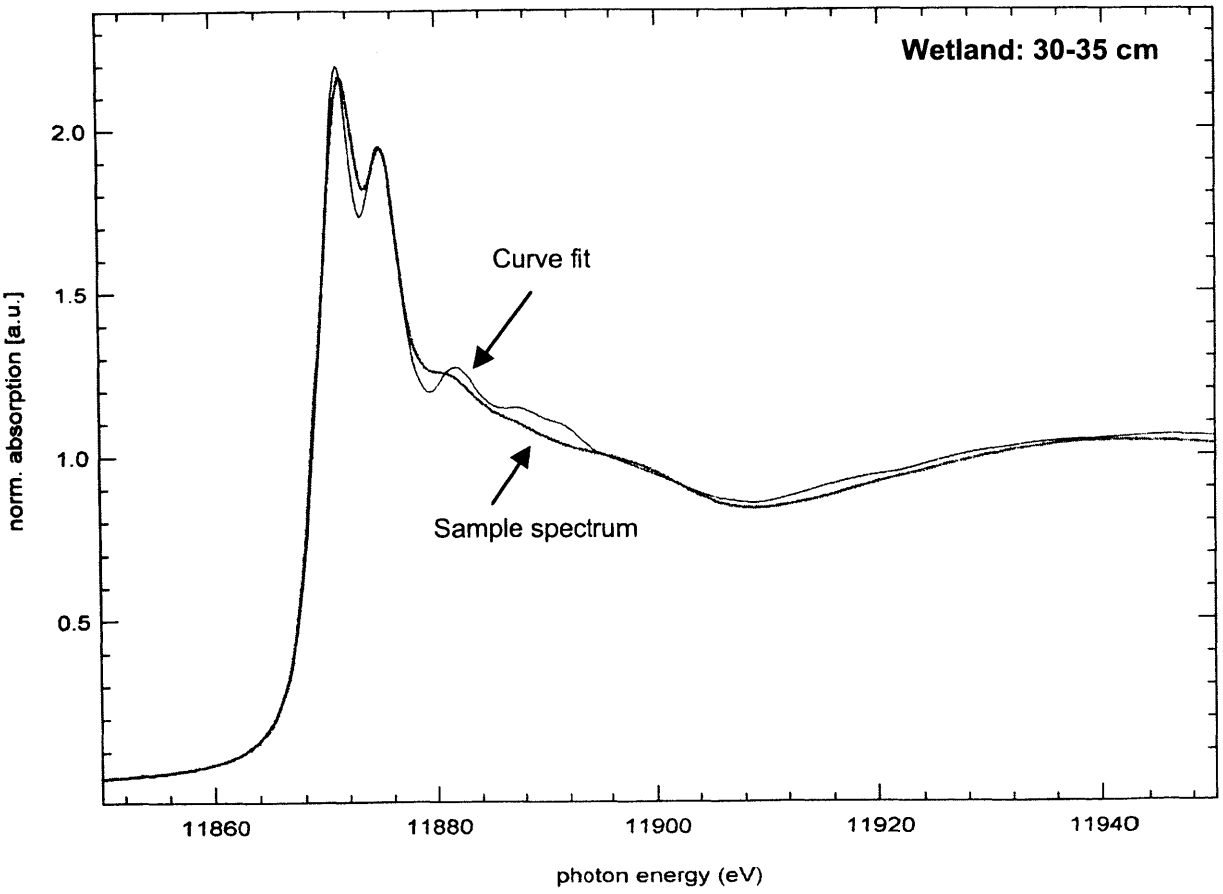

Figure II. Wetland Depth 65-70 cm. The As oxidation state distribution in a subsample of the 65-70 cm depth was determined to be 39% As(V)-O and 61% As(III) (44% As(III)-O + 17% As(III)-S). In this depth, the concentration of As is only about 13 μg/g, which explains the noise observed even though 10 scans were averaged.

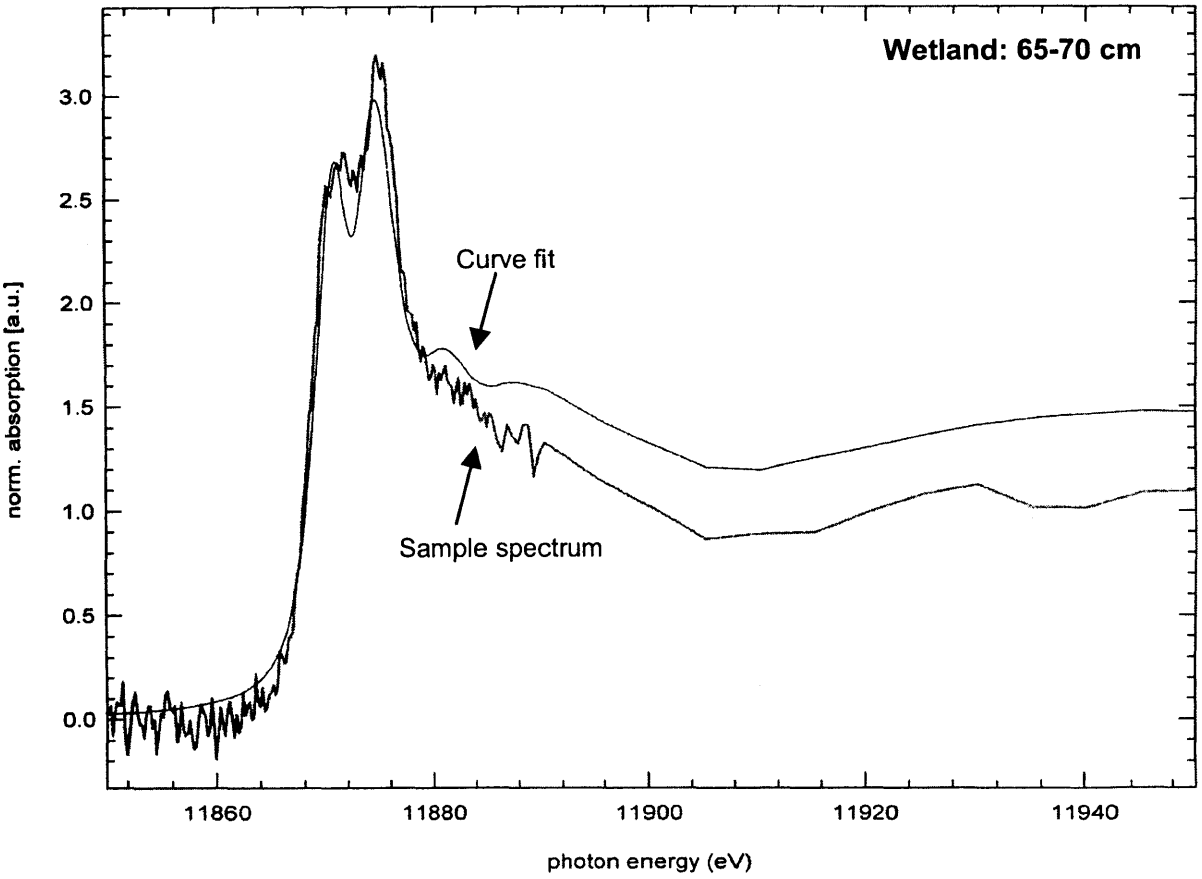

Figure III. Wetland Depth 90-95 cm. For this depth, the As oxidation state distribution was determined to be 50% As(V)-O and 50% As(III) (40% As(III)-O + 10% As(III)-S). The concentration of As was approximately 26 μg/g for this depth. The spectrum below is an average of 10 scans. More noise observed for this depth compared to the 65-70 cm depth may arise from sediment heterogeneity (i.e. lower concentration for this particular subsample).

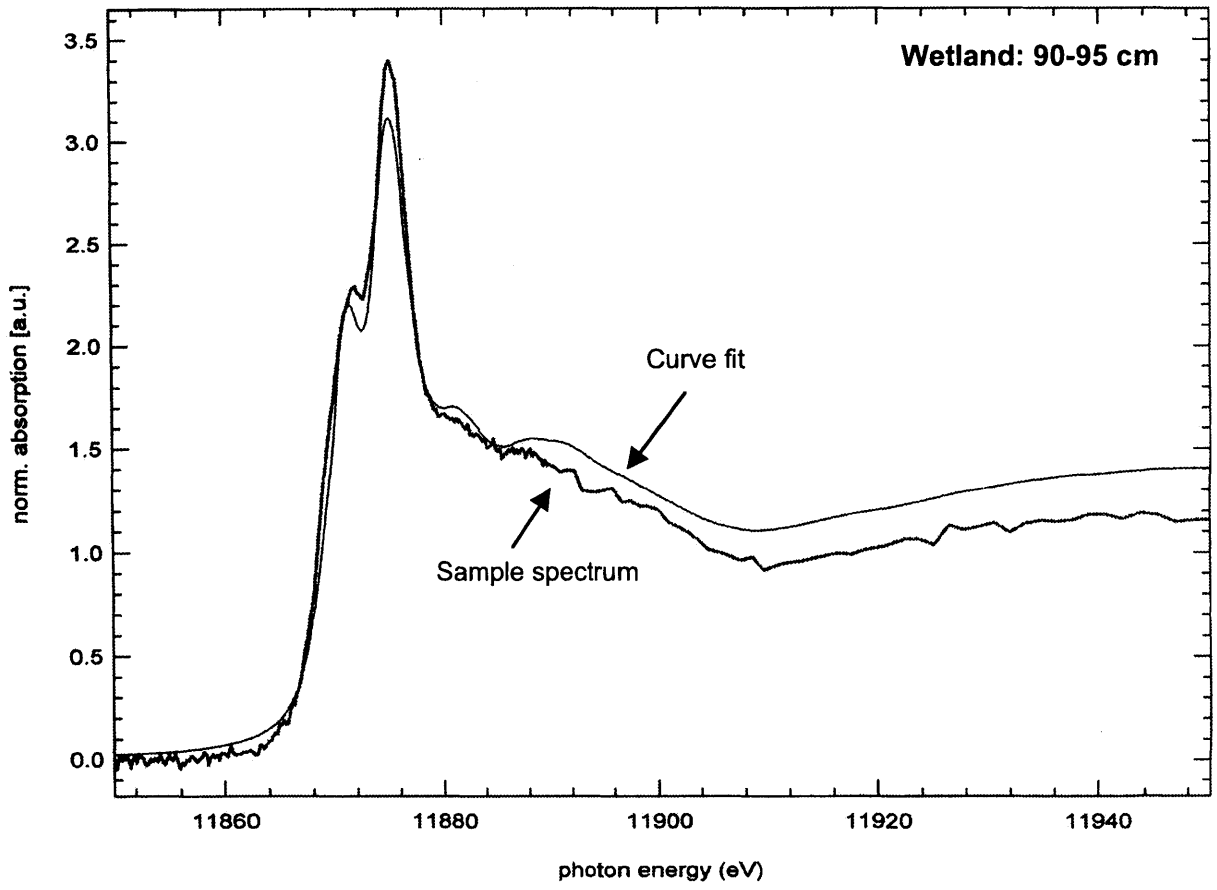

D.2. Figure IV. Spectrum of the XANES region of the energy spectrum for the riverbed core. For the 20-25 cm depth, the As oxidation state distribution was determined to be 22% As(V)-O and 78% As(III) (70% As(III)-O + 8% As(III)-S). The sediment in this depth averaged 680 μg As/g sediment. The sample was run overnight for 24 scans using an energy resolution of 0.35 eV.

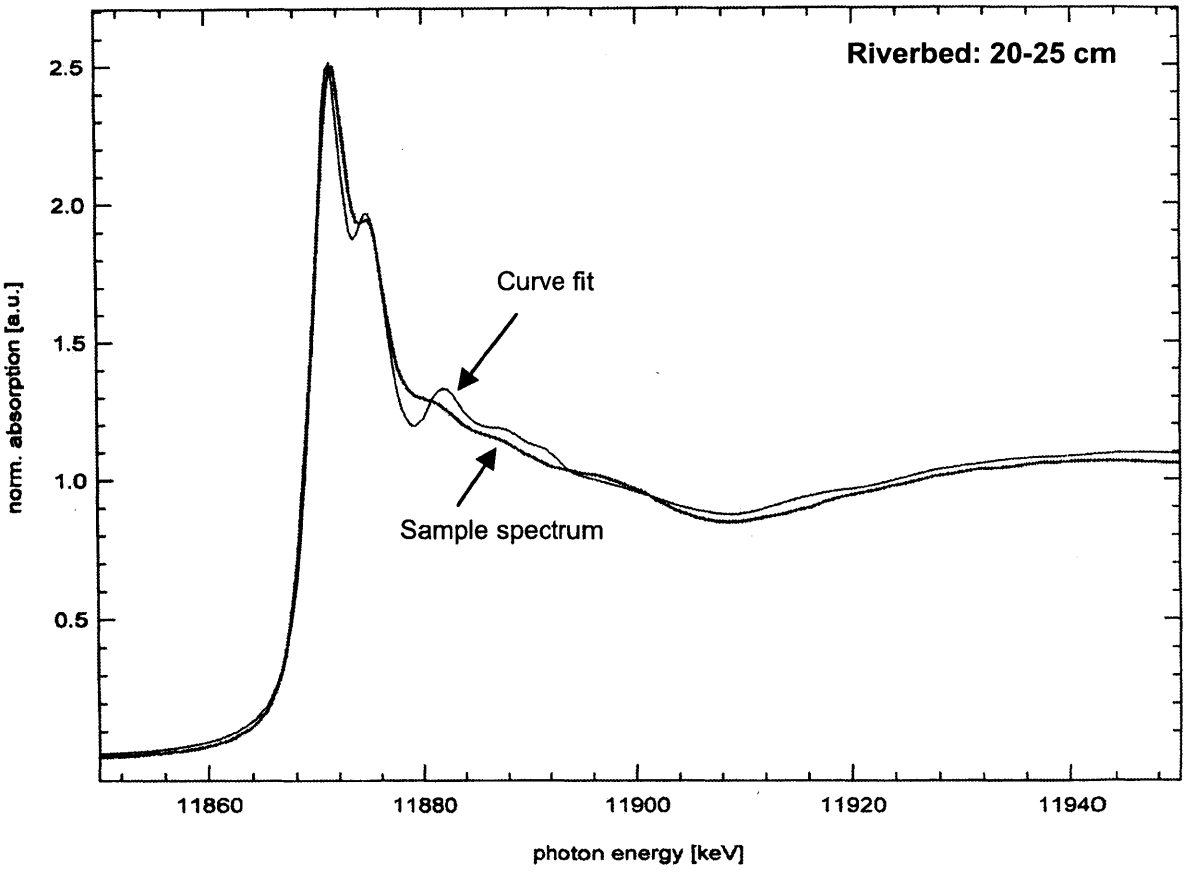

D.2. Figure V. Spectrum of the XANES region of the energy spectrum for the riverbed core. For the 20-25 cm depth, the As oxidation state distribution was determined to be 20% As(V)-O and 80% As(III) (41% As(III)-O + 39% As(III)-S). The sediment of this depth contained approximately 74 μg As/ g sediment. The spectrum is an average of 15 scans.

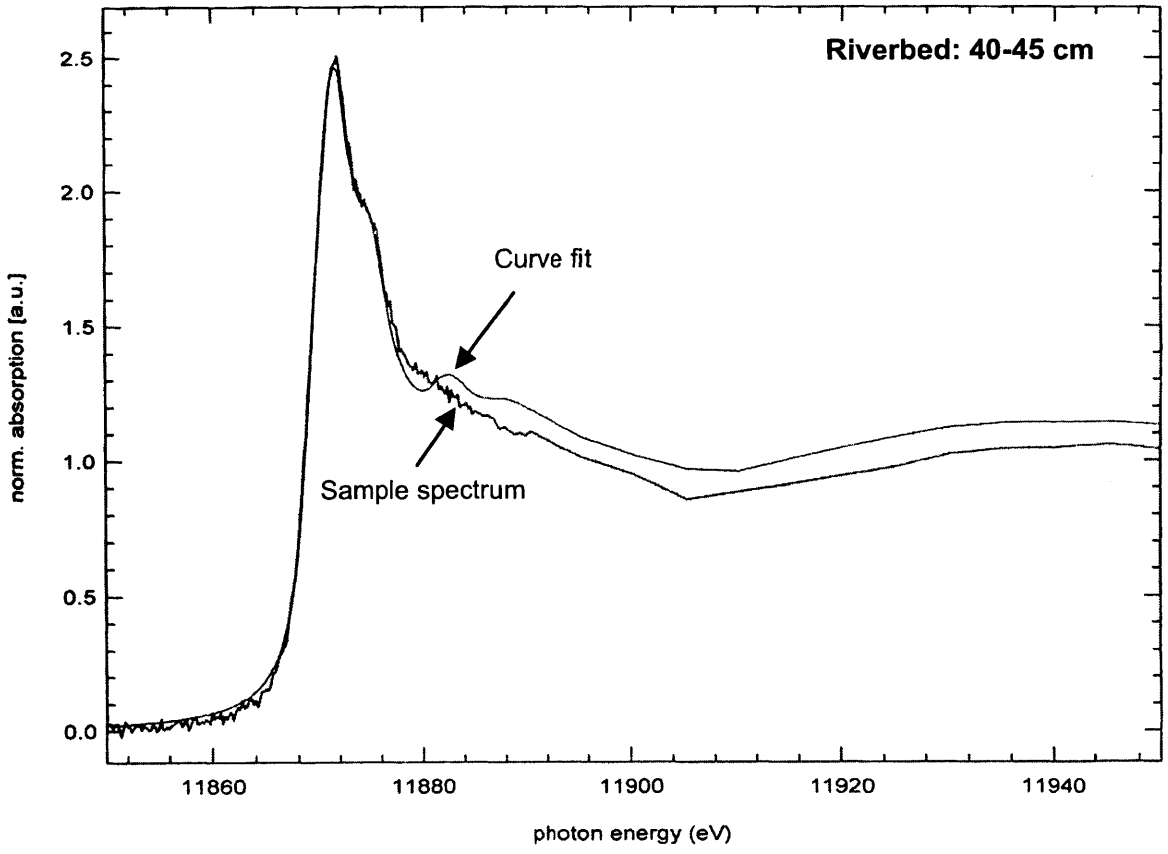

Figure VI. Riverbed Depth 95-100 cm. For this depth, the As oxidation state distribution was determined to be 15% As(V)-O and 85% As(III) (47% As(III)-O + 38% As(III)-S). The average As concentration in this depth was 286 µg/g. The spectrum is an average of 5 scans.

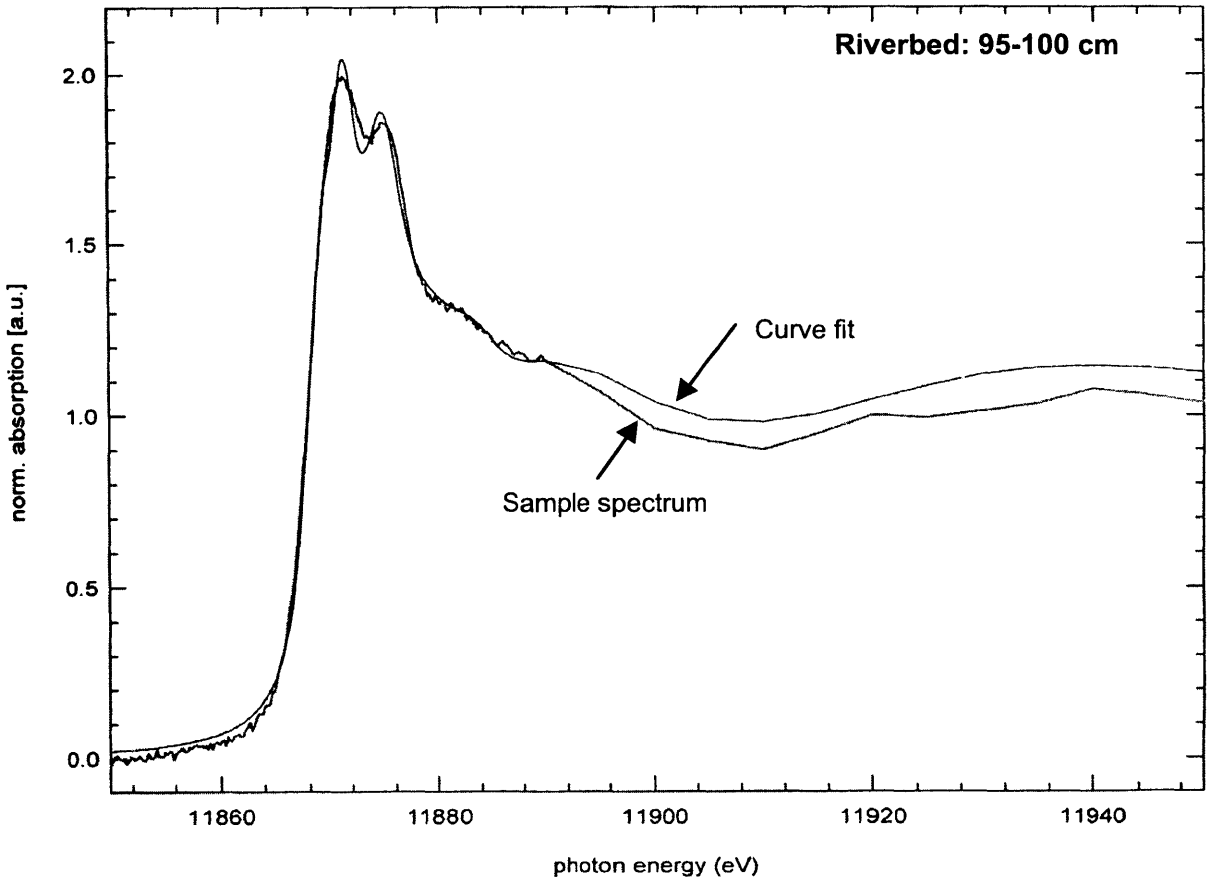

Figure VII. Arsenic model compounds. Edge positions measured relative to the standard reference As foil were as follows: FeAsS - 11866.4, As_2S_3 (amorphous, As(III)-S) - 11867.8, As_2O_3 (As(III)-O) - 11869.4, NaH_2AsO_4 (As(V)-O) - 11873.23 eV. Model compounds were run under the same conditions as the standards during the same beam time.

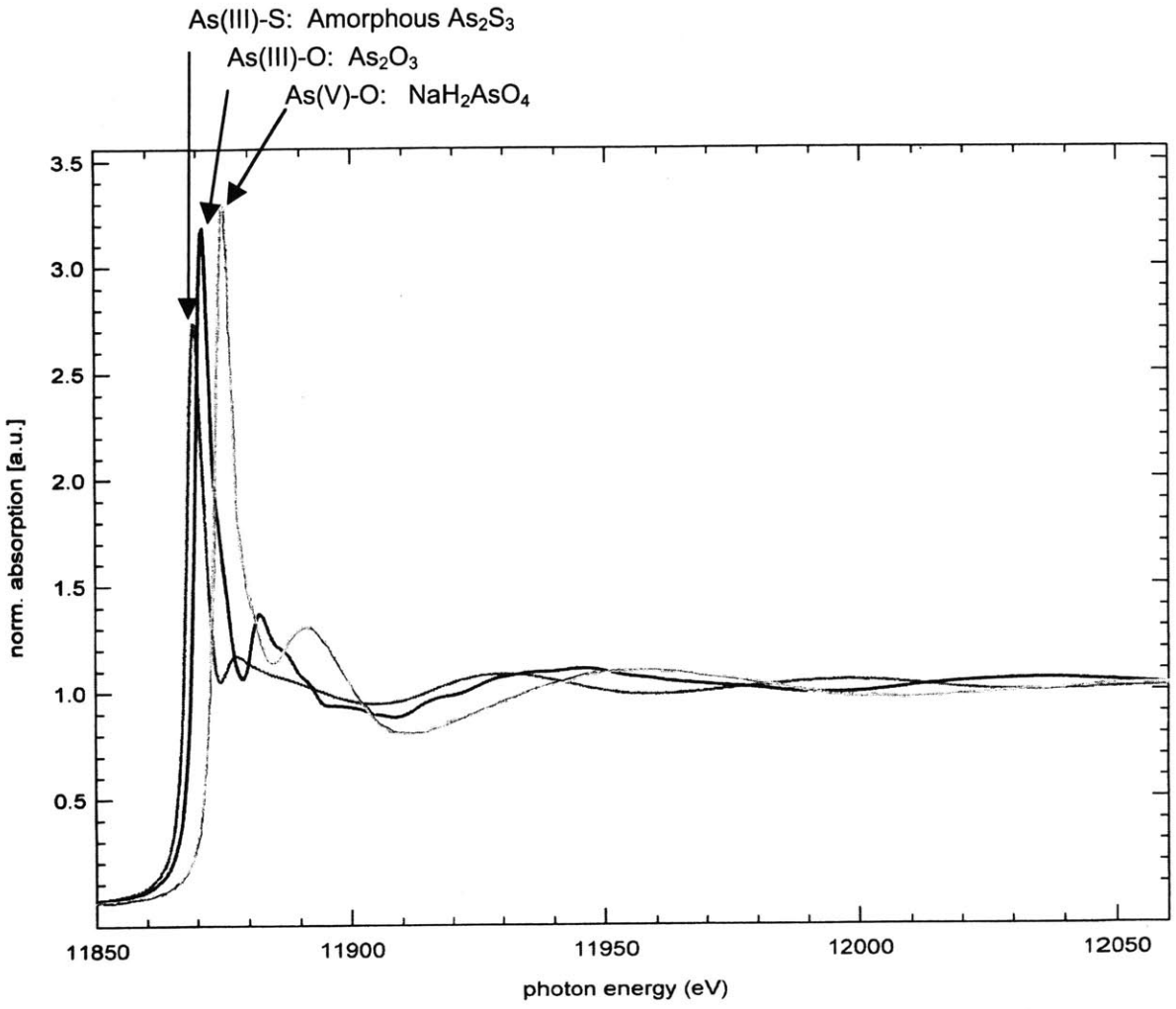

Appendix E.

E.1. Figure I. Rough distribution of dominant plant species found in different regions of the Wells G & H wetland as determined by a visual assessment from the east upland area and the river. Except for a few areas of *P. australis* monoculture stands, the wetland is dominated by *T. latifolia* followed by a mixture of *T. latifolia* with *L. salicaria* and *C. stricta*. We collected root cores from the region marked by the arrow. Within this region, cores were located strictly in between *T.latifolia* plants to avoid collecting roots from other plants in the cores. The distinct characteristics of the root systems of *C. stricta* (very dense, tight cluster of roots) and *L. salicaria* (shallow, sparse roots) were not observed in any of the root cores obtained.

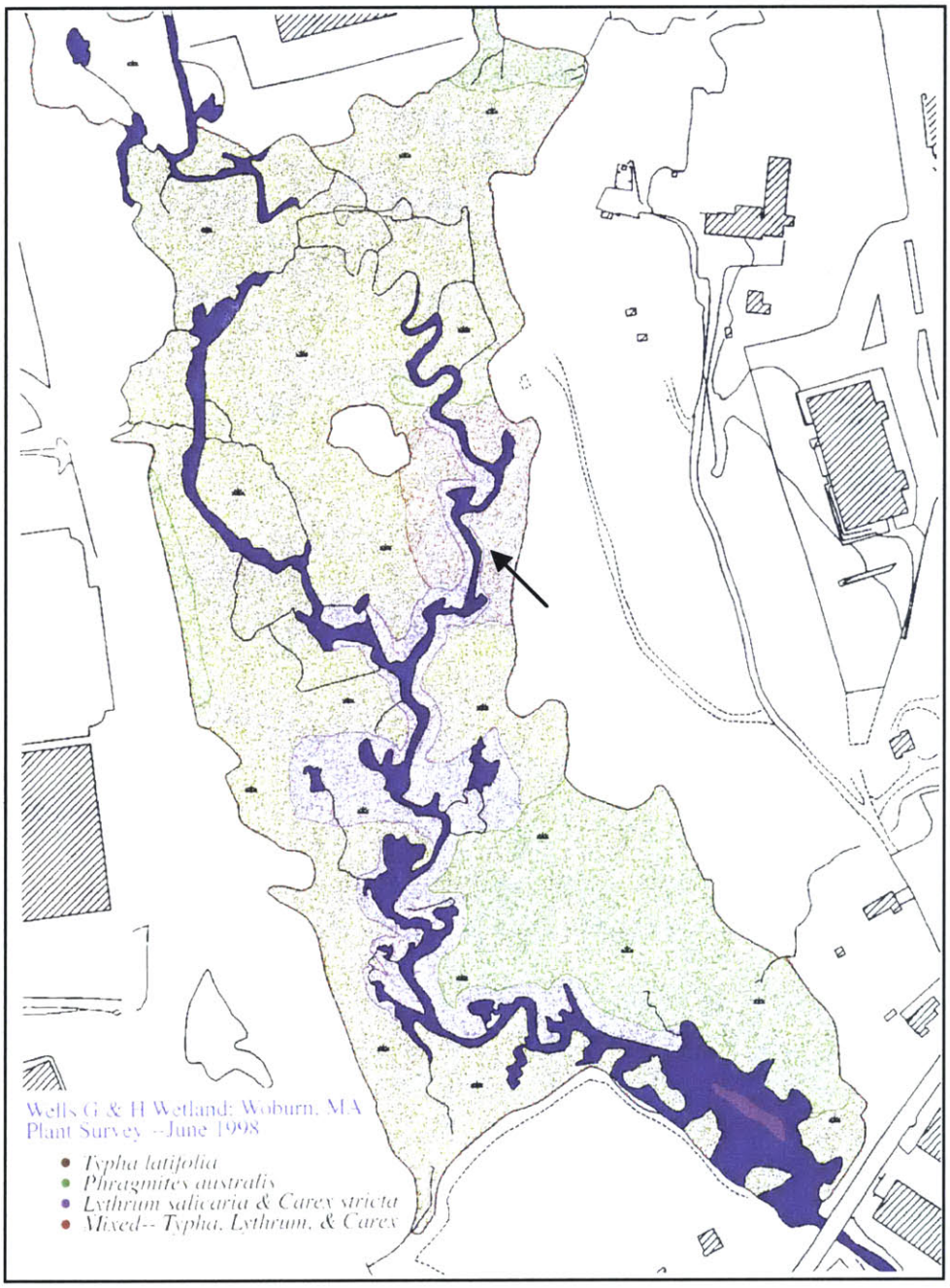

E.2. Figure II. SEM backscatter image of air-dried, water-washed *T. latifolia* roots analyzed by XRF microtomography. Variable pressure in the sampling chamber avoided the need for sample impregnation with resins, which allowed us to visualize small scale structural features (unlike in Fig. V). Image is shown in backscatter mode, where bright areas reflect high Z elements. In agreement with XRF microtomograms, the only area of the root with high concentrations of Fe (high Z) is the exterior plaque.

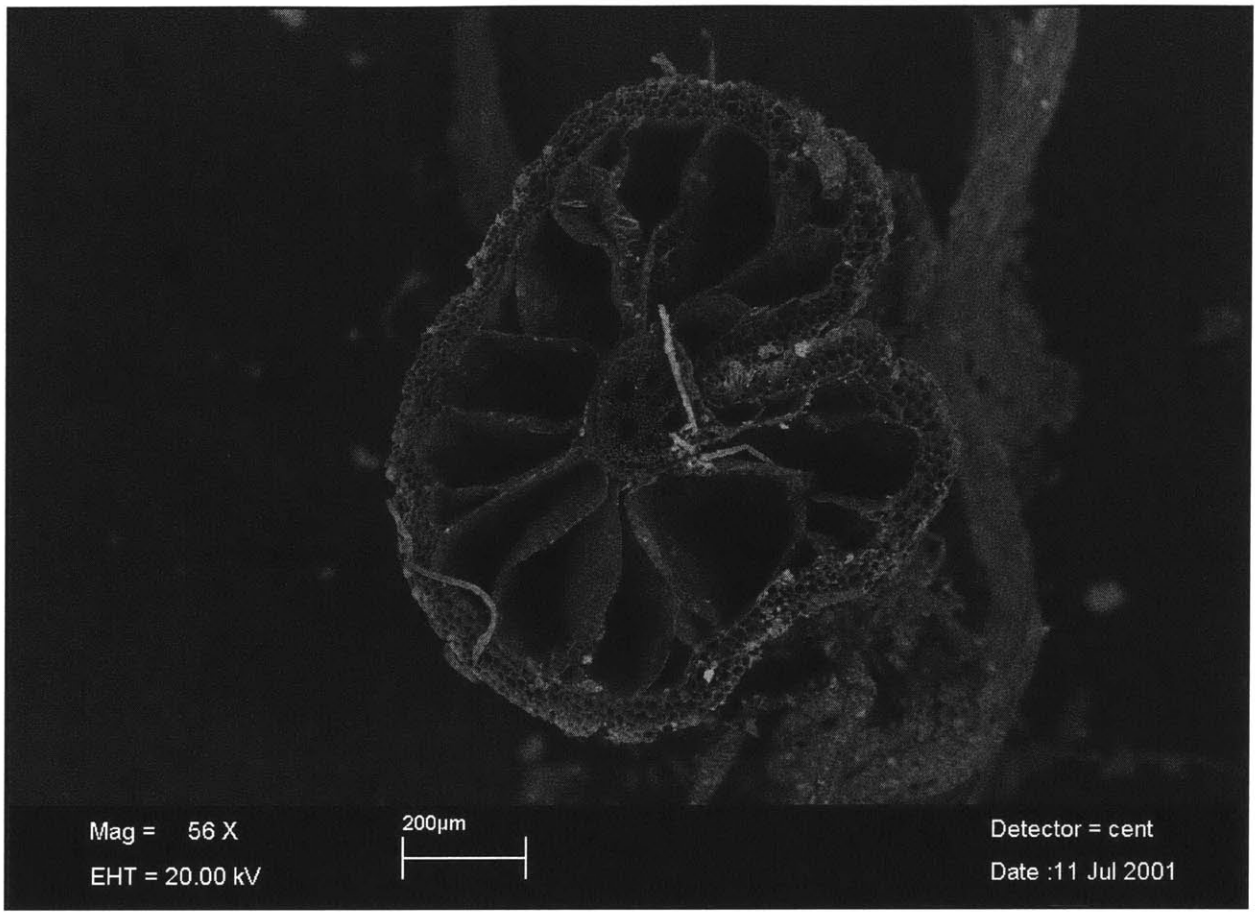

Figure III. Another viewpoint of the root plaque, which appears as a bright ring on the outside of the root. Sample preparation of root cross-sections for SEM requires that either roots are sliced through or impregnated with resin and sliced. Potential contamination introduced from the exterior of the root into the interior may occur during root slicing if the samples do not contain resin. However, resin impregnation does not allow structural features to be observed, particularly the plaque. XRF microtomography allows for elemental mapping through a root cross-section without slicing the root, and trace elemental concentrations can be detected.

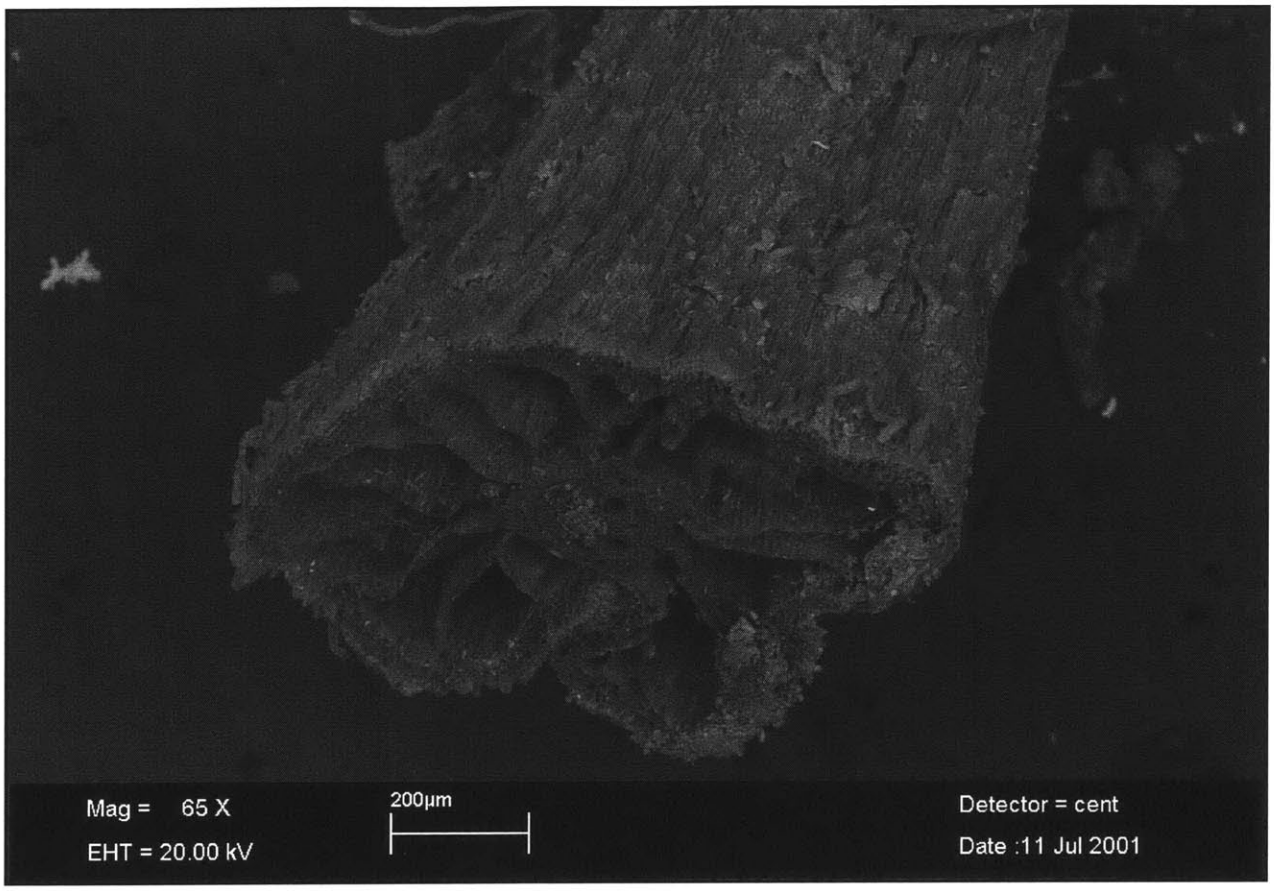

E.3. Figure IV. SEM backscatter image (BSE) of a freeze-dried *T. latifolia* rhizome and element maps collected for the same rhizome section by energy-dispersive XRF. The rhizosphere sediment, in literature reported to extend up to 1 mm from the root surface, is enriched in Fe, Si, and Al according to the x-ray elemental maps below. Ca, K, and Cl are more evenly distributed in the root as well as the rhizosphere sediment, likely due to plant nutritional requirements. Concentrations of As were below the detection limits.

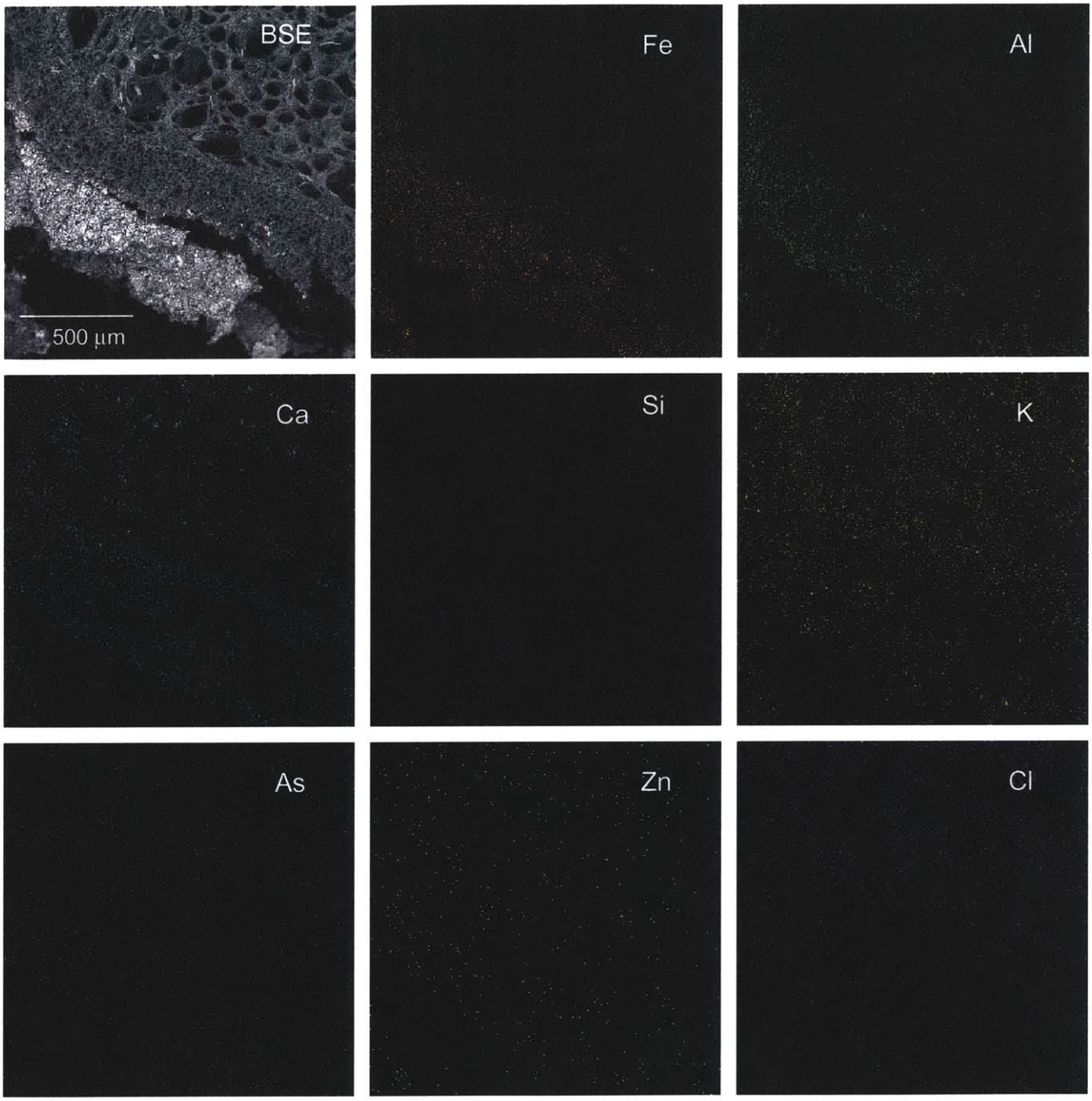

Figure V. Close-up image of the rhizome rhizosphere sediment shown in Figure II. The BSE image reveals the heterogeneity of particle size and shape in the sediment. Particles brought to the root surface appear to have been cemented together to form rhizosphere sediment. Fe, Al, and Ca appear to be evenly distributed within the rhizosphere sediment, whereas Si appears in hot spots within isolated phases. As, Ti, and S do not show any apparent distribution pattern in the rhizosphere sediment, due to low concentrations.

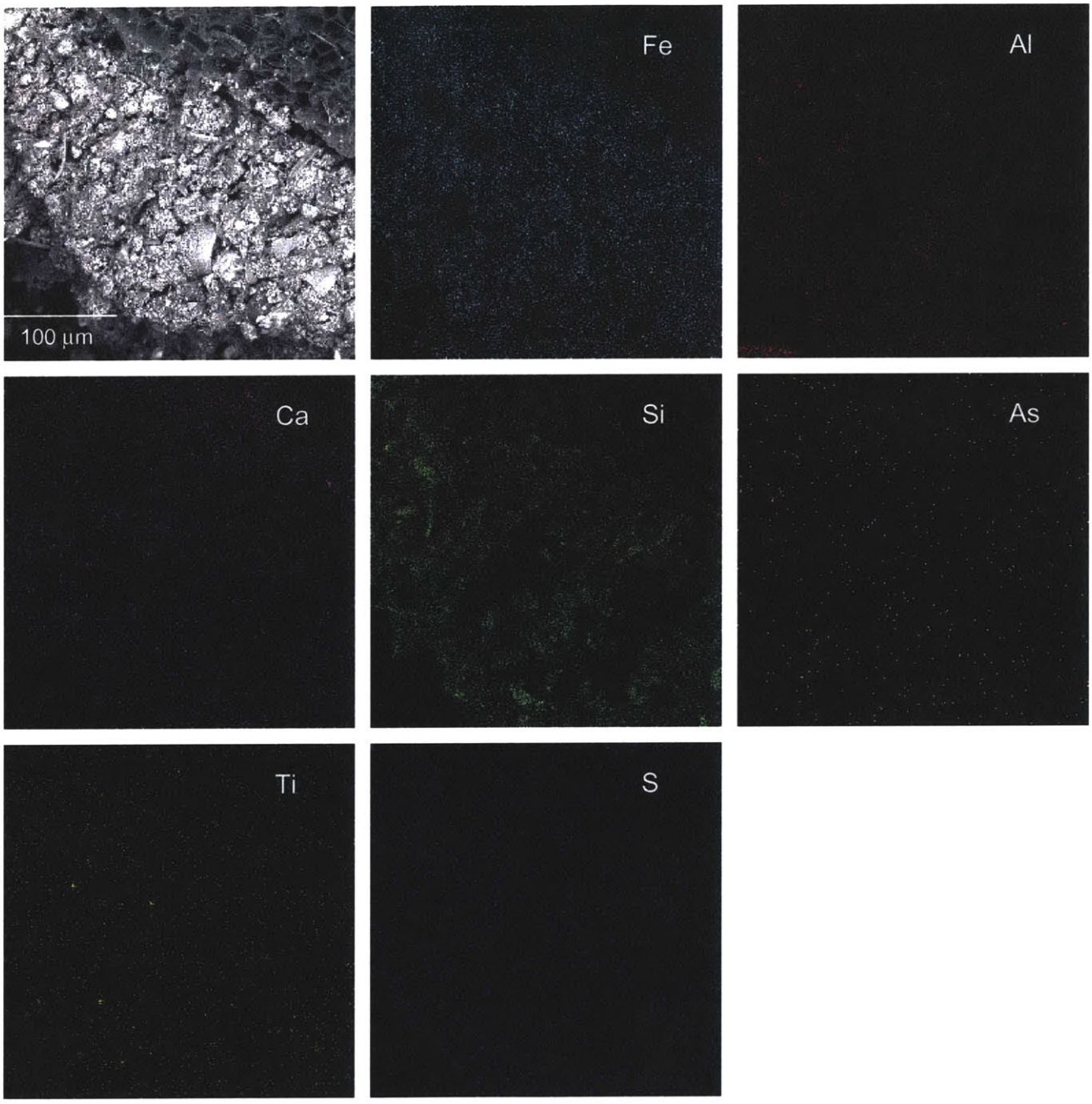

E.4. Figure VI. SEM BSE image (A) of resin-impregnated sediment subsample from the Wells G & H Wetland, at approximately 45 cm depth. Numbered spots shown are analyses of relative concentrations of metals by secondary ion mass spectrometry (SIMS) operating the beam in step-scan mode. Results in (B) and (C) show relative Fe and relative As concentrations across the step scan, where y-axis error bars are 1σ reproducibility for the averaged ratio. Elevated concentrations of Fe and As were observed within the root boundaries, which initially led us to examine the hypothesis that roots can store As and Fe internally. Cross-sectional metal distribution determinations by XRF microtomography showed that, in live roots, Fe and As are confined to the exterior of the root (Ch. 4). Based on these findings and images of Fe-laden root fragments observed by optical microscopy (App. C), we hypothesized that dead root fragments may store Fe and As after the cell walls decompose. Based solely this image of an old root fragment, however, we cannot rule out the possibility that this root is from another type of wetland plant that may take up As. Additional research into this hypothesis is required to conclusively determine whether As and Fe is stored within roots after senescence.

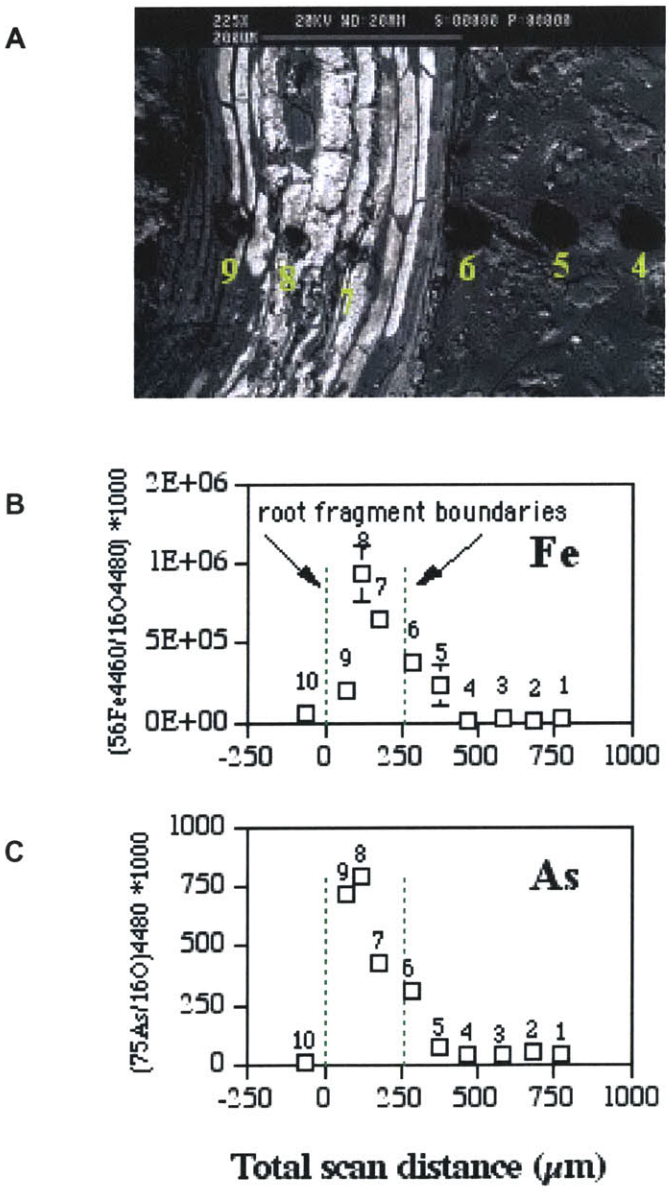

E.5. Figure VII. Fluorescence microtomography images of a cross section through a 120 μm diameter freeze-dried *T. latifolia* root, which are very similar to the images of a 300 μm root shown in Ch. 4. The images were obtained by measuring fluorescence at each element s white line energy produced by the 16.3 keV x-ray beam. The root was translated through the beam by 3 μm steps, followed by 5 degree rotations and another rotation for a total of 180 degrees. Dwell time at each point was 1 second, thus yielding an analysis time of approximately 4 hours. Higher intensities of fluoresence corresponding to higher concentrations are nearer the hot end of the color spectrum (white then red, orange, etc). The Fe plaque in the small root, like the larger root in Ch. 4, was of similar thickness (10-20 μm).

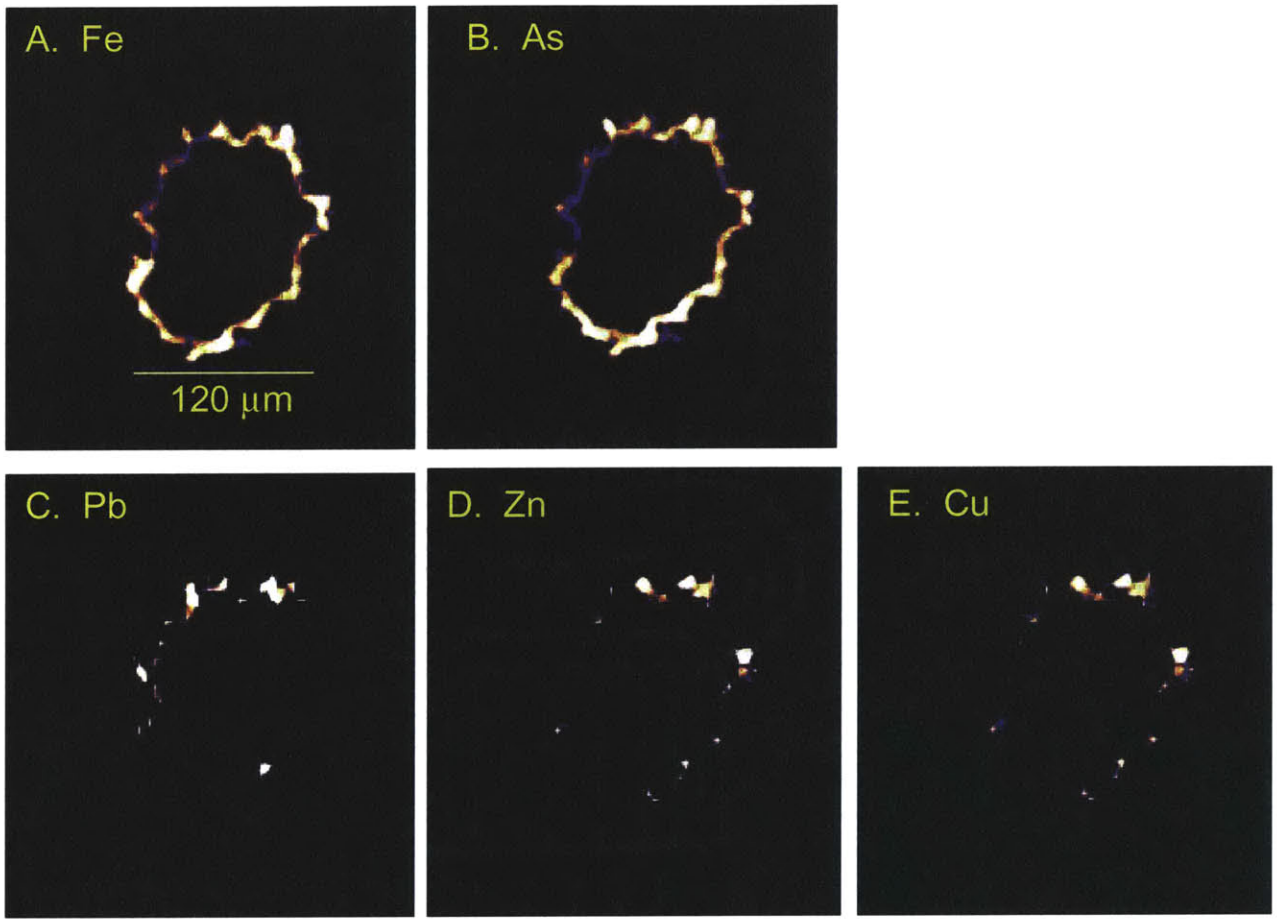

Figure VIII. Correlation plot of As versus Fe for the 120 μm root shown in Fig.VII. Each point is the fluorescence intensity for a 5 μm step, with a 3 μm beam width. Intensity is directly proportional to count rate for all detectors. The plot shows that As and Fe are highly correlated at the small scale of 3 μm.

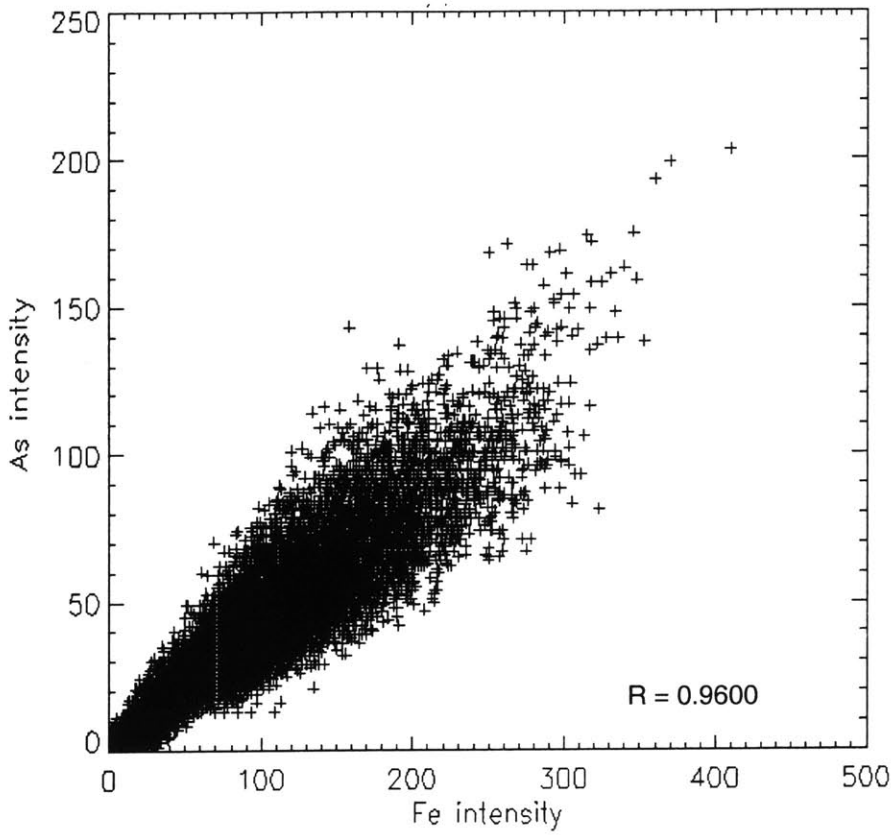

Figure IX. Fluorescence microtomography images of a rhizome wall section, with the interior shown to the left of the bright area of the plaque. Images were collected using a 12.0 keV x-ray beam, with 1 second dwell time at each position for each element s white line energy. The rhizome was translated through the beam in 10 μm steps, then rotated by 5 deg, and retranslated until a total of 180 degrees. The images show that for even the rhizome, As and Fe are highly correlated, and Cu and Zn are correlated in two discrete regions.

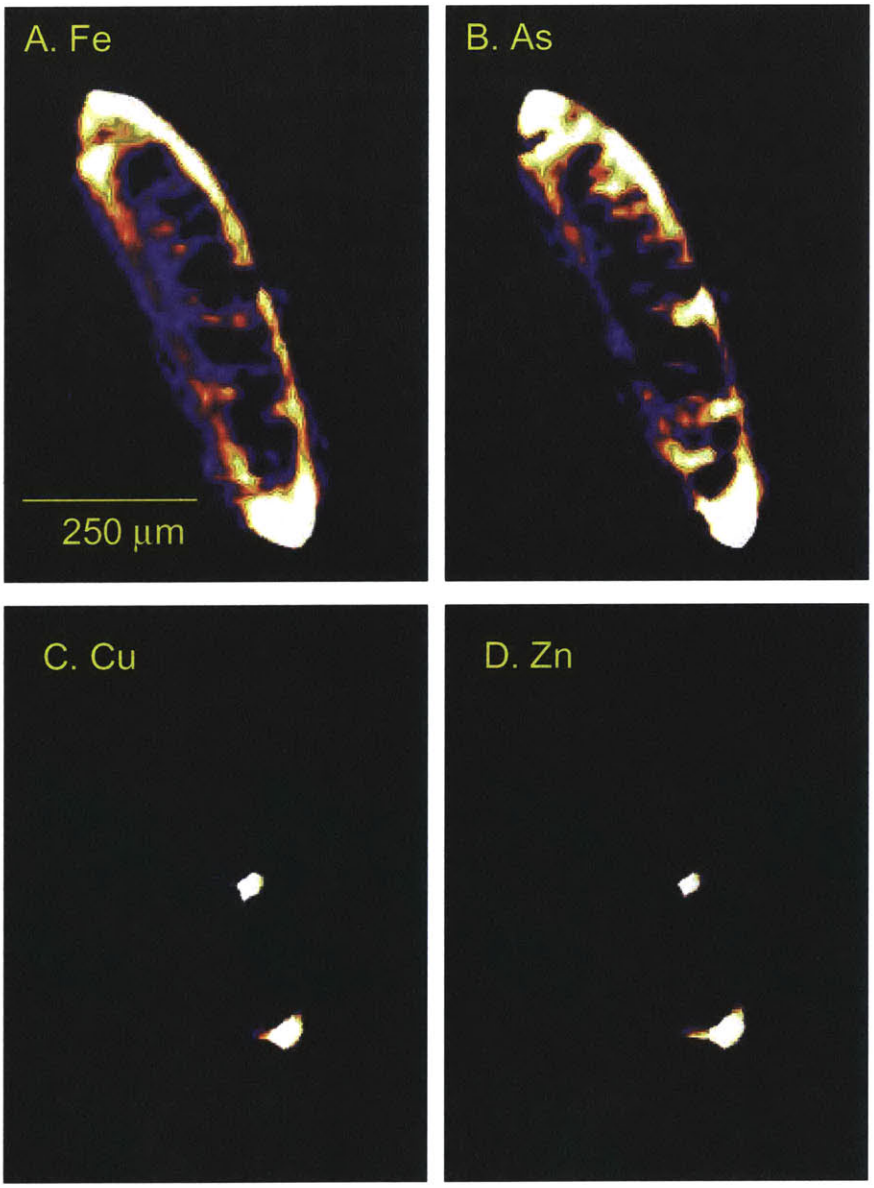

Figure X. Arsenic XANES scan of an unpreserved root cross-section using a defocussed 400 μm beam width and height. Data points are represented by connected circles. The solid line is the data curve fit using As(III) and As(V) on FeOOH as model compounds, which shows that the plaque is comprised of approximately 16% As(III) and 84% As(V). This XANES spectra is very similar to the one shown in Ch. 4, although the spectra here is for a root region near the apex (5 mm from the root tip) and the Ch.4 XANES spectra is from an older section of root (>1 cm from root tip).